SANDIA REPORT
SAND2023-01803
Printed April 2023

Sandia National Laboratories

MELCOR Accident Progression and Source Term Demonstration Calculations for a Molten Salt Reactor

Kenneth Wagner
Brad Beeny
Troy Haskin
David Luxat
Rod Schmidt

Prepared by
Sandia National Laboratories
Albuquerque, New Mexico
87185 and Livermore,
California 94550

Issued by Sandia National Laboratories, operated for the United States Department of Energy by National Technology & Engineering Solutions of Sandia, LLC.

Available to DOE and DOE contractors from
U.S. Department of Energy
Office of Scientific and Technical Information
P.O. Box 62
Oak Ridge, TN 37831

Telephone: (865) 576-8401
Facsimile: (865) 576-5728
E-Mail: reports@osti.gov
Online ordering: http://www.osti.gov/scitech

Available to the public from
U.S. Department of Commerce
National Technical Information Service
5301 Shawnee Rd
Alexandria, VA 22312

Telephone: (800) 553-6847
Facsimile: (703) 605-6900
E-Mail: orders@ntis.gov
Online order: https://classic.ntis.gov/help/order-methods/

ABSTRACT

MELCOR is an integrated thermal hydraulics, accident progression, and source term code for reactor safety analysis that has been developed at Sandia National Laboratories for the United States Nuclear Regulatory Commission (NRC) since the early 1980s. Though MELCOR originated as a light water reactor (LWR) code, development and modernization efforts have expanded its application scope to include non-LWR concepts. Current MELCOR development efforts include providing the NRC with the analytical capabilities to support regulatory readiness for licensing non-LWR technologies under Strategy 2 of the NRC's near-term Implementation Action Plans. Beginning with the Next Generation Nuclear Project (NGNP), MELCOR has undergone a range of enhancements to provide analytical capabilities for modeling the spectrum of advanced non-LWR concepts. This report describes the generic plant model developed to demonstrate MELCOR capabilities to perform molten salt reactor (MSR) safety evaluations. The generic plant model is based on the molten salt reactor experiment (MSRE) design, which operated from 1965-1969. The historical design reports provide sufficient information to build a MELCOR full-plant model. The MSRE fuel is dissolved in the molten salt coolant. The fuel fissions when it passes through the graphite core. The primary loop has a pump within a pump bowl and an intermediate loop molten salt to molten salt heat exchanger. The reactor is located in a reactor cell that includes a flow path to over-pressure vapor condensing and gas retention tanks. There is an offgas system connected to the pump bowl and other system locations that circulates helium to charcoal and absolute filters before exiting through the plant stack. An example calculation is performed to show the plant response to a molten salt spill accident. The accident selected for evaluation follows the maximum credible accident (MCA) from the MSRE safety analysis.

ACKNOWLEDGEMENTS

This work was funded by the NRC as part of the development and demonstration activities defined in the NRC Non-Light Water Reactor Vision and Strategy Volume 3: Computer Code Development Plans for Severe Accident Progression, Source Term, and Consequence Analysis [1]. The authors gratefully acknowledge the contributions from Jason Schaperow, Shawn Campbell, and Hossein Esmaili of the US NRC for their valuable technical guidance.

Austin Lo and Friederike Bostelmann of Oak Ridge National Laboratories (ORNL) performed the MSRE SCALE analyses that provided the radionuclide decay heat power, radionuclide inventory, the core axial and radial power profile, and the reactivity feedbacks for this analysis. Their analyses are documented in ORNL/TM-2022/1844 and are part of the same NRC-sponsored effort.

CONTENTS

LIST OF FIGURES

LIST OF TABLES

ACRONYMS AND DEFINITIONS

Abbreviation	Definition
ASHRAE	American Society of Heating, Refrigerating and Air-Conditioning Engineers
COR	Core
CV	Control Volume
CVH	Control Volume Hydrodynamics
DOE	United States Department of Energy
FHR	Fluoride-Salt-Cooled High-Temperature Reactor
FL	Flow Path
FLiBe	Li_2BeF_4
GEM	Gibbs Energy Minimization
GPM	Gallons Per Minute
GRTR	Generalized Radionuclide Transport and Retention
HEPA	High-Efficiency Particulate Air
HS	Heat Structure
LWR	Light Water Reactor
MCA	Maximum Credible Accident
MSR	Molten Salt Reactor
MSRE	Molten Salt Reactor Experiment
NGNP	Next Generation Nuclear Plant
NRC	United States Nuclear Regulatory Commission
NUEP	Nuclear Energy University Program
ORNL	Oak Ridge National Laboratory
RN	Radionuclide
scfh	Standard cubic feet per hour
scfm	Standard cubic feet per minute

1. INTRODUCTION

MELCOR is an integrated systems-level thermal hydraulics and source term code for reactor safety analysis [1]. It has been developed at Sandia National Laboratories for the United States Nuclear Regulatory Commission (NRC) since the early 1980s. Current MELCOR development efforts include providing the NRC with the accident analysis capabilities to support regulatory readiness for licensing non-light water reactor (non-LWR) technologies under Strategy 2 of the NRC's near-term Implementation Action Plans [2]. Beginning with the Department of Energy (DOE) Next Generation Nuclear Project (NGNP), MELCOR has undergone a range of enhancements to provide analytical capabilities for modeling the spectrum of advanced non-LWR concepts. A detailed description of the development process, including identification of technical gaps, is provided in NRC's "Non-Light Water Reactor (Non-LWR) Vision and Strategy, Volume 3 – Computer Code Development Plans for Severe Accident Progression, Source Term, and Consequence Analysis" (NRC ADAMS Accession No. ML20030A178). This report describes the generic MELCOR plant model developed to demonstrate MELCOR capabilities to date to perform molten salt reactor (MSR) safety evaluations.

The MELCOR MSR model is applied to provide an example of a source term analysis. The scope of the source term demonstration project includes development and application of a MELCOR full-plant model using publicly available references and data. The project also includes source term demonstration calculations for other non-LWR designs (e.g., a heat pipe reactor) that are documented in separate reports [3][4][5].

MELCOR characterizes the evolution of the accident from the early thermal-hydraulic response through the core heat up, including the release and transport of radionuclides from the primary system to the containment or confinement buildings and the environment. The code is a knowledge repository from decades of experiments and model development with a historical focus on LWR phenomenology. However, MELCOR has been extended with new models to address non-LWR technologies. The key MELCOR MSR models are discussed in Section 2.

MELCOR relies on the SCALE code system to provide the radionuclide inventories, kinetics parameters, power distributions, and decay heat, especially through the ORIGEN code. SCALE is a multi-disciplinary tool developed by Oak Ridge National Laboratory (ORNL) for the NRC to combine nuclear system simulation tools into one cohesive package [6]. SCALE provides a comprehensive, verified and validated, tool set for nuclear data, criticality safety, reactor physics, radiation shielding, radionuclide inventory characterization, activation, depletion and decay, and sensitivity and uncertainty analysis under a software quality assurance program. Since the 1970s, regulators, licensees, and research institutions around the world have used SCALE for safety analysis.

The MELCOR MSR input model used for the source term analysis is based on the ORNL Molten Salt Reactor Experiment (MSRE) [7]. The demonstration MSRE MELCOR input model development included (a) the reactor system, (b) incorporation of the SCALE inventory, axial and radial power profiles, decay heat tables, and reactivity feedback coefficients, (c) the containment, (d) the vapor condensing and gas retention tanks, (e) the offgas filter and auxiliary filter systems, and (f) plant control and radionuclide tracking algorithms. Section 3 describes the MSRE model used in the source term calculations.

The MSRE MELCOR plant model is used to simulate a molten salt spill from the reactor vessel due to a break in the piping to the drain tank. The accident analysis followed the maximum credible

accident (MCA) scenario documented in the MSRE reactor safety analysis report [8]. Some exploratory calculations were performed to illustrate the impact of variable scenario assumptions as well as variations in the safety system availability. The accident progression and the source term results are described in Section 4. A summary is presented in Section 5.

This report describes the MELCOR MSRE full-plant deck and its application to the MCA scenario. In addition, this work was presented at a public workshop on September 13, 2022. The video recording and presentation material are available at the following links:

- Video – https://youtu.be/nHHV528O0p0
- Slides – NRC ADAMS accession number ML22353A101 [9]

2. MELCOR MSR MODELING FEATURES

The MELCOR code is organized into "packages" that correspond to different groupings of reactor regions, physics, or other code functionalities [10]. A nuclear power plant is modeled using the building block components of control volumes, heat structures, and flow paths. These basic components are used to represent the primary system, the reactor vessel, the reactor cell (containment), the reactor building, and the secondary system, which will be described in the next section. These fundamental modeling features are used for all reactor types. The level of modeling detail or discretization is user-specified based on the objectives of the analysis. An example for the MSRE design is described in this report [7] in the next section.

In addition to the control volumes, heat structures, and flow paths, there are a few MSR-specific models. The next subsections describe some of the key MELCOR models used in the MSR demonstration calculations. Section 2.1 gives an overview of the MSR-specific models. Sections 2.2, 2.3, and 2.4 provide some additional details about code models for the fluid fuel, the FLiBe equation of state, and the Generalized Radionuclide Transport and Retention (GRTR) models, respectively.

2.1. Overview of MELCOR MSR-specific models

The modeling of the MSRE in MELCOR utilizes some new modeling features. First, MELCOR has been updated to support molten salt and sodium (Na) reactor fluids. For molten salt fluid properties, the thermophysical properties of FLiBe were added from Reference [11]. The FLiBe fluid properties are used for the molten salt with the dissolved fuel and the secondary side molten salt without dissolved fuel.

Next is the new fluid fuel fission power model. For other reactor types, the fuel is solid and initially contained within the core. However, the MSR fuel is dissolved into the molten salt and fissions when it passes through graphite structures in the core region of the reactor vessel. The new fluid fuel fission power model specifies the fission power for fluid fuel in the core region and the transport of delayed neutron precursors outside of the core region.

Finally, a new model was added to manage the radionuclides that circulate within the molten salt. The radionuclide inventory in the molten salt fuel and the associated radionuclide decay heats are specified from the SCALE analysis. The fluid fuel and the associated radionuclides from fission are tracked in MELCOR using the GRTR model. The decay heat associated with the flowing radionuclides is managed as groups of elements in radionuclide classes. The GRTR model is a subset of the MELCOR Radionuclide (RN) package, which manages the radionuclide transport and deposition physics. The Decay Heat (DCH) package provides the class-specific decay heat power to the RN package for every radionuclide in all locations.

2.2. Fluid fuel model

MELCOR ordinarily uses the COR package to model solid fuel behavior. However, the MSRE uses a fluid fuel. Consequently, a different approach is used for the MSR. The fluid fuel model is implemented as a new model in the control volume hydrodynamics (CVH) package. The fluid fuel model specifies the fission power in the core region. The fluid fuel model includes specification of separate regions for inside the graphite core and outside the core where the molten fuel salt normally circulates as shown in Figure 2-1. The MSR fission power is added to the fluid fuel in the core. The fission power can vary according to an axial and radial power profile, which was provided from the SCALE analysis. There is no fission power in the circulating fuel region outside of the core. However, the delayed neutron precursors that transport into and out of the circulating region are tracked.

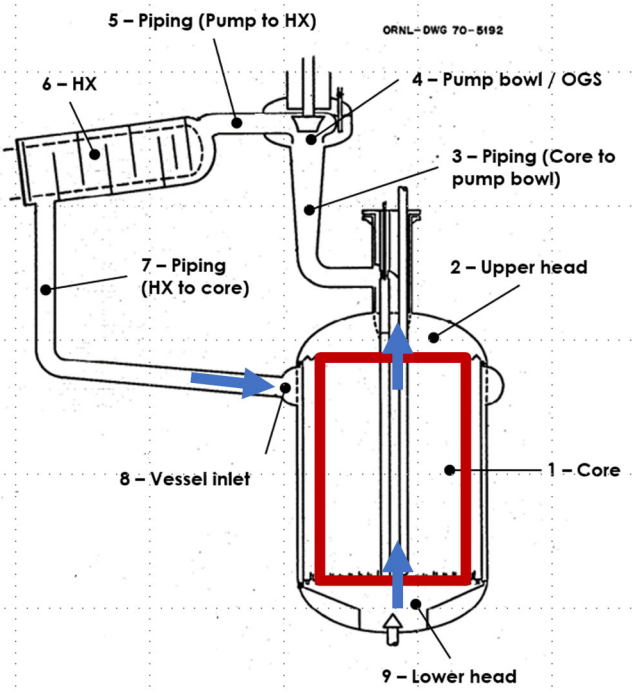

Figure 2-1 MELCOR MSR fluid fuel model.

The fluid fuel model includes a modified version of the point kinetics equation for the transient fission power [12]. The modified point kinetics equation, which accounts for the flow of delayed neutron precursors is shown in Equation (1),

$$\frac{dP}{dt} = \frac{\rho - \overline{\beta}}{dt} P(t) + \sum_{i=1}^{6} \lambda_i C_i^C + S_o \qquad \text{(Eqn. 1)}$$

where,

P	fission power (W)
t	transient time (s)
ρ	reactivity (s)
$\overline{\beta}$	total effective delayed-neutron yield (i.e., defined below)
β_i	static delayed-neutron yield for the ith group
Λ	neutron generation time (s)
λ_i	decay constant for ith delayed-neutron group (s^{-1})
S_o	rate of thermal power generated by an active neutron source (W/s)
C_i^C	fission power generated by ith group delayed-neutron precursors in the core (W)

For flowing fuel, the concentration of the delayed precursors inside the core region C_i^C(t) and outside of the core in the loop C_i^L(t) are tracked as follows,

$$\frac{dC_i^C(t)}{dt} = \frac{\beta_i}{\Lambda}P(t) - \left(\lambda_i + {}^1/_{\tau_C}\right)C_i^C(t) + \frac{V_L}{\tau_C V_C}C_i^L(t-\tau_C) \qquad \text{(Eqn. 2)}$$

$$\frac{dC_i^L(t)}{dt} = \frac{V_C}{\tau_C V_C}C_i^C(t) - \left(\lambda_i + {}^1/_{\tau_L}\right)C_i^L(t) \qquad \text{(Eqn. 3)}$$

where,

C_i^C(t)	fission power generated by i[th] group delayed-neutron precursors in the core (W)
C_i^L(t)	fission power lost by the i[th] group delayed-neutron precursors outside the core (W)
β_i	static delayed-neutron yield for the i[th] group
Λ	neutron generation time (s)
λ_i	decay constant for i[th] delayed-neutron group (s^{-1})
τ_C	time constant of the flow through the core (s)
τ_L	time constant of the flow outside of the core (s)
V_C	volume of the fluid in the core (m^3)
V_L	volume of the fluid outside of the core (m^3)

The various terms in Equations 2 and 3 are described as follows,

a	Increase in power by delayed neutron precursors in the core due to fission
b	Decrease in power by delayed neutron precursors in the core due to decay and flow out of the core
c	Increase in power by delayed neutron precursors in the core due to flow into the core from outside the core
d	Increase in power by delayed neutron precursors outside the core due to flow from the core
e	Decrease in power by delayed neutron precursors outside the core due to decay or flow into the core

Finally, the total effective delayed-neutron yield in the core is updated each timestep as follows,

$$\bar{\beta} = \beta - \beta(t)_{lost} = \sum_{i=1}^{6}\beta_i - \left(\frac{\Lambda}{P(t)}\right)\sum_{i=1}^{6}\lambda_i C_i^L(t) \qquad \text{(Eqn. 4)}$$

The fission power from the fluid fuel point kinetics model is distributed across the core according to the specified axial and radial power distribution. The fluid fuel model can respond to external reactivities calculated in the control function package for thermophysical variations from normal operating conditions. The feedbacks from SCALE included (a) the molten salt liquid temperature and (b) the graphite temperature. The feedbacks are summarized in Section 3.6. Another feedback was added for voiding to terminate the fission power when the liquid fuel did not exist in the core. The termination of fission power in voided CVH control volumes was subsequently implemented into the fluid fuel physics model.

The power due to the radionuclide decay heat is provided by the DCH package to the RN package. In each CVH control volume inside and outside of the core, the mass of each radionuclide class is tracked. Prior to the shutdown of the fission reaction due to the control rods being inserted (or perhaps voiding in a drain scenario), the specific RN class decay powers (W/kg) are fixed to the shutdown value from the SCALE analysis. Thereafter, the decay heats follow the RN class decay heat tables from SCALE.

Finally, a portion of the fission power can be deposited into the graphite due to neutron heating. ORNL estimated the graphite heating due to neutron capture to be ~670 kW [7]. The graphite heating was scaled by the total fission power and distributed across the heat structures representing the graphite stringers according to the radial and axial power distribution provided by SCALE.

2.3. MELCOR FLiBe equation of state

The MSRE molten salt fuel included variations of lithium, beryllium, and zirconium fluoride salts that contain uranium, or uranium and thorium fluorides. For the demonstration calculation, MELCOR's fluoride salt, or FLiBe (Li_2BeF_4), thermophysical properties are used for both the molten salt fuel and the secondary unfueled fluoride salt. The FLiBe equation of state was obtained from Idaho National Laboratory [11]. When simulating an MSR, special input directives are used to identify FLiBe as primary fluid rather than water. MELCOR reads the FLiBe fluid properties database, which provides the specific volume (m^3/kg), the specific internal energy (J/kg), the coefficient of thermal expansion (1/K), the isothermal compressibility (1/Pa), the specific heat capacity at constant pressure, c_P (J/kg-K), and the specific entropy (J/kg-K). The coefficient of thermal expansion and isothermal compressibility are determined using these properties.

A key addition implemented in the MELCOR demonstration calculations for a fluoride-salt-cooled high-temperature reactor project was an extrapolation to frozen conditions [13]. FLiBe salt solidifies at approximately 460°C. During the evolution of a transient, the temperature may reach the freezing point. To allow frozen conditions without significant code architectural changes, a thermodynamic supercooling model was added to the equation of state such that the liquid and vapor phases may exist below the freezing temperature. The freezing extension was required for the MSRE model as trace amounts of FLiBe vapor transported through the relatively cool offgas system. Similarly, a small molten fuel salt leak onto the MSRE reactor cell floor could freeze.[1] The model addition allowed the MSRE steady state and transient calculations to be performed.

2.4. MELCOR GRTR model

The GRTR model is being developed for increased flexibility in modeling liquid field radionuclide behavior. GRTR is a submodel of the RN package and has been fully integrated. The GRTR model adds capabilities to assess radionuclide behavior in molten salt systems such as solubility, soluble and insoluble (i.e., colloid) radionuclide transport, deposition, and vaporization. The GRTR model was originally implemented to call the Thermochimica Gibbs free energy minimization (GEM) solver to calculate the radionuclide vapor pressures, chemical forms, and solubilities [14]. Due to limitations in the molten salt thermodynamic database [15], the approach was modified to calculate the solubility using radionuclide-specific Antione vapor pressure curves. Where data is available from the molten salt database (e.g., Cs and CsF), built-in vapor pressure curves generated by Thermochimica were

[1] The MSRE demonstration calculation assumed the entire primary system spilled onto the floor, which remained at high temperature. However, a small leak is more likely to cool and freeze.

added. The new approach allows exploration of responses and uncertainty evaluations (e.g., vapor pressure neglecting solubility) until more radionuclides are added to the molten salt thermodynamic database. The modified approach is also computationally faster.

Figure 2-2 shows the GRTR inputs, the physico-chemical dynamic models, and the transport models. GRTR receives the mass of radionuclides entering the molten salt pool from the fuel or the gas space by the COR and RN packages, respectively. The radionuclides in GRTR are tracked as a soluble form, an insoluble form (i.e., colloids), or non-condensable gases that advect with the liquid molten salt between control volumes. The physico-chemical models include vaporization, mass transfer between soluble and insoluble forms, and deposition onto structures. The transfer between soluble and vapor forms is specified using solubility curves with an optional time-constant for dissolution. The colloid deposition onto structures includes the sorption of soluble radionuclides into graphite and the colloid deposition onto structural surfaces. GRTR is intended to be flexible for all reactor types with user flexibility on the number of forms and interacting physics (see Figure 2-3 for detailed example of an MSR).

The GRTR model evaluates the radionuclide state variables using the control volume's liquid temperature and pressure from the CVH package. The GRTR advective flows into and out of the control volume are provided by the RN package using molten salt flowrates from the CVH package.

The GRTR model was still under development at the time of the MSRE salt spill demonstration calculations. The MSRE salt spill demonstration calculation only used the GRTR cesium vaporization model. The vaporization prediction was limited to Cs and CsF due to limitations in the molten salt thermodynamic database [15]. However, the spilled molten salt temperatures were below where any significant transfer from the liquid to the vapor above the liquid surface occurs. The GRTR model was also specified to release all the noble gases after the spill. The MELCOR code development staff are adding flexibility to incorporate alternative thermochemical databases and built-in physics options for the form-wise transfers.

A companion report on non-LWR reactor modeling is planned, which will summarize the lessons learned during the non-LWR demonstration calculations. It will identify ongoing or recommended work to improve modeling and the prediction of the non-LWR source term. The GRTR development plans include the incorporation of some functionality from SCALE/ORIGEN. The ORIGEN routines will allow a mechanistic evaluation of radionuclide decay outside of the core, which could include the transfer of mass from one radionuclide class and GRTR form to another. New transfer features are also being added to include location-specific physics. The location-specific models will allow modeling of airborne releases due to splashing, entrainment, and bubbling (e.g., due to the helium sparger flow in the pump bowl).

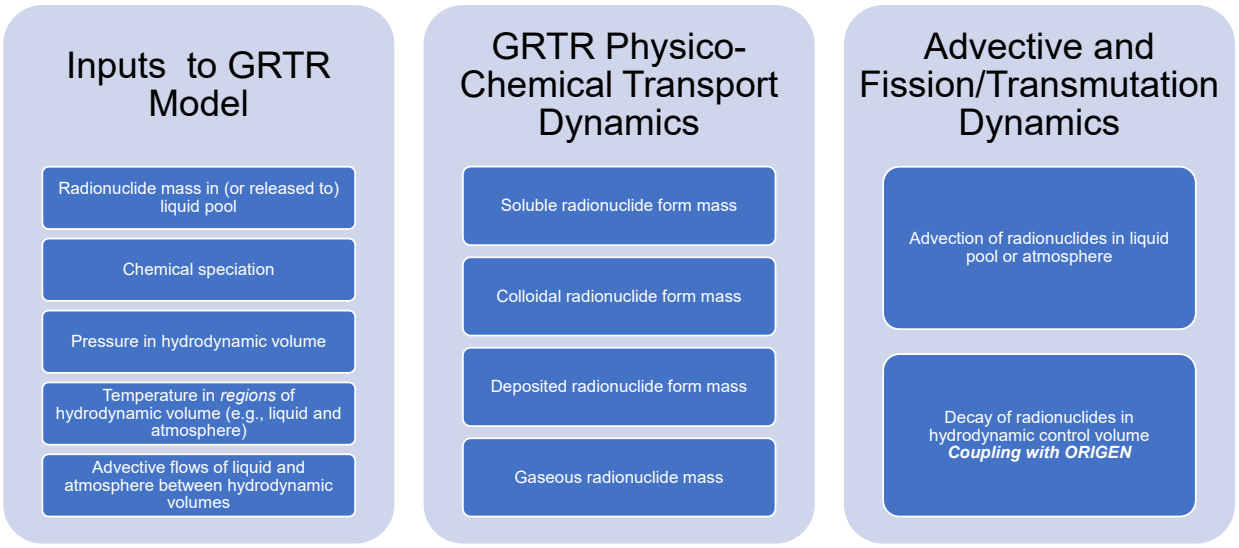

Figure 2-2 MELCOR GRTR inputs, models, and transport.

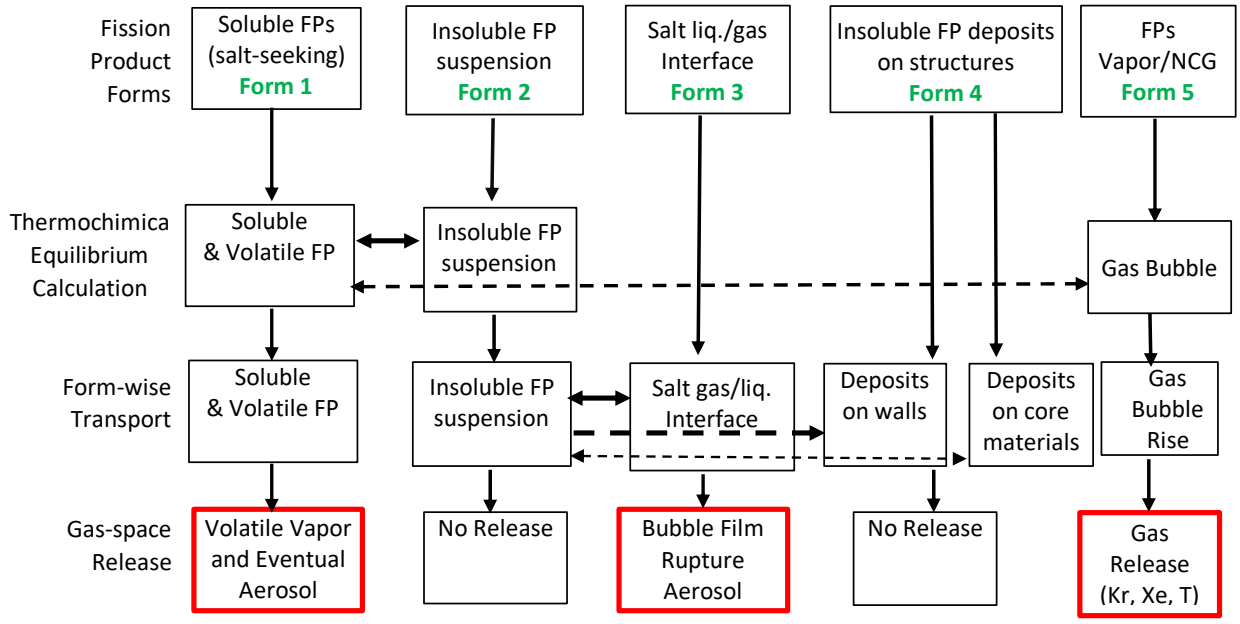

Figure 2-3 Example of a GRTR application for a molten salt system.[2]

[2] GRTR allows specification of the number of forms and their interactions. The example in Figure 2-3 was developed for a molten salt reactor. The horizontal arrows correspond to mass transfer processes between forms. Only the forms pointed to by an arrowhead indicate mass transfer. Masses of released species are given in the bottom row in red-bounded boxes.

3. MODEL DESCRIPTION

The development of the MELCOR MSRE input model was primarily based on the MSRE design report [7]. The information from Reference [7] was supplemented with additional information in the safety analysis report [8]. The reactor cell, the vapor condensation system, the reactor building volume, and the maximum credible accident boundary conditions were obtained from the safety analysis report [8]. The information available in References [7] and [8] is relatively comprehensive. Nevertheless, some dimensions were not available and therefore estimated from available drawings. Some of the important estimated values included the primary system piping lengths, vessel elevations, the pump bowl gas volume, the details of the primary heat exchanger geometry, and many reactor cell dimensions. Assumptions or estimations for the missing parameters were made to complete the demonstration model.

The radionuclide inventory and decay heat tables were obtained from a supporting SCALE analysis by ORNL [16]. SCALE was also used to generate the axial and radial power profiles and the reactivity feedbacks. Other key inputs from the SCALE analysis included the deposited radionuclides in the primary system and radionuclides in offgas system upstream of the charcoal filters.

Section 3.1 provides an overview of the MSRE. The reactor vessel, the primary and secondary systems, and the containment building nodalizations are described in Section 3.2. The MSRE uses an offgas system to remove noble gases from the fluid fuel, which is described in Section 3.3. ORNL provided the radionuclide inventory and the decay heat, which is described in Section 3.4. The fission product release from the molten salt spill scenario is very different from fixed fuel reactor designs and is described in Section 3.5. SCALE also provided reactivity feedbacks for the point kinetics point model, which are described in Section 3.6. Finally, the steady state initialization is shown in Section 3.7.

3.1. MSRE overview

The MSRE reactor system schematic is shown in Figure 3-1. The reactor vessel interfaces with the hot leg to the pump bowl. The salt pump is located in a partially closed off region of the pump bowl. The pump bowl surrounds the salt pump. There is a spray flow into the gas space above the pump bowl molten salt surface. The pump bowl has flow connections to the mainstream flow circuit. The salt pump circulates the molten salt through a heat exchanger and then back to the reactor vessel. The secondary side of the primary heat exchanger is an unfueled molten salt loop. The secondary loop rejects its heat through air radiators in a ventilation plenum leading to the plant stack. Some of the key MSRE design parameters are summarized in Table 3-1.

The MSRE reactor vessel nodalization was developed using the geometry and technical information in Reference [7]. The reactor vessel is 2.44 m high with a diameter of 1.5 m. The volume of molten salt in the core is 0.70 m^3. There is 0.855 m^3 of molten salt in the other reactor internals, for a total of 1.56 m^3. The total primary system molten fuel inventory is 1.996 m^3. Consequently, the fluid volume in the remainder of the primary loop is 0.443 m^3 (see Table 3-2). The core power density is 20 MW/m^3, which is significantly higher than a PBMR (4.8 MW/m^3) but much lower than a current-generation pressurized water reactor (105 MW/m^3).

The MSRE vessel includes an inlet flow distributor, an annular downcomer, the lower reactor head, the core, and the upper head (see Figure 3-2). The core is a large graphite structure with flow channels (see Figure 3-3). It is constructed from 600 graphite stringers (Figure 3-4), which combine to form the molten salt flow channels. The fluid fuel fissions as it flows through the stringer flow

channels in the graphite core. The fluid exits out of the top of the reactor vessel towards the pump bowl.

The circulating fluid fuel salt (0.075 m^3/s) enters the side of the vessel into a half toroidal flow distribution pipe that surrounds the reactor vessel. The flow distribution pipe directs the fluid salt through 84 holes to ensure a uniform flow entering the annular downcomer. Upon leaving the vessel, the fluid fuel salt flows upward into the pump. The pump impeller directs the main stream of the fluid fuel into the horizontal hot leg between the pump bowl and the primary heat exchanger. A partially filled tank (i.e., the pump bowl) is hydraulically connected to the impellor region of the pump.

The pump bowl serves several purposes. It is the only free surface in the primary system. The system pressure is maintained via the helium offgas system connection to the pump bowl and overflow tank. It is assumed that the cover-gas system maintains a 34.5 kPa (5 psig) overpressure. A recirculation spray flow from the pump exit is directed into the gas space of the pump bowl to promote removal of noble gases from the nuclear fission in the core. Finally, the pump bowl provides for the fluid expansion and contraction as the system heats or cools, respectively.

The flow exits the pump horizontally towards the primary system heat exchanger (Figure 3-5). The primary fuel salt flows through the shell side of the heat exchanger and non-fueled molten salt flows through the tube side and removes heat. There are 160 heat exchanger tubes in a U-shape configuration. The secondary molten salt flow rate is 0.536 m^3/s. The molten salt exits the heat exchanger and flows to the reactor vessel via a cold leg pipe.

Because the MSRE is a research reactor, it does not include a power conversion system. Instead, the secondary side of the MSRE connects to radiators in a plenum leading to the plant stack. A fan forces air across the radiators to cool the secondary side molten salt. The secondary side molten salt enters the heat exchanger at 593 °C and exits at 552 °C. The secondary fluid inlet pressure is 0.58 MPa. The radiators consist of 120 tubes of 9.1 m length and 0.019 m inner diameter. The radiator air fan flowrate is 94.4 m^3/s. The air temperature rises 111 °C across the radiator.

Reference [7] includes a description of the MSRE reactor cell (i.e., the containment) but few dimensions. The reactor cell contains the vessel, the primary system loop, and most of the secondary loop except the radiators. The reactor vessel is insulated by a thermal shield structure. The shield forms an annular region that is filled with carbon steel balls and circulating water. The thermal shield completely surrounds the vessel. The thermal shield water flow system is designed to remove 600 kW. A 15 cm insulation layer is located in the gap between the shield and the reactor vessel. There are heaters adjacent to the vessel. The heaters can provide up to 68 kW to maintain the vessel fluid fuel above its melting temperature (e.g., during startup).

Similar to the vessel thermal shield (i.e., also called a furnace), the pump bowl and overflow tank are surrounded by a furnace with electrical heaters. The pump bowl furnace includes 13 cm of insulation with heaters next to the pump bowl. The pump bowl does not include a radiation shield (i.e., the carbon steel balls and water).

As shown in Figure 3-1, the reactor cell connects to the drain tank cell. The fluid fuel from the primary system is drained into the tanks when the reactor is not operating. The containment pressure boundary includes the reactor cell and the drain tank cell. The total volume is 320 m^3.

The reactor and drain tank cells are inerted with 95% N_2. A vacuum pump maintains the reactor cell pressure at 0.875 bar absolute (12.7 psia). The nominal in-leakage rate is 0.42 standard liters per hour, which corresponds to a 0.23 mm diameter leak path.

The maximum credible accident (MCA) is defined as a fuel salt spill in the reactor cell with a coincident spill of water. From the MSRE safety analysis report [8],

> *"Equilibration of all the fuel salt with the cell atmosphere and just enough water to form the maximum amount of saturated steam would result in the maximum pressure in the secondary container. With no relief device, pressures as high as 110 psig could result."*

The containment design includes a vapor suppression tank and a gas retention tank to mitigate this pressure rise (see Figure 3-7). The piping to the tanks is normally isolated from the reactor cell using two bursting disks. A 10 cm (4") pipe with a 1.03 bar (15 psig) bursting disk is in parallel with the primary 30.5 cm (12") pipe with a 1.38 bar (20 psig) bursting disk to the vapor condensing tank. The vapor condensing tank has 34 m^3 (1200 ft^3) of water and uses a sparger to condense the steam. The gas space of the vapor condensing tank is connected to a 93 m^3 (3300 ft^3) gas retention tank. Any non-condensable gas exiting the surface of the water is retained in the gas space of the vapor condensing tank or in the gas retention tank. A vacuum relief valve allows backflow from the vapor condensing tank if the reactor cell pressure decreases below the vapor condensing tank pressure.

The MSRE used an expansive offgas filtration system. A simplified diagram is shown in Figure 3-8. A helium source supplies 6000 liter/day through the primary pump bowl and the overflow tank. The pump bowl helium effluent connects to a series of holdup volumes (large volume & low flow) inside and outside of the reactor cell. There are two filter trains with 0.623 m^3 (22 ft^3) of charcoal. Typically, only one train is operating and the other is isolated. There is also an auxiliary charcoal filter that is usually offline. The auxiliary filter can be used for filtered venting of the reactor cell.

The relatively low flow from the charcoal filters connects at a filter plenum with the 9.9 m^3/s (21,000 cfm) reactor building ventilation flow. The combined flow from the offgas and the ventilation system enters three 32 m^2 (3x350 ft^2) fiberglass roughing filters, which have a 90-95% efficiency for dust and larger particles. The roughing filters are used to protect and reduce the mass loading on the absolute filters.

Three 2.23 m^2 (3x24 ft^2) high-efficiency particulate air (HEPA) "absolute" filters are downstream of the roughing filters. The absolute HEPA filters have a 99.97% efficiency for 0.3-micron particles or larger. The filtered flow enters the exhaust fan and exits through the 30-m (100-ft) plant stack.

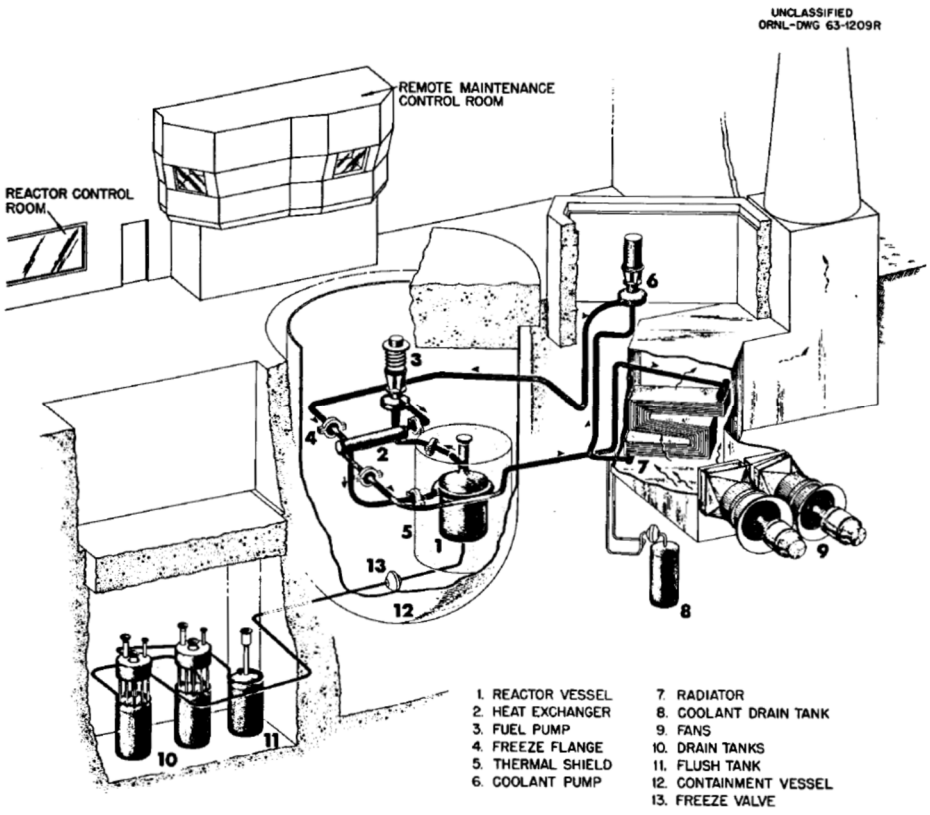

Figure 3-1 MSRE schematic [7].

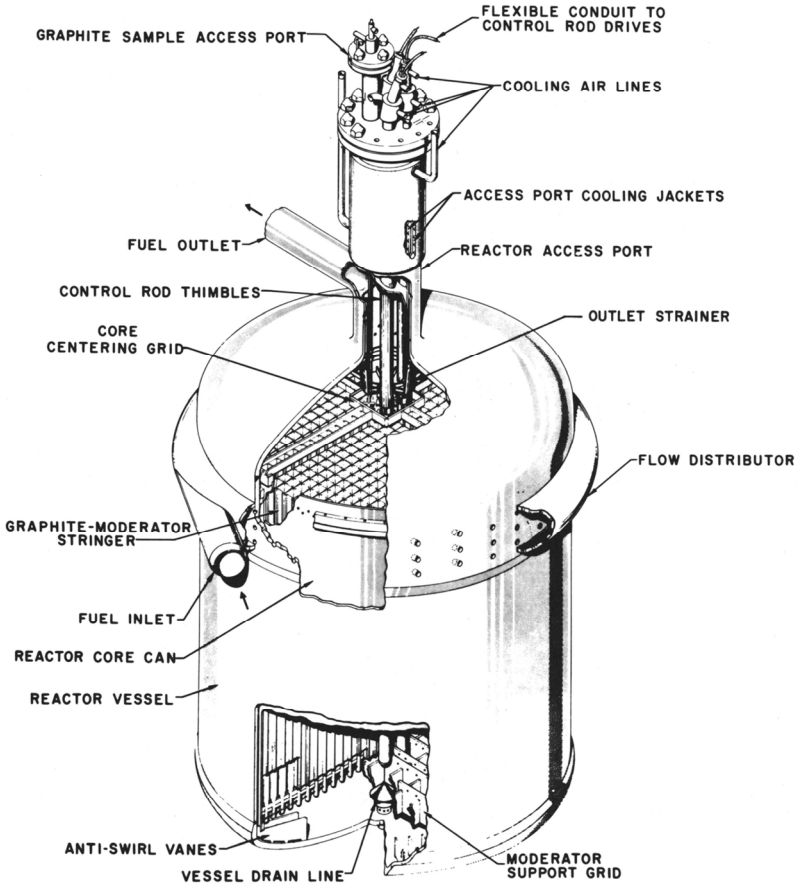

Figure 3-2 MSRE reactor vessel [7].

Figure 3-3 MSRE graphite core [7].

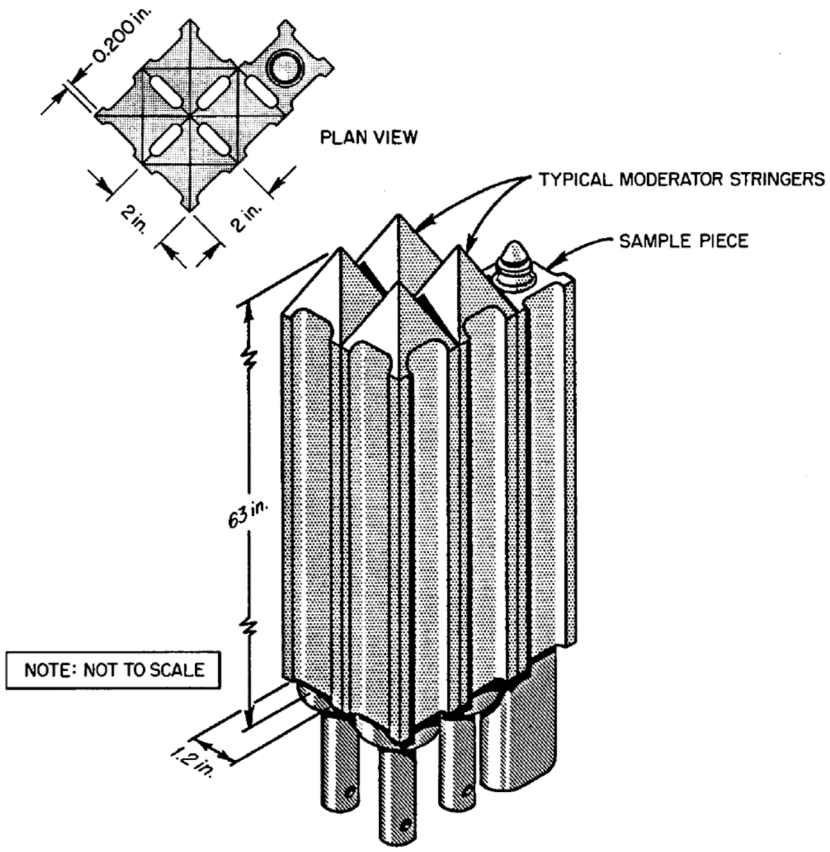

Figure 3-4 MSRE graphite stringer [7].

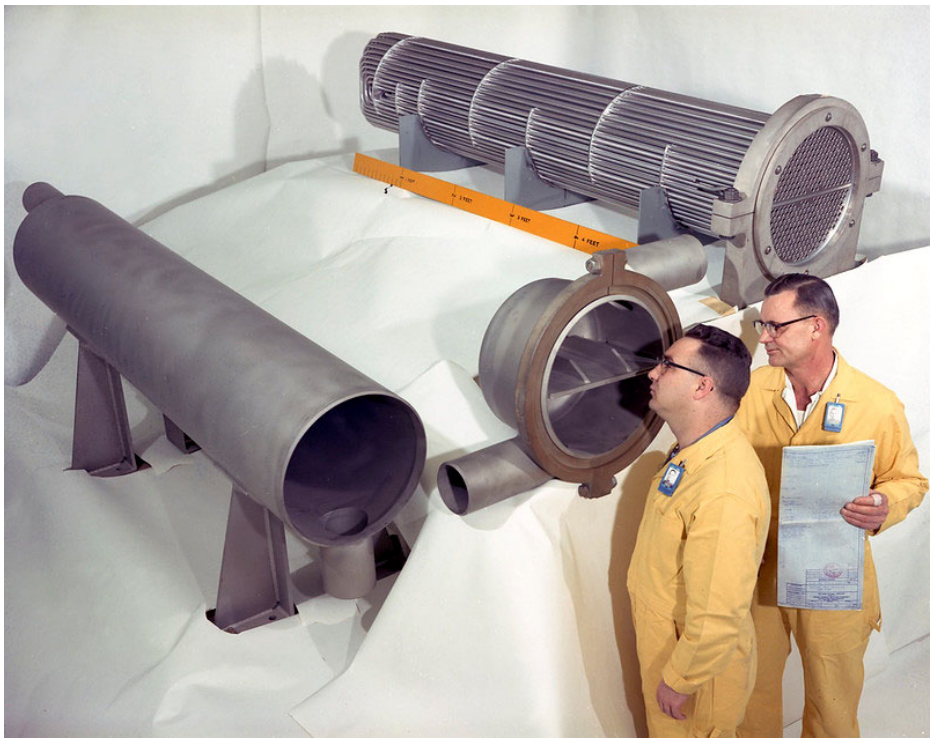

Figure 3-5 MSRE primary heat exchanger [7].

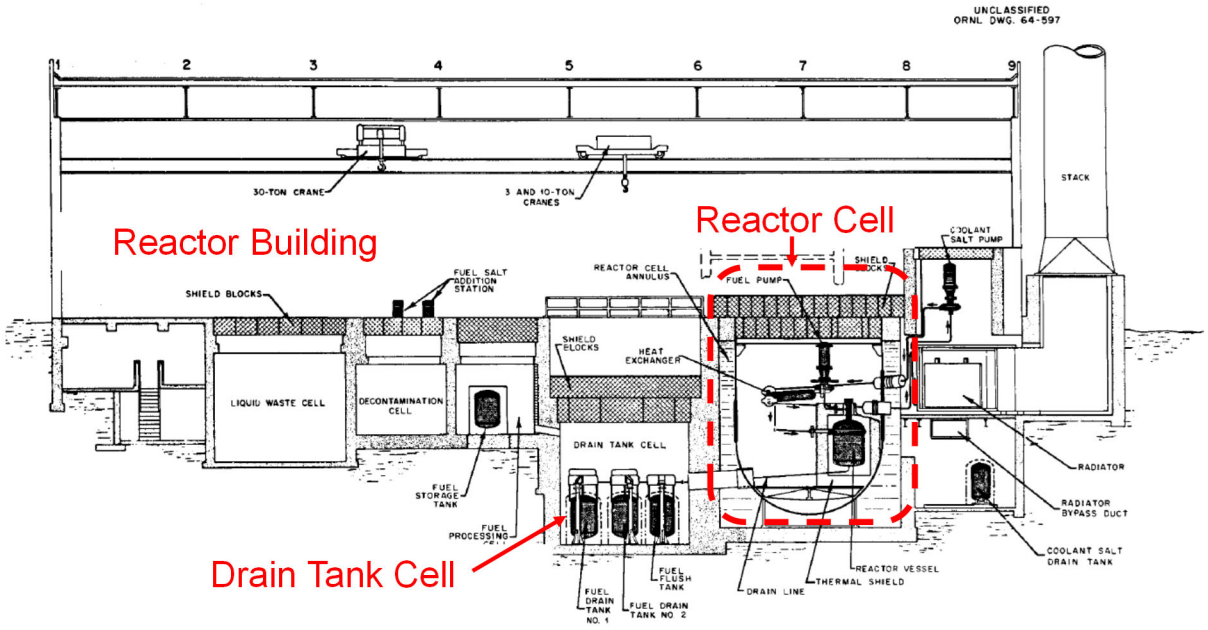

Figure 3-6 MSRE side view showing the reactor cell, the drain tank cell, and the surrounding reactor building [7].

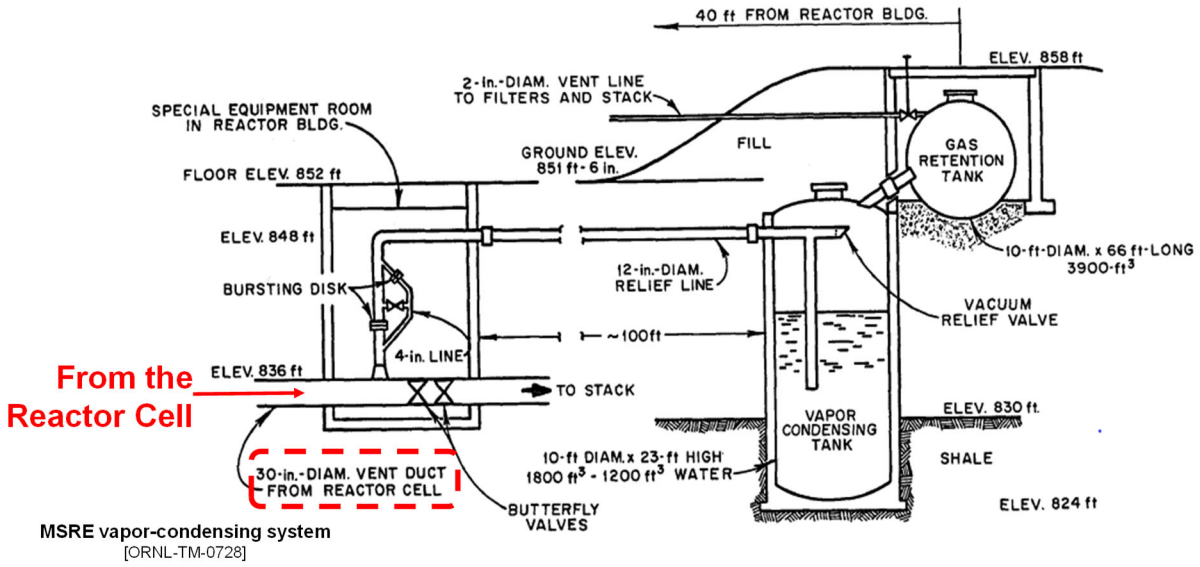

Figure 3-7 MSRE containment bursting disks and the vapor condensing and gas retention tanks [7].

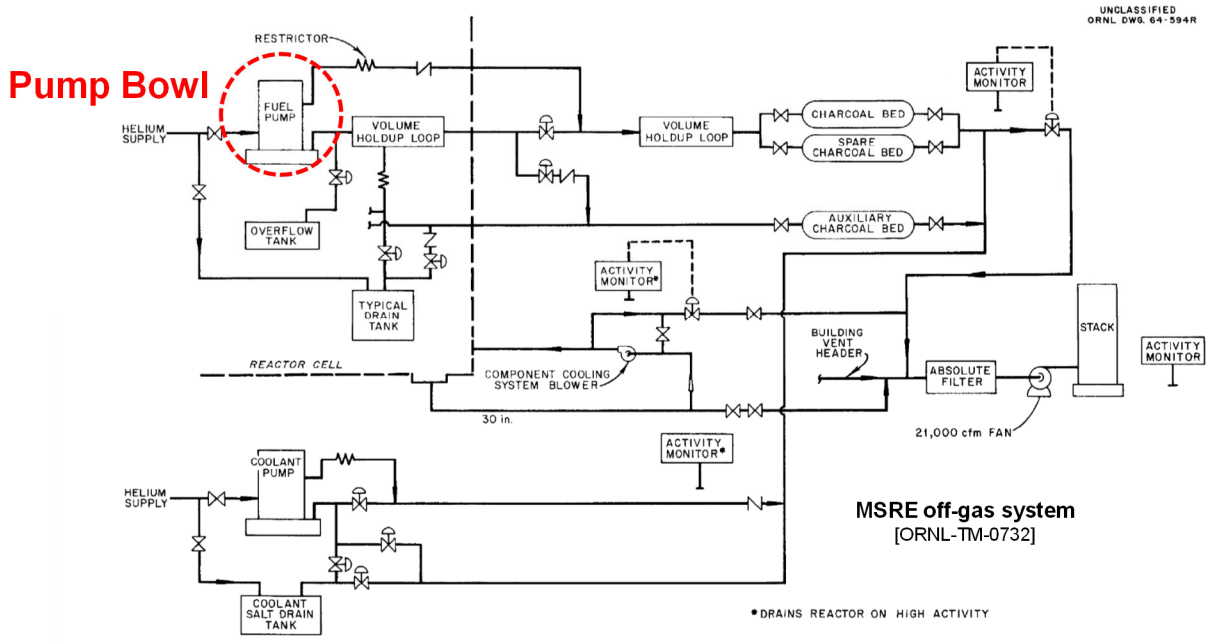

Figure 3-8 MSRE offgas system [7].

Table 3-1 Key MSRE design parameters [7].

Parameter	Value
Reactor thermal power	10 MW *
Coolant	$LiF\text{-}BeF_2\text{-}ZrF_2\text{-}UF_2$
Enrichment	34.5 wt.% ^{235}U
Moderation	Graphite stringers
Power density	20 MW/m^3
Reactor vessel pressure	Near atmospheric
Reactor inlet temperature	635 °C
Reactor outlet temperature	668 °C
Primary system flowrate	0.075 m^3/s
Loop transit time	25.2 sec
Operating time	375 days

* The initial criticality was 10 MW but subsequently operated at 8 MW. The MELCOR analysis used 10 MW thermal power based on the MSRE design document [7].

Table 3-2 MSRE fluid volumes [7].

Region	Volume (m^3)
Core	0.708
Upper head	0.297
Reactor vessel to pump	0.059
Pump main stream	0.025
Pump bowl outside main stream volume	0.091
Pump to heat exchanger	0.023
Heat exchanger	0.173
Heat exchanger to reactor vessel	0.062
Reactor vessel inlet (nozzle, volute, downcomer)	0.275
Lower head	0.283
Total	1.996

3.2. MSRE model nodalization

The MSRE model nodalization and key modeling features for the reactor vessel, the primary and secondary systems, and the containment are described in Sections 3.2.1 through 3.2.3, respectively.

3.2.1. Reactor vessel nodalization

The MSRE reactor vessel nodalization in MELCOR utilizes building block inputs from multiple packages. The building block approach to the input provides flexibility to model alternate reactor designs with varying levels of resolution. The reactor core is the key region in the vessel, which includes the graphite stringer structures and the fluid channels. In the MSRE model, this is specified using control volumes, flow paths, and heat structures rather than using the COR Package. The MSR fluid fuel model provides the power to the various fluid fuel regions in the core.

The reactor vessel control volume and flow path nodalization is shown in Figure 3-9, which is modeled in cylindrical coordinates. The MSRE core nodalization has 10 axial levels and 5 radial rings. CV-110 models the core inlet plenum region at the bottom of the vessel. The core region where the fluid fuel fissions is located in Rings 1 through 5, which includes CV-210 through CV-219, CV-220 through CV-229, CV-230 through CV-239, CV-240 through CV-249, and CV-250 through CV-259. Attached to each of the control volumes in the core are heat structures representing the graphite stringers. The fluid fuel flows axially through the graphite stringers and exits into the outlet plenum (i.e., CV-130). The fluid fuel enters the vessel through the distribution plenum (CV-100) and flows down the annular downcomer (CV-105) towards the inlet plenum.

The axial and radial nodalization were selected to facilitate the transfer of data from the SCALE analysis to the MELCOR model. As shown in Figure 3-10, the SCALE axial nodalization was simplified by combining 3 SCALE axial levels for each MELCOR axial level. The simplified MELCOR axial nodalization is typical of best practices for reactor transient analysis. The radial nodalization was also simplified for incorporation in MELCOR. SCALE Rings 1 and 2 were combined together and also Rings 6 and 7. The combined rings had much smaller volumes than

SCALE Rings 3, 4, and 5. Consequently, they were grouped to reduce the volume variations between rings while still retaining the calculated variations in the radial power distribution.

The relative powers from the SCALE analysis were combined into the various MELCOR regions and renormalized based on the fluid volume. The resultant axial and radial power distribution was used directly in MELCOR fluid fuel model. The SCALE analysis predicted a small fraction of the fission power occurred in the stringer inlet and exit zones, which was also included in the MELCOR model. The power profile is assumed to be fixed, which is consistent with a point kinetics modeling approach (see Section 3.6).

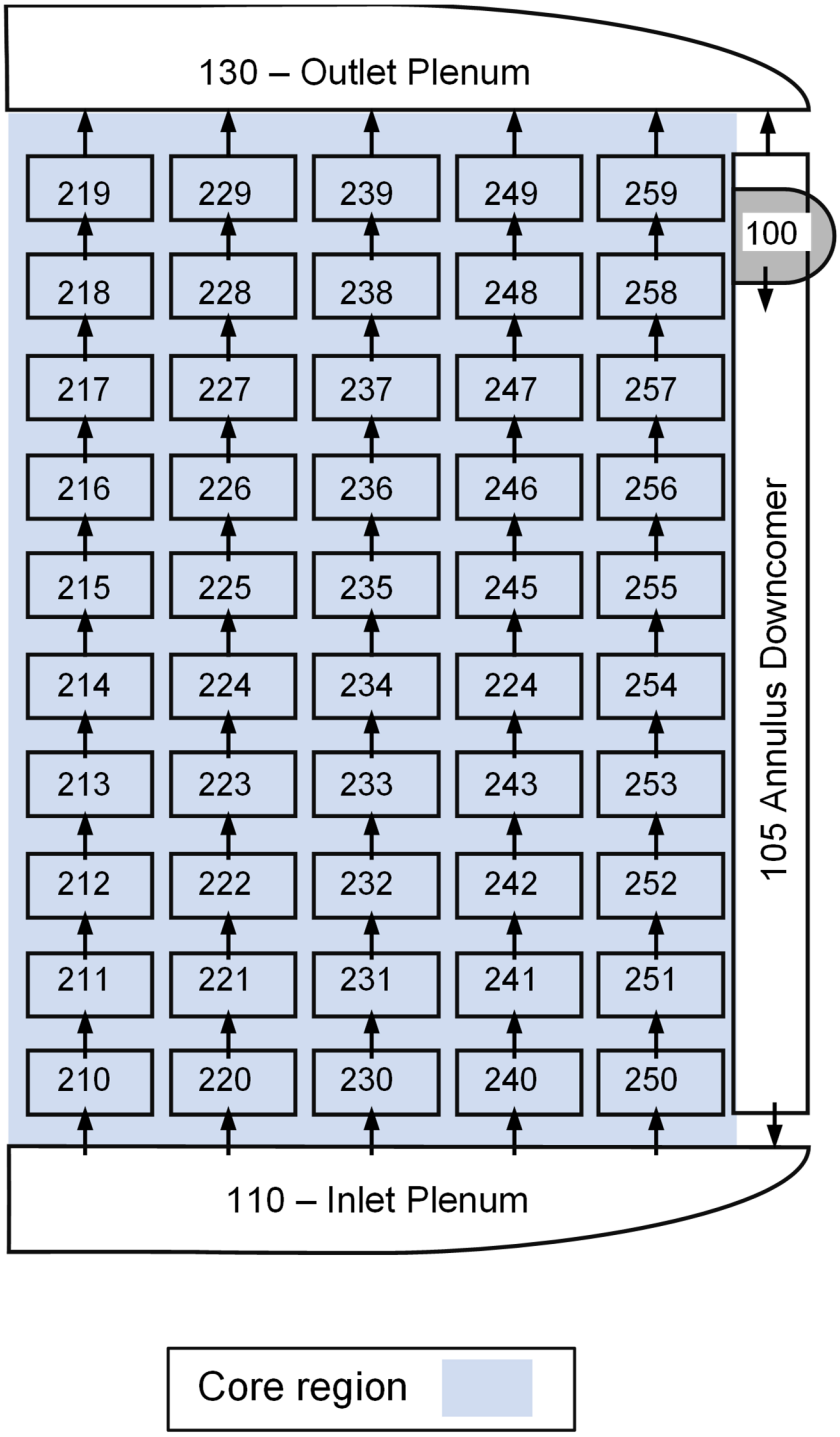

Figure 3-9 MSRE reactor vessel nodalization.[3]

[3] Modeled in cylindrical coordinates and showing from the center (left side) to the outside (right side) of the vessel. CV-210 to CV-219 are the center of the reactor and the highest power region.

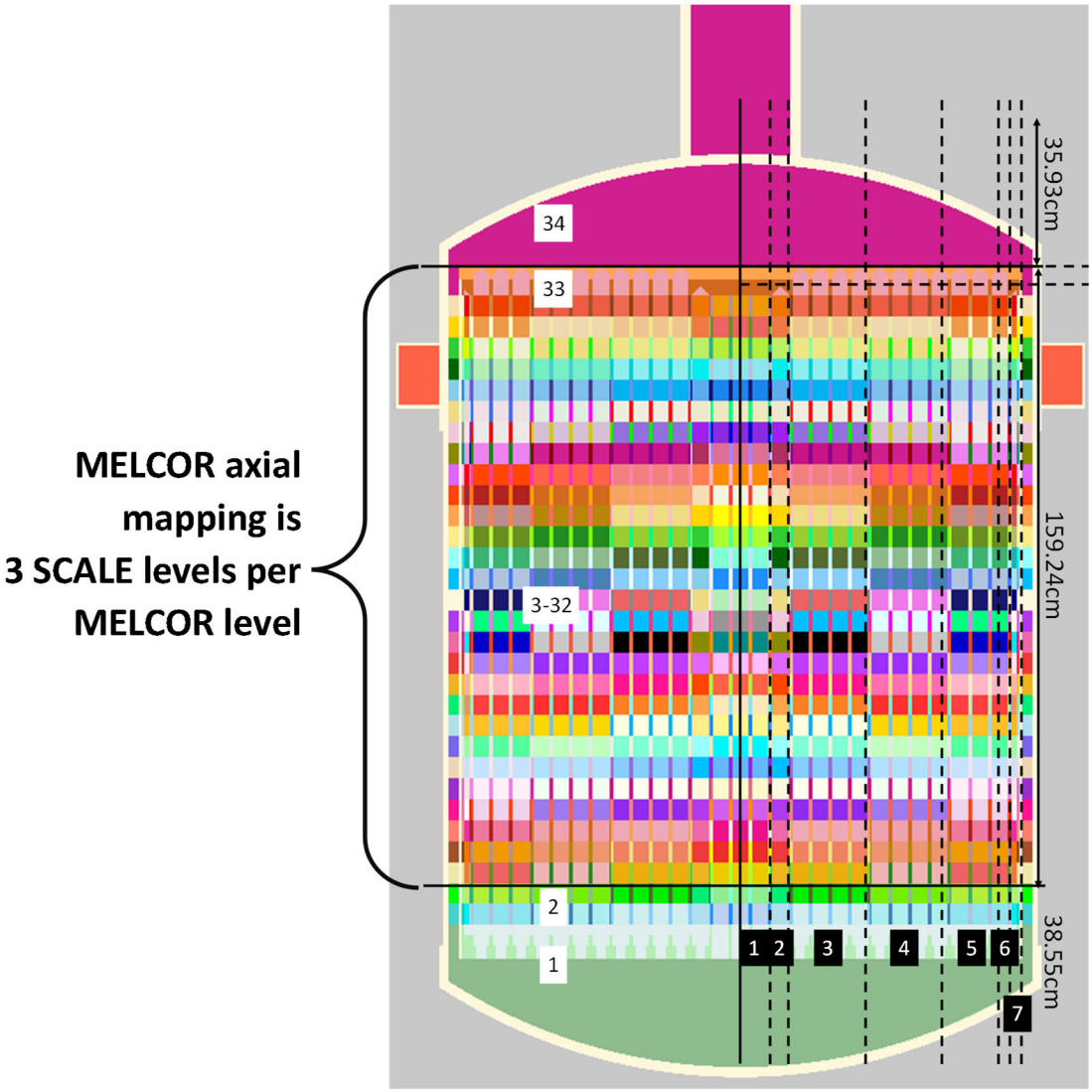

SCALE Radial Zone (r)	1 & 2	3	4	5	6 & 7
MELCOR Radial Zone (r)	1	2	3	4	5
Percent of stringers	3.5%	19.3%	35.3%	36.7%	5.2%

Figure 3-10 Mapping from the SCALE MSRE reactor vessel nodalization.

3.2.2. Primary and secondary system nodalization

The primary and secondary system nodalization is shown in Figure 3-11. As described in Section 3.1, the MSRE has a vertical hot leg (CV-300) leaving the reactor vessel into the pump bowl. The pump bowl includes the region with the pump impellor (CV-305) and an upper pool (CV-306). The fluid fuel exits the pump into a horizontal hot leg (CV-310) towards the secondary heat exchanger. The primary fluid flows through the shell side of the heat exchanger, which includes separate control volumes for the upper and lower portions (CV-320 and CV-321, respectively). The fluid fuel exits the heat exchanger into the cold leg (CV-330), which connects to the reactor vessel. The molten salt in the secondary side of the heat exchanger flows through the tube-side of the heat exchanger. The secondary heat exchanger inlet boundary conditions are specified in CV-400. The secondary tubes

are also split into the upper and lower portions of the heat exchanger (i.e., CV-401 and CV-402, respectively). The secondary fluid exits into CV-403. The heat transfer from the primary side of the heat exchanger to the secondary is calculated using a log-mean temperature difference with an effective heat transfer coefficient.

The right-hand side of Figure 3-11 shows the helium flows into the offgas system. There are 1279 liters per day helium purge flows that enter the overflow tank (CV-307) and around the pump shaft (CV-305). A larger 3456 liters per day purge flow is supplied to the vapor space in the pump bowl (CV-306). The helium flow exits into the offgas system (see Section 3.4).

Also shown on Figure 3-11 are two recirculation flows from the exit of the pump (CV-305). 3.15 liters/sec (50 gpm) of the pump exit flow is recirculated back into the pump bowl as a spray. The molten salt is sprayed into the pump bowl gas space. The spray is used to enhance separation of the noble gases created by the core fission process. A small portion of the flow (0.95 liters/sec or 15 gpm) is directed for cooling of the pump shaft.

Finally, the core fission power to the fluid fuel, the core and loop radionuclide decay heat power, and the direct graphite neutron heating are 8.86 MW, 0.47 MW, and 0.67 MW, respectively. The MELCOR calculation used the initial startup power of 10 MW.[4] The primary system flowrate is 75.7 liters/sec (1200 gpm) and the secondary flow rate is 63.6 liters/sec (850 gpm). The core inlet and outlet temperatures are 635 ^{o}C (1175 ^{o}F) and 663 ^{o}C (1226 ^{o}F), respectively.

[4] The MSRE had an initial startup power of 10 MW but subsequently run at 8 MW [16]. The MELCOR calculations used the design value of 10 MW.

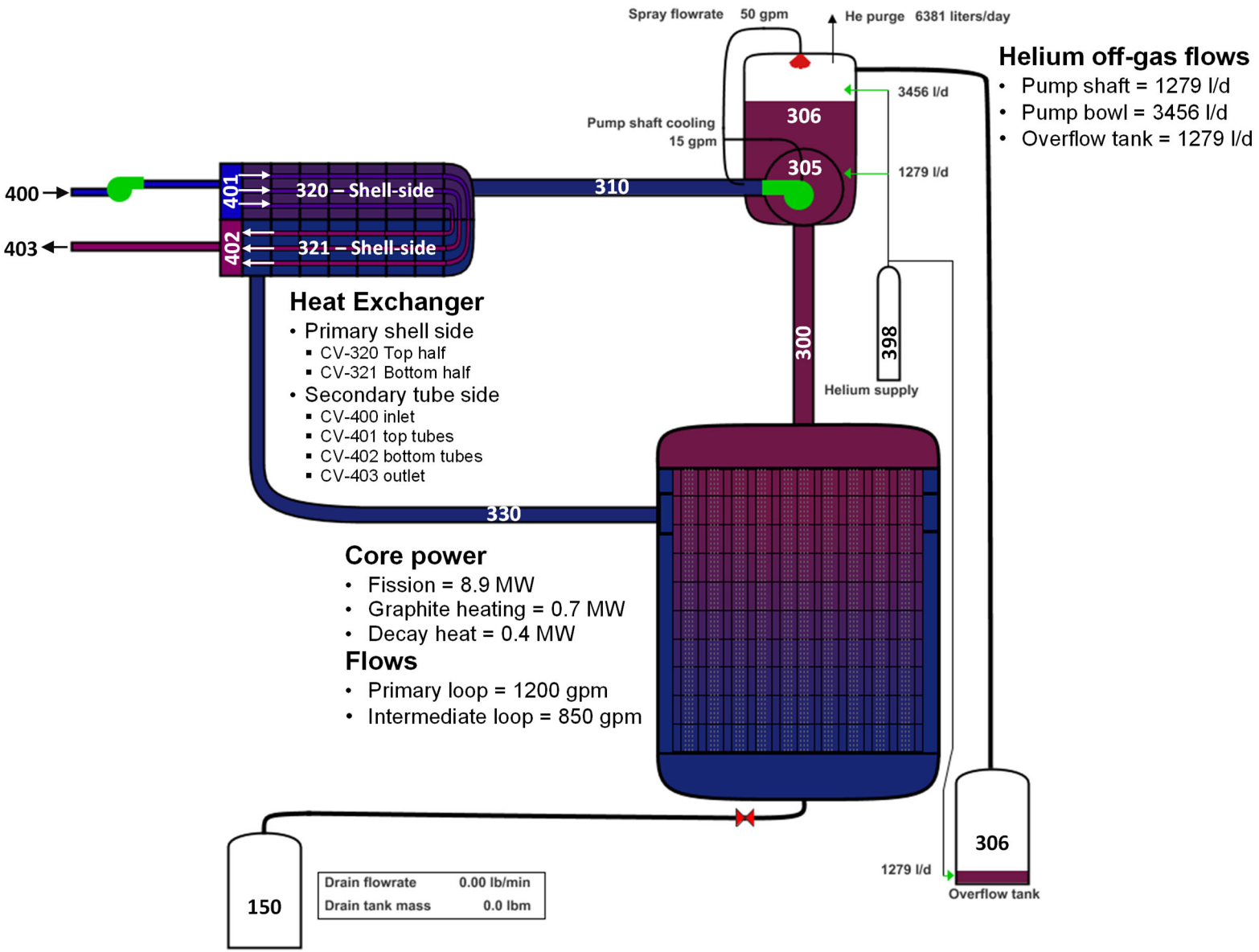

Figure 3-11 MSRE primary and secondary CVH and FL nodalization.

3.2.3. Reactor containment nodalization

The MSRE containment nodalization is shown in Figure 3-12. The scope of the containment includes the reactor cell (CV-510), the connected drain tank room (CV-515), the vent line from the reactor cell (CV-525), the piping to the vapor condensing tank (CV-530), the vapor condensing tank (CV-535), and the gas retention tank (CV-540). The containment is surrounded by a reactor building (CV-520). The reactor cell is normally isolated from the vapor condensing tank by two burst disks (FL-535 and FL-540). The burst disks open at a differential pressure of 103 kPa (15 psi) and 138 kPa (20 psi), respectively. The lower pressure burst disk is located on a smaller 10 cm (4") diameter line. If the reactor cell pressure continues to rise, then the higher pressure burst disk will open the larger 30 cm (12") line. The flow is directed via FL-545 to 1.83 m (6 ft) below the vapor condensing tank liquid surface. The submerged flow promotes quenching of any steam directed from the reactor cell. Any non-condensed gas leaving the surface of the water is retained in the gas space in the vapor condensing tank above the water level or the gas retention tank. The gas retention tank can be vented to the filters and the stack (FL-560). If the pressure in the reactor cell drops below the gas pressure in the vapor condensing tank, then a vacuum relief valve (FL-555) allows flow back to the reactor cell.

The nominal in-leakage from the reactor cell is known due to the metering from the vacuum pump that maintains a negative pressure in the reactor cell. The normal operating pressure is 87.6 kPa (-2 psig) with an inward leak rate of 11.8 liters/min (0.42 scfh). The effective leakage area is a 1.83 mm diameter hole. The reactor cell design pressure is 337 kPa (40 psig).

The reactor vessel and pump bowl are surrounded by thermal insulating structures called furnaces. The reactor vessel furnace (i.e., also called a thermal shield [5]) is modeled with a multi-material heat structure (HS-1601) representing the silica insulation, the carbon steel container, and the shield comprised of water and steel balls. The gas space inside the thermal shield is modeled with CV-160. The pump bowl thermal shield has a similar design but does not include the water and steel balls. The top (HS-3990) is covered with a fiber insulation and the sides and bottom (i.e., HS-3991 and HS-3992, respectively) are wrapped with a silica insulation. The interior heaters were not modeled.

The reactor cell is surrounded by the reactor building (i.e., Building 7503). In the safety analysis, it is assumed the building leaks at 10% volume per day [8]. The building design over-pressure was not known but assumed to be +1.72 kPa (+0.25 psig). Based on the 10% per day leak rate and the assumed building design over-pressure, the effective leakage areas from the building was estimated and is modeled as two 1.4 cm diameter leakage paths to the environment.

The reactor building leakage paths are assumed to be located at low and high locations on the reactor building outer wall. When there is an external wind, one flow path is assigned to the upwind side of the building and the other is on the downwind side. The guidance for modeling building wind effects with MELCOR is described in Reference [17]. External wind effects are included in DOE facility safety analyses where there are not strong driving forces for fission product release. The wind increases the building infiltration and exfiltration rates. Both an upwind infiltration location and a downwind location were included in the model. The wind effects are modeled as an additional Bernoulli pressure term in the flow path pressure solution,

[5] There are electrical heaters between the thermal shield and the vessel that can be operated to prevent freezing. The furnace designation is most applicable when the electrical heaters are operating to prevent freezing of the molten salt. The thermal shield function limits the heat loss from the reactor and reduces the neutron flux outside the vessel.

$$dP_{Wind} = \frac{1}{2}\rho C_p v^2$$

where,

dP_{Wind}	Bernoulli wind pressure term, (Pa)
ρ	Fluid density, (kg/m^3)
C_p	Building coefficient, (-)
v	Wind velocity, (m/s)

The values for building coefficients are typically obtained using computational fluid dynamics evaluations. When wind effects are modeled in the MELCOR MSRE demonstration calculations, generic values were obtained from the American Society of Heating, Refrigerating and Air-Conditioning Engineers (ASHRAE) handbook (see Table 3-3 [18]).

Table 3-3 Typical building coefficients [18].

Wind Direction	Value
Upwind	0.7
Downwind	-0.4
Side and top of the building	-0.35

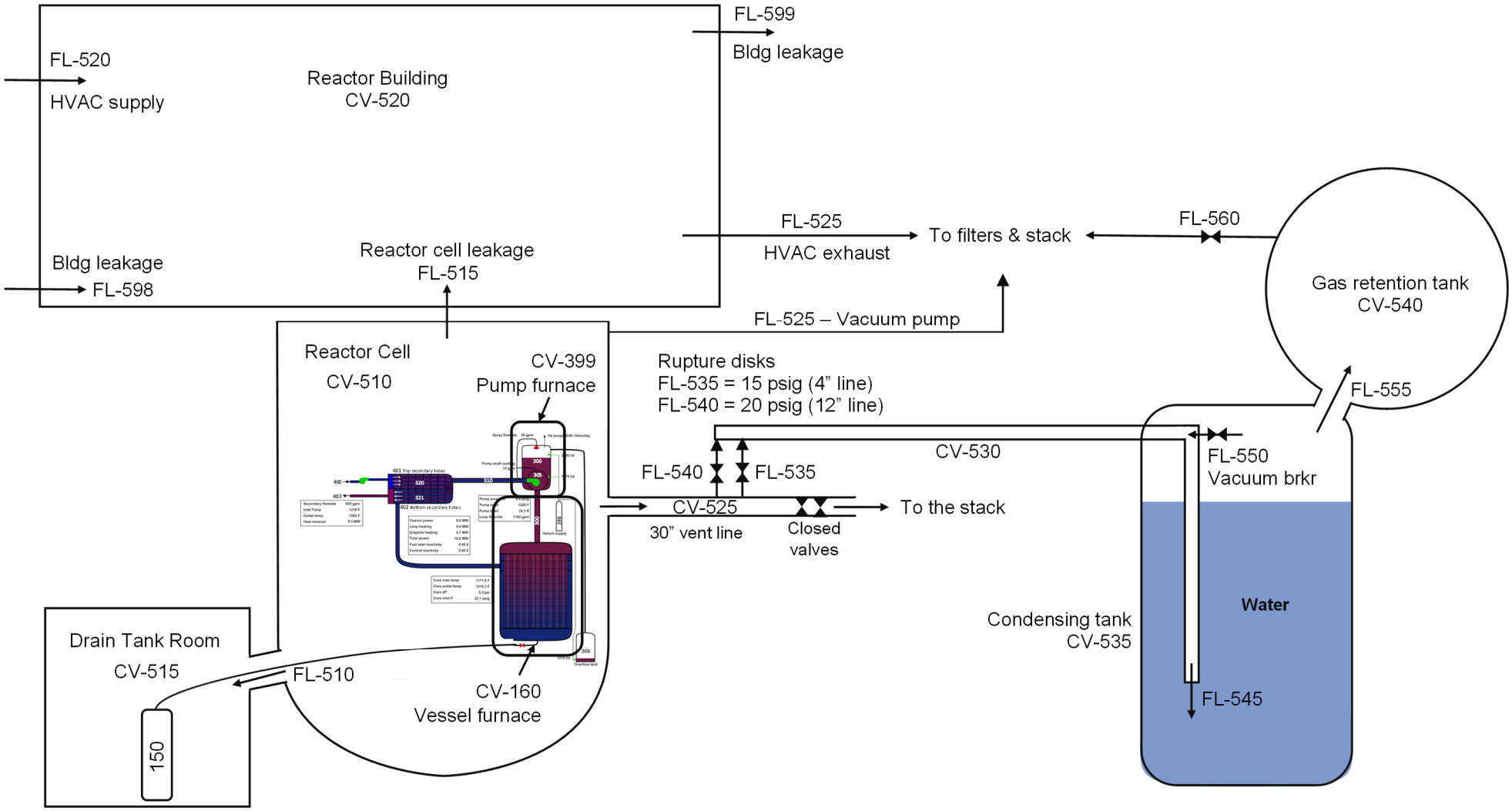

Figure 3-12 MSRE reactor containment and reactor building CVH and FL nodalization.

3.3. MSRE offgas system

The MSRE uses an offgas system to filter radionuclide releases. The MELCOR offgas nodalization (see Figure 3-13) includes two parts, one connected to the pump bowl and another pathway connected to the reactor cell. The offgas system from the pump bowl includes the hold-up volume inside the reactor cell (CV-600) and the holdup volume region (CV-605) between the reactor cell to the two charcoal filter trains. A 1.2 m (4-ft) section of the piping after the reactor cell is cooled by an external gas flow of 0.236 m^3/s (500 scfm), which is modeled with CV-601 and the two connecting flowpaths. The two charcoal beds (CV-610 and CV-615) include segments with successively increasing diameter pipes (i.e., 3.8 cm, 7.6 cm, and 15.2 cm diameter). Each charcoal filter train holds 658 kg of charcoal, which is included in the charcoal filter model for the thermal response. The filter is assumed to retain gaseous iodine with a decontamination factor of 100 (i.e., 99% efficiency). The outside of the charcoal filter train is immersed in water, which was modeled with a specified heat transfer coefficient corresponding to boiling water.

The two filter trains exit into a connecting pipe to the filter inlet plenum. The filter offgas flow mixes with the 9.9 m^3/s (21,000 cfm) reactor building ventilation system flow. The flow from the plenum passes through roughing and absolute filters before entering the exhaust fan that flows to the plant stack. The roughing filter is specified to filter dust and large aerosols before they reach the absolute filter. There are three 32 m^2 roughing filters, which are 90-95% efficient. It was assumed that the roughing filters remove 92.5% of the aerosols greater than 25 microns. There are three 2.23 m^2 absolute filters with a 99.97% efficiency for particles larger than 0.3 micron [7]. It was assumed that aerosols smaller than 0.3 micron passed through the filter. The exhaust fan draws the flow through the filters and discharges to the 30.5 m (100-ft) plant stack. Any radionuclides from the offgas flow are diluted by the building ventilation flow (9.9 m^3/s or 21,000 cfm).

If the reactor cell becomes contaminated, the auxiliary charcoal is used to filter the airspace at 1.7 m^3/hr (1 cfm). The auxiliary filter flowpath is manually operated when needed. The auxiliary charcoal bed holds 240 kg of charcoal. The auxiliary charcoal bed flow connects to the filter pit with the other flow streams. Similar to the primary offgas charcoal filters, the auxiliary filter is assumed to only retain gaseous iodine with a decontamination factor of 100.

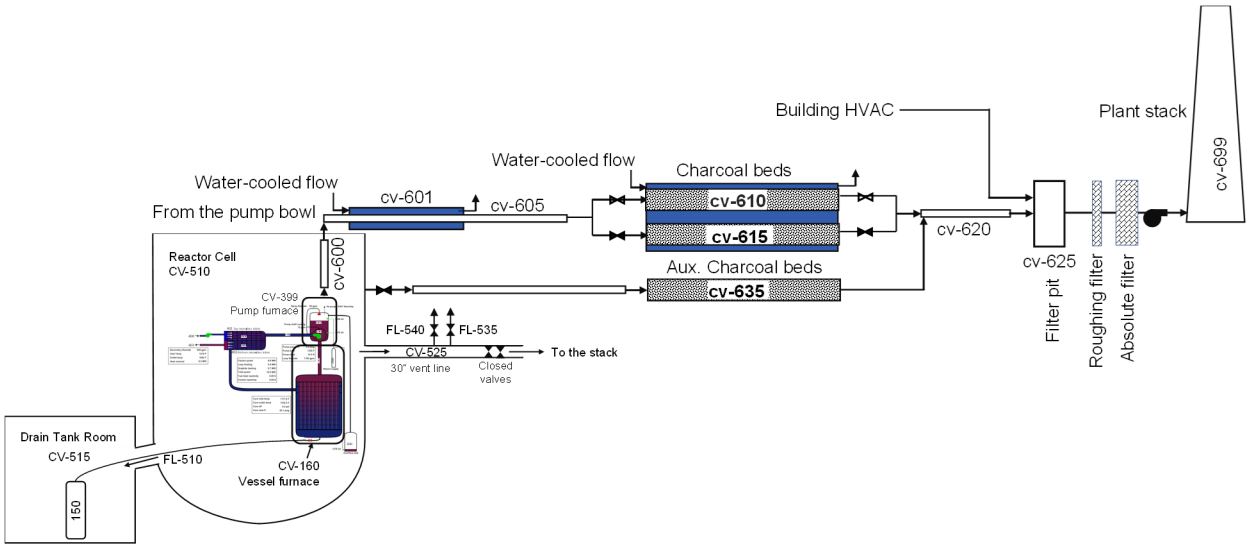

Figure 3-13 MSRE offgas nodalization.

3.4. Radionuclide inventory and decay heat input

The MELCOR default radionuclide class assignments were established for light water reactors by combining elements with similar vapor pressures and chemical behaviors. For molten salt reactor applications, some adjustments are warranted to better reflect observed behavior in the MSRE. In particular, ORNL has done some work to align elements based on their solubility in molten salt and map it to the periodic chart. Most notably, the noble metals were observed to be insoluble and susceptible to plating out on structures in the loop. Figure 3-14 shows the assignment of many elements according to their solubilities. Through collaboration with SCALE team, Table 3-4 shows the resulting element assignments.

The basic structure of the default MELCOR radionuclide classes were maintained with a few reassignments to be consistent with the insights from Reference [19]. In particular, only the insoluble elements identified in Figure 3-14 were included into the Mo radionuclide class, which included Mo, Ru, Pd, Ag, Ge, Sn, As, and Sb. The elements in the Mo class not identified as insoluble on Figure 3-14 were removed and reassigned into a new radionuclide class, which is identified as the V class for Vanadium. Since Ru was moved to the Mo class, the default class previously named Ru was changed to the Re class for rhenium.

The always soluble elements from Figure 3-14 were consolidated into the Cs, I2, and Hg classes. This included formation of the Hg[6] class. Some of the elements in the default Cs and I2 classes were not defined as soluble in Figure 3-14. However, they were retained in the Cs and I2 classes based on their chemical similarity. Finally, all the elements identified as sometimes soluble elements in Figure 3-14 were consolidated in the new Nb class, which included Nb, Zn, Cd, Se, and Te.

In summary, the 12 default LWR radionuclide classes in MELCOR were expanded to 15 classes for the MSRE using insights from Reference [19]. Where the solubility characteristics were known, the elements were grouped together. The new groupings consolidated the insoluble elements into the

[6] Hg was combined with the always soluble Ga and In elements based on a recommendation from ORNL, although not specifically classified on Figure 3-14. The inventory of Hg was larger than Ga and In, so Hg was assigned as the representative element and the class name.

Mo class; the soluble elements were consolidated into the Cs, I2, and Hg classes, which also included some elements with chemical similarity from the LWR default classes; and the sometimes soluble elements were consolidated into the Nb class. The other elements remained in their default classes. However, the movement of the representative element into one of the new classes based on solubility led to new class names based on new representative elements assignments (i.e., S, Re, and V). Finally, the I_2 group simulated the airborne transport of iodine, which represents 5% of the iodine inventory. The other 95% of the iodine inventory is assumed to combined with a portion of the cesium inventory to form cesium iodide aerosols. The remaining cesium combines with cesium fluoride.

The radionuclide inventory and decay heat inputs were calculated using the ORIGEN module of SCALE [16]. The ORIGEN analysis developed the burn-up that approximated the 375 days of continuous refueling of the MSRE. The data provided from SCALE includes separate decay heat curves for each radionuclide class in Table 3-4. In addition, ORNL provided masses and decay heat curves at all 9 locations shown in Figure 2-1, whereas fixed fuel reactors applications would have masses and curves for one location (i.e., the core). The variations in the specific inventory (kg per m^3 of molten salt) at the 9 locations could be significant for some nuclides (e.g., I-137 with a half-life similar to the MSRE loop transient time). However, MELCOR lumps many nuclides and elements into each radionuclide class. A comparison of the various radionuclide class (i.e., the groupings in Table 3-4) results showed relatively small differences in the specific radionuclide decay heats (W/kg) and mass concentration (kg per m^3 of molten salt) across the 9 regions. Consequently, it is a reasonable assumption[7] to use the average system radionuclide class decay heat tables. The radionuclide class inventories are shown in Table 3-5, and the overall decay heat power is shown in Figure 3-15.

The SCALE analysis considered deposition of insoluble and sometimes soluble radionuclides onto surfaces in the primary circuit during the 375-day simulation. Using the observed deposition rates for the MSRE from Reference [20], the total deposition of the insoluble and sometimes soluble radionuclides metals after 375-days was determined. Reference [20] also provides the locations where the radionuclides deposited, which is shown in Table 3-6. The deposited radionuclides included contributions from the Mo and the Nb radionuclide classes (see Table 3-4). The Nb radionuclide class includes elements that are sometimes soluble. The Mo radionuclide class includes insoluble elements (i.e., primarily noble metals). Since the deposited radionuclides continue to decay after deposition, their decay heat was included in the MELCOR MSRE model. The SCALE analysis accounted for the subsequent daughtering and time-dependent deposition effects (e.g., varying time away from the fission source after depositing). The heat source is applied to the surface of the primary system heat structures according to the distribution in Table 3-6.

ORNL also estimated on the continuous removal of noble gases into the offgas system [16]. An important decay chain in the offgas system is Xe-135, which decays to Cs-135 with a 9.2 hr half-life.[7] Using SCALE for the radionuclide decay and the offgas flowrate, ORNL provided the offgas inventory and the associated decay heat in the offgas system prior to the charcoal filters. The MELCOR MSRE model was initialized with the specified radionuclide masses (i.e., including Cs-135) and their decay heat.

---

[7] A companion report on non-LWR reactor modeling is planned, which will summarize the lessons learned during the non-LWR demonstration calculations. There is ongoing work to incorporate models from SCALE into MELCOR, which will allow decay chain tracking. The report will identify that traditional modeling was reasonable for the MSRE primary loop but more detailed modeling is needed for some nuclides in the offgas system.

Table 3-4 MELCOR radionuclide classes

Class Name	Representative Element	Member Elements
Xe	Xe	He, Ne, Ar, Kr, Xe, Rn, H, N
Cs	Cs	Li, Na, K, Rb, Cs, Fr, Cu
Ba	Ba	Be, Mg, Ca, Sr, Ba, Ra, Es
I2	I	F, Cl, Br, I, At
S	S	S, Po
Re	Re	Re, Os, Ir, Pt, Au, Ni
V	V	V, Cr, Mn, Fe, Co, Ta, W
Mo	Mo	Mo, Tc, Ru, Rh, Pd, Ag, Ge, As, Sn, Sb
Nb	Nb	Nb, Zn, Cd, Se, Te
Ce	Ce	Ti, Zr, Hf, Ce, Th, Pa, Np, Pu, C
La	La	Al, Sc, Y, La, Ac, Pr, Nd, Pm, Sm, Eu, Gd, Tb, Dy, Ho, Er, Tm, Yb, Lu, Am, Cm, Bk, Cf
U	U	U
Hg	Hg	Hg, Ga, In
Pb	Pb	Pb, Tl, Bi
B	B	B, Si, P
CsI	CsI	CsI

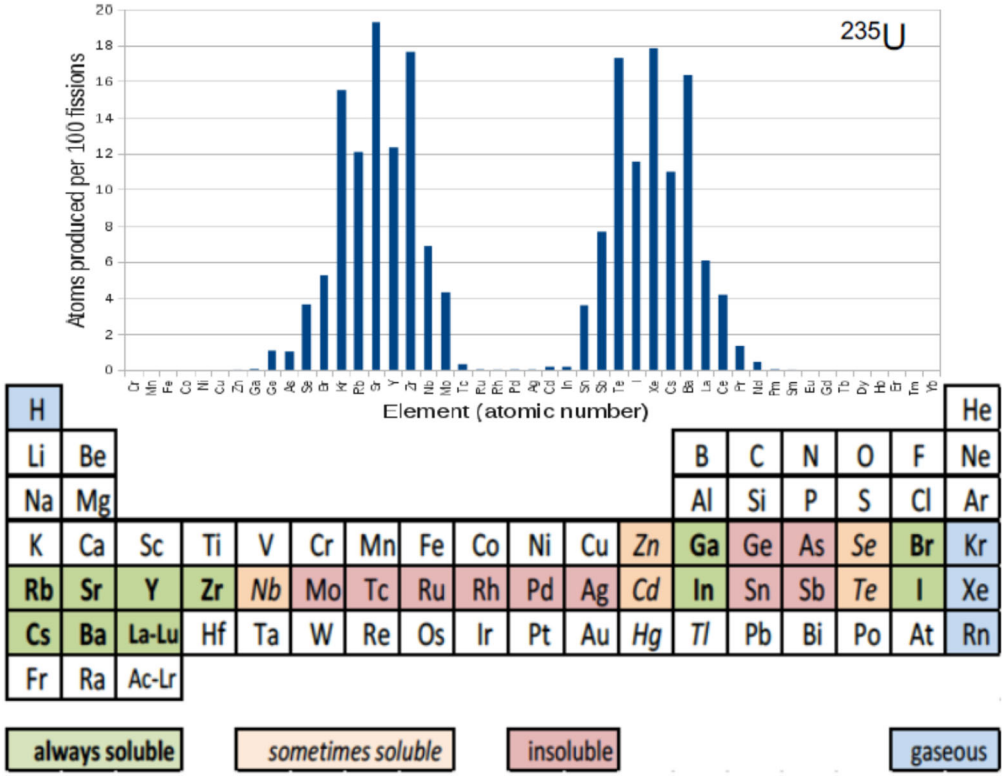

Figure 3-14 Identification of element solubility in molten salt [19].

Table 3-5 MSRE radionuclide class masses.

MELCOR RN class	MELCOR Class Mass (kg)
XE	2.8537E-04
CS	1.7449E-01
BA	2.3628E-01
I2	1.4509E-05
S	9.3574E-17
RE	6.6738E-12
V	1.5726E-16
MO	2.5702E-03
NB	1.5670E-04
CE	5.4295E+02
LA	7.0837E-01
U	2.1546E+02
HG	1.9337E-05
PB	8.5349E-13
B	0.0000E+00
CSI	5.6438E-04

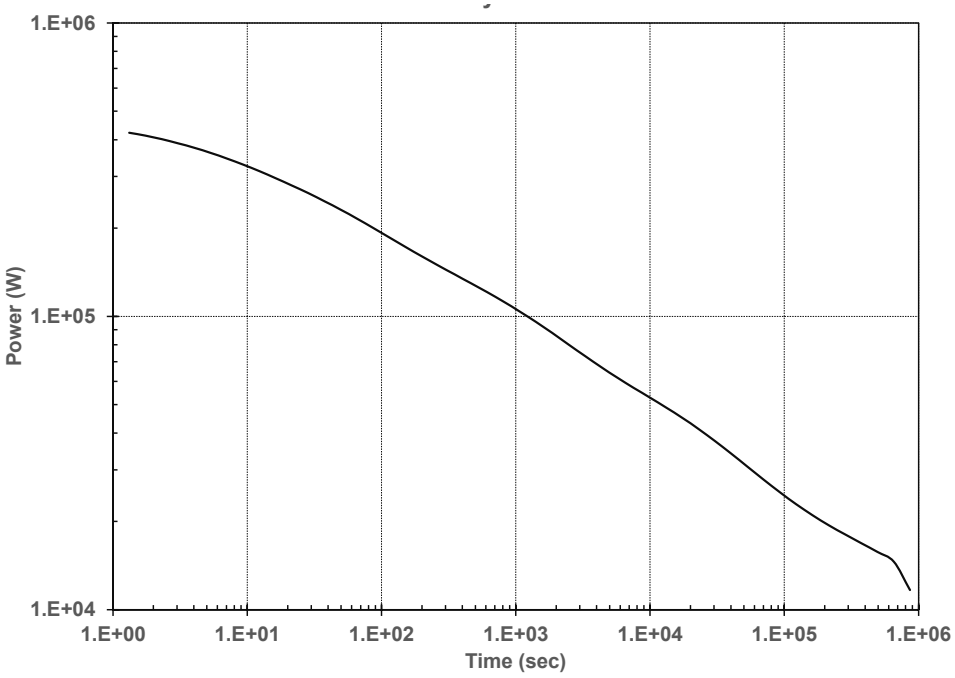

Figure 3-15 MSRE decay heat curve.

Table 3-6 MSRE noble metal deposition locations [20].

Location	Percentage
Heat exchanger	40%
Loop	50%
Pump bowl, overflow, offgas	9%
Core graphite	1%

3.5. Fission product release from the molten salt

The MSRE demonstration calculations are based on a leak in the drain piping between the bottom of the vessel and the connecting drain tank (see Figure 3-6). The salt spill scenario includes a complete spill of all the fluid fuel onto the reactor cell floor. The molten fuel salt is very effective at retaining both the soluble and insoluble radionuclides. However, a few radionuclide release mechanisms are hypothesized. For example, the more volatile radionuclides can vaporize from the fluid surface. The vaporization potential is a function of the radionuclide vapor pressure with consideration of the radionuclide's solubility. As discussed in Section 2.4, the thermodynamic database for radionuclides in molten salt is very limited. However, the potential for Cs and CsF vaporization was included in the calculations. The Cs and CsF vaporization turned out to be negligible due to the relatively low fluid fuel temperature of the spilled salt.

Other methods of radionuclide release could occur from hydrodynamic aerosol generation due to splashing, spray gas entrainment, and bubble bursting. The GRTR model was still being developed at the time of the analyses and the hydrodynamic aerosol generation models were not completed. The hydrodynamic aerosol generation models will be location-specific to capture effects from spills, sprays, and bubble bursting. For example, a molten salt spill could spray and breakup due to gas entrainment, which generates droplets and aerosols (e.g., see the DOE handbook [21] for experiments characterizing aerosol generation in spills). The noble gas release at the surface of the spill may create bursting bubbles (e.g., the MSRE observed a large foam and mist formation in the pump bowl when U-233 fuel[8] was used [20]). In lieu of the pending GRTR aerosol generation models, the salt spill demonstration calculation used the radionuclide release fractions from the MSRE safety analysis [8], which is discussed further in Section 4.2.

A companion report on non-LWR reactor modeling is planned, which will summarize the lessons learned during the non-LWR demonstration calculations. It will identify ongoing or recommended work to improve non-LWR modeling and the prediction of the non-LWR source term. The new GRTR aerosol generation models and alternate radionuclide vaporization models will be identified in the report.

3.6. Point kinetics modeling

MELCOR includes a point kinetics fluid fuel model for the dynamic calculation of the reactor power. The model was developed to support the evaluation of the MSRs (see Section 2.2). ORNL determined the reactivity feedbacks for the MSRE using SCALE. Separate temperature feedbacks were determined for the fluid fuel and the graphite stringer reflectors (see Figure 3-16). The

[8] The mist suggests mechanisms for aerosol formation from gas bubbles (e.g., noble gases) bursting at the liquid surface. However, the formation of the foam is not completely understood. The MSRE demonstration analysis assumed the performance attributes of the U-235 fuel, which did not have significant foam and mist generation.

feedbacks were incorporated into the MELCOR MSRE fluid fuel point kinetics model. As described in Section 2.2, a void feedback was added to terminate the fission power when liquid fuel did not exist in the core. The void feedback was not quantified in SCALE. It was simply a logical modeling constraint to stop fission when the core voids.

Determined reactivity coefficients by temperature/density perturbation:

- Calculated reactivity at multiple temperature/density points
- Fitted reactivity
- Determined reactivity coefficient as derivative of fitted curve

Component	Fresh core	375 days
β_{eff} [pcm]	704 ± 14	697 ± 22
Graphite temperature reactivity coefficient [pcm/K]	-5.13 ± 0.05	-4.83 ± 0.07
Fuel salt temperature *and density* reactivity coefficient [pcm/K]	-8.27 ± 0.12	-8.28 ± 0.12

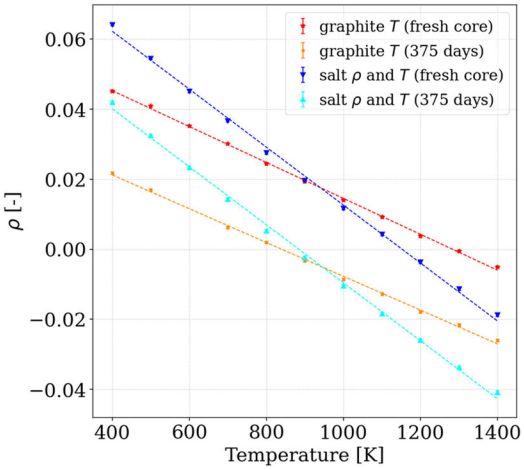

Figure 3-16 MSRE reactivity feedback curves [9].

3.7. Steady state initialization

The MSRE model was stabilized to steady state conditions that were provided in Reference [7]. Figure 3-17 through Figure 3-23 show the comparison to key steady state variables from Reference [7]. The steady state values from Reference [7] are labeled "MSRE" in Figure 3-17 through Figure 3-23. The model was started at stagnant conditions to avoid startup convergence issues with slightly mismatched initial conditions. Nevertheless, the primary and secondary pumps quickly stabilized the flows to the rated values (see Figure 3-17). A simple pump with a proportional-integral controller was used to establish a primary system flow of 0.07571 m^3/s (1200 gpm). A time-specified velocity boundary condition was used to establish a secondary flow of 0.05363 m^3/s (850 gpm).

The circulating molten fuel salt energy balance is shown in Figure 3-18. The rated power is 10 MW, which is the sum of the fluid fission power (8.86 MW), the heat flow back to the circulating fuel fluid due to neutron heating of the graphite stringers (0.67 MW), and the decay heat from the radionuclides in the fluid (0.47 MW). The heat flow from the graphite stringers initially oscillates until the stringer temperature profile is established from the direct neutron heating (see Figure 3-19). The long-term response shows a balance between the energy addition from the neutron heating to the heat flow from the graphite back into the molten fuel fluid. The primary side heat transfer to the secondary also oscillates initially but converges to 10 MW, which is the net primary system heat addition.

The core inlet and outlet temperatures are shown in Figure 3-20. The core inlet temperature is controlled to the desired temperature by a proportional-integral controller on the heat exchanger heat transfer. The core inlet temperature is 635 °C (1175 °F). The calculated core outlet temperature

is 663 °C (1225 °F), which is in good agreement with the value reported in Reference [7]. The good agreement with the outlet temperature shows a good prediction of the fluid fuel thermophysical properties, the net heat addition, and the core flow rate.

The system pressure in the vapor spaces above the molten salt was reported in Reference [7] to be near atmospheric pressure. In the MELCOR model, the system pressure was assumed to be at a 34.5 kPa (5 psig) overpressure. The system pressure (Figure 3-21) was controlled via a valve on the off-gas flow. The helium supply system injects a total of 6000 liters/day into the pump bowl, the pump shaft, and the overflow tank. Once the system pressure is balanced, the offgas flow stabilizes to 6000 liters/day (see Figure 3-22).

Finally, the molten salt inlet and outlet temperatures into the secondary side of the primary heat exchanger are shown in Figure 3-23. The inlet temperature is specified to the reference value of 552 °C (1025 °F). The calculated outlet temperature is 511 °C (1096 °F), which is 2.2 °C (4 °F) below the value in Reference [7]. Since the secondary flowrate (Figure 3-17), the secondary inlet temperature (Figure 3-23), and the energy transfer to the secondary (Figure 3-18) matched the reference values, the thermal-physical properties of the secondary side fluid may be slightly different than the ones used in Reference [7], or the reported value was rounded up. The MELCOR model used the same thermophysical properties for the primary fuel fluid and the secondary molten salt. Nevertheless, the agreement was reasonably close and not expected to impact the results.

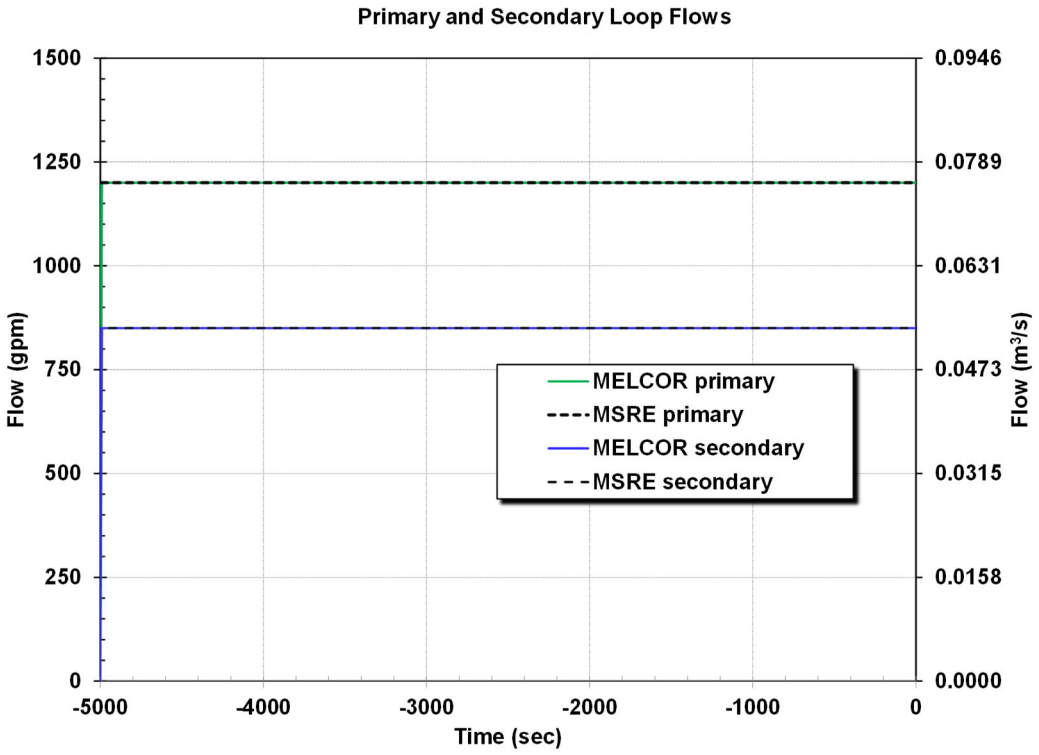

Figure 3-17 Steady state primary and secondary system core flows.

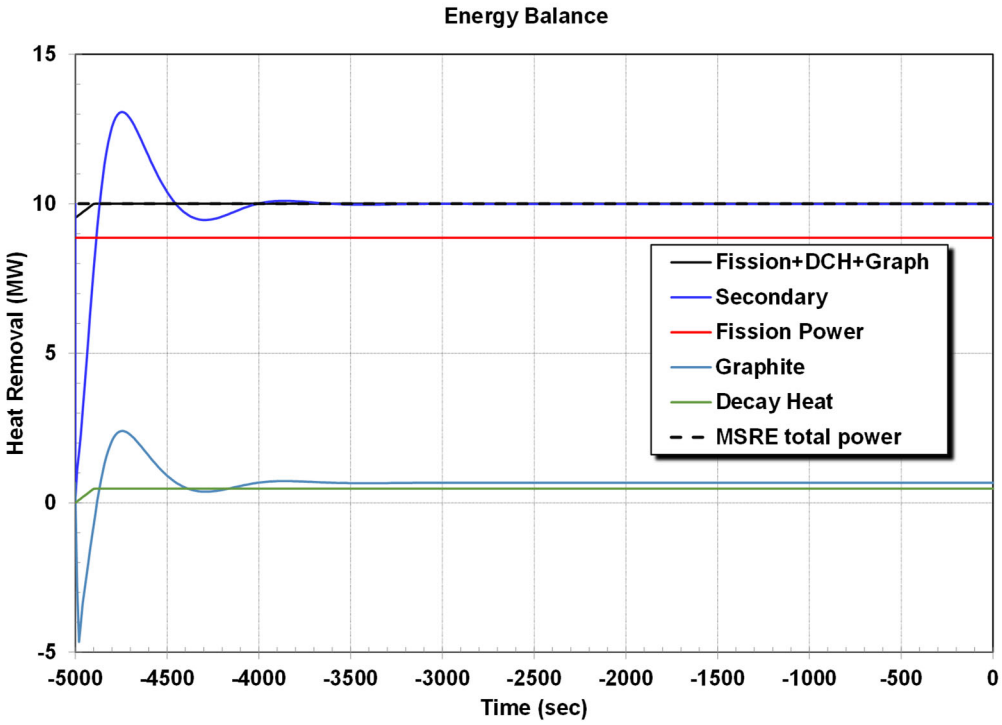

Figure 3-18 Circulating molten fuel salt energy balance.

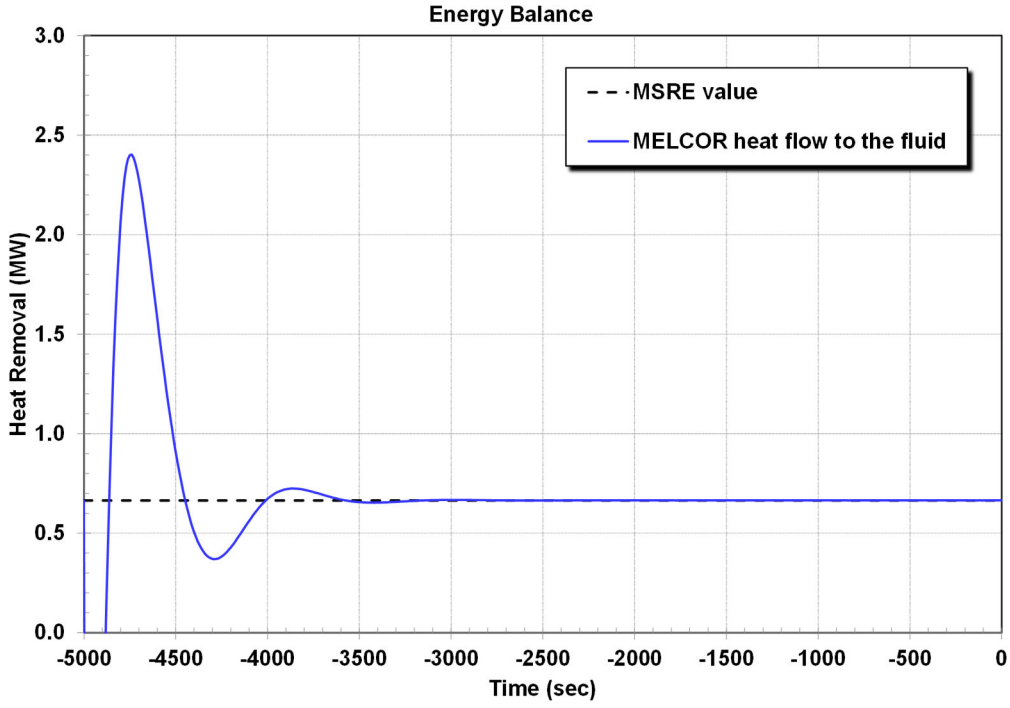

Figure 3-19 Heat flow from the graphite stringers to the molten fuel salt.

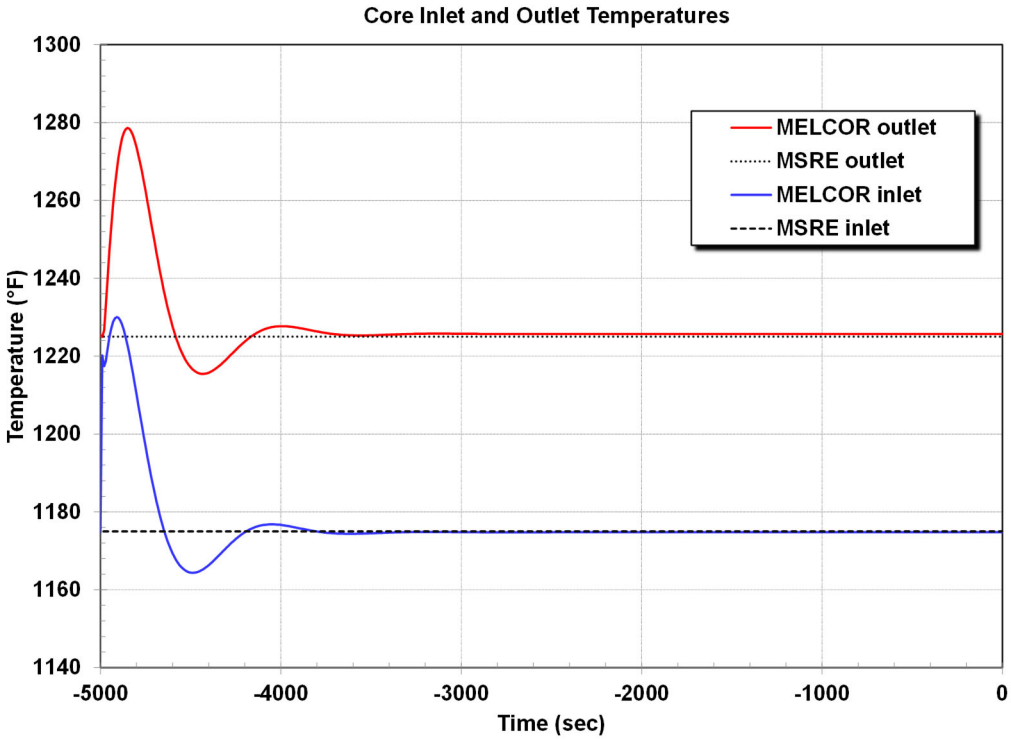

Figure 3-20 Steady state hot leg and cold leg temperatures.

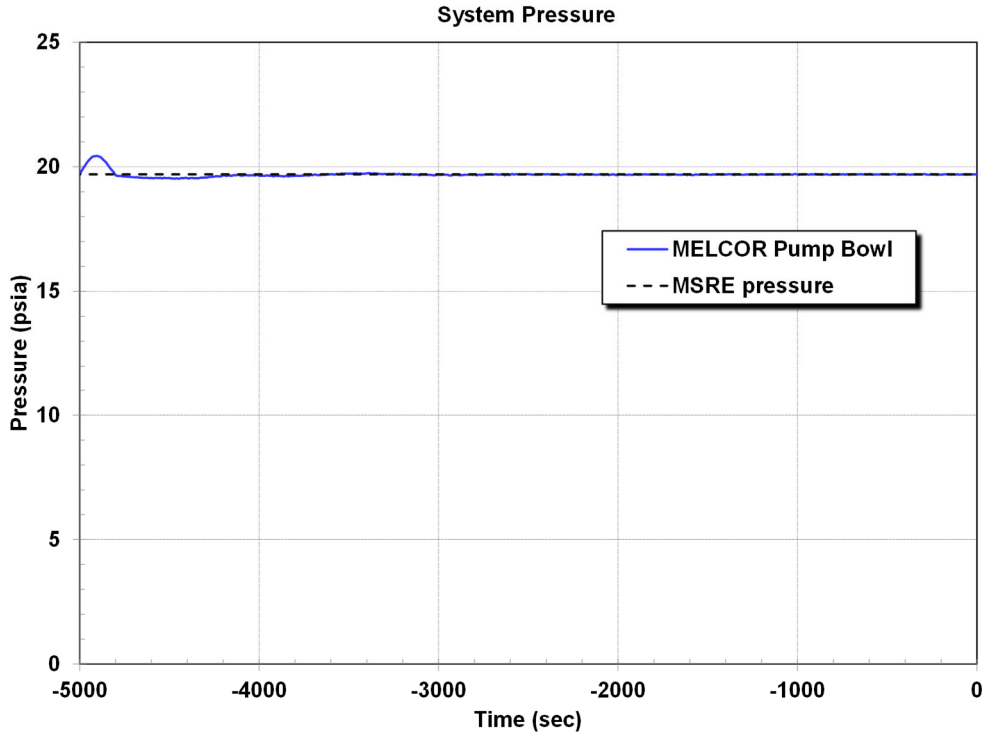

Figure 3-21 Steady state pump bowl pressure.

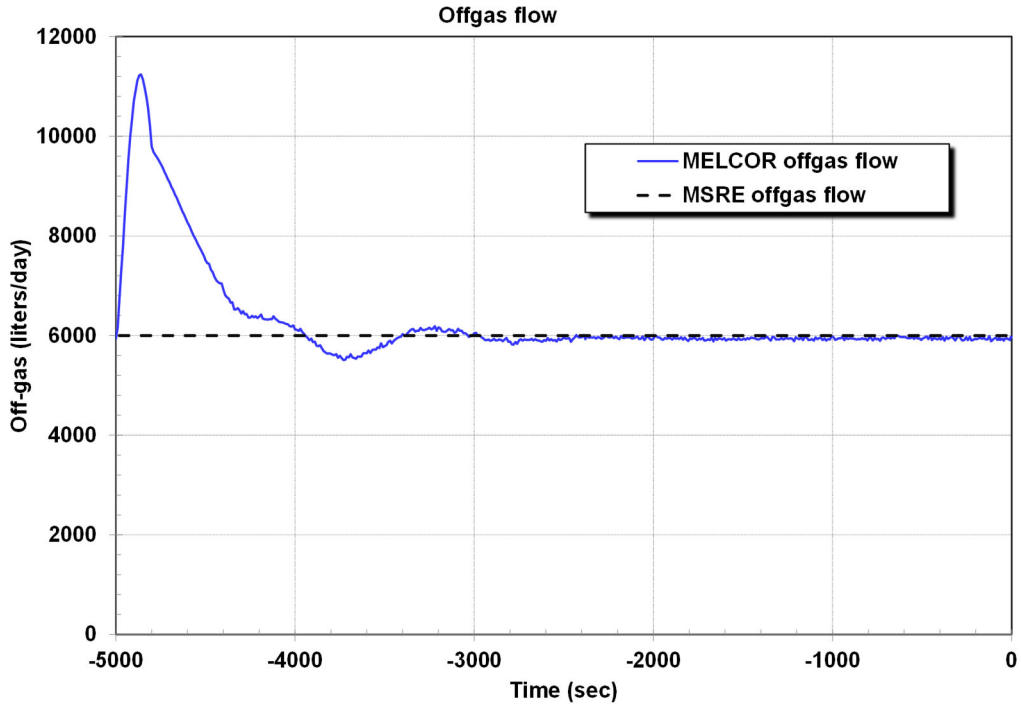

Figure 3-22 Steady state offgas flowrate.

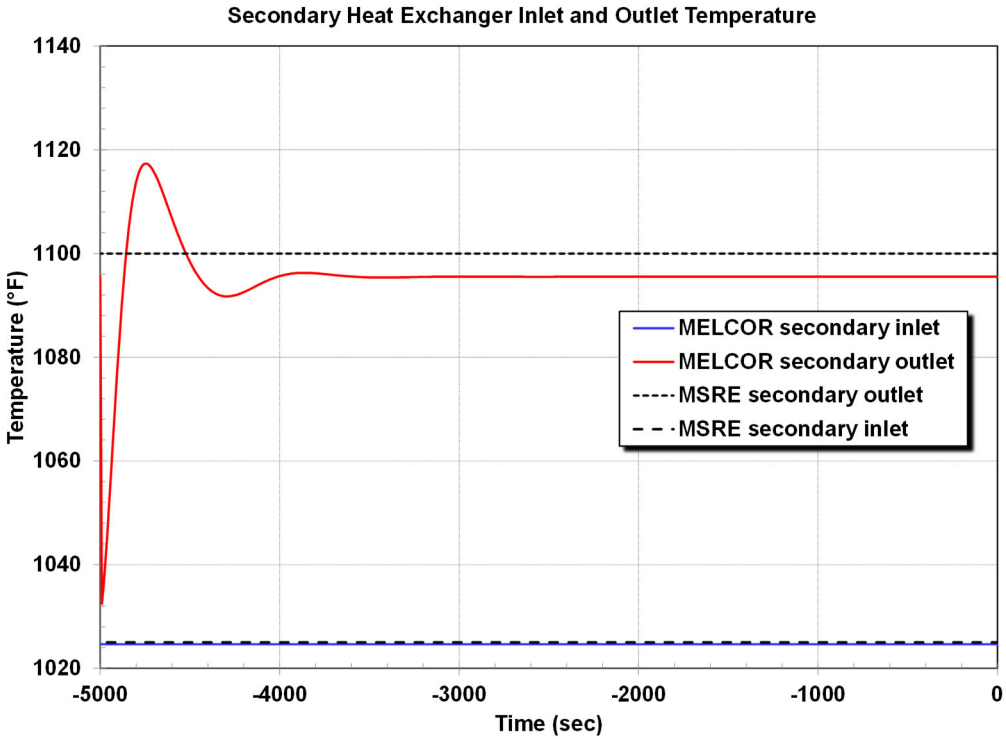

Figure 3-23 Steady state secondary-side inlet and outlet temperatures.

4. EXAMPLE RESULTS

The MSRE demonstration calculation was a molten salt spill into the reactor cell. Two variations of the MSRE model were used to simulate the molten fuel salt spill. The full MSRE model described in Section 3 with molten fuel salt was used to simulate the initial spill into the reactor cell (i.e., the first MSRE model). The second MSRE model focused on the ex-vessel radionuclide transport and release and included the effects from a coincident water spill with the molten fuel salt into the reactor cell.

The transient was initiated in the first model with a break in the fuel drain pipe at the bottom of the reactor vessel. The molten salt drained from the vessel and the recirculation loop onto the reactor cell floor. The first hour of the transient was simulated using the first model, which included draining all the molten fuel salt from the primary system and the associated reactor cell response. The salt spill accident progression is described in Section 4.1.

The long-term source term response was modeled using the containment (Sections 3.2.3) and the offgas portions of the input model nodalization (Sections 3.3). The modeling approach for the long-term model (i.e., the second model) is described in Section 4.2. The long-term response model results included two basic sequence variations: a salt spill, and a salt spill with a coincident water spill. The results from the long-term molten salt spill sequences without a coincident water spill are presented in Section 4.3 and the results of the salt spill with a coincident water spill are described in Section 4.4. Finally, some sensitivity calculations were performed with varying the reactor cell and the reactor building leakage rates with an external wind, which are described in Section 4.5.

4.1. Molten fuel salt spill results

The full MSRE model was used to simulate the molten salt spill into the reactor cell. The sequence is initiated with an event (e.g., seismic) that causes a loss-of-onsite power and a break in the drain pipe at the bottom of the reactor vessel. The salt pump trips offline with the loss of power and the control rods enter the core to terminate the fission reaction. All the molten fuel salt from the vessel and the primary system spills into the reactor cell. As shown in Figure 4-1, approximately 3860 kg (8500 lbm) of molten fuel salt drains into the reactor cell. The peak bulk temperature of the spilled salt reached 635 °C (1175 °F) by 4 minutes but gradually cooled to 582 °C (1080 °F) by 60 minutes. Figure 4-2 compares the normal molten fuel salt inventory to 10 minutes after the start of the spill.

The spill rate slows as the reactor cell pressurizes due to heating (Figure 4-3) and the hydrostatic head of the molten salt in the vessel decreases. The reactor cell pressure initially rises from -13.7 kPa (-2 psig) to +43 kPa (+6.3 psig) but slowly depressurizes.[9] The leakage into the reactor cell changes from the normal inflow to an outflow after the pressurization. The reactor cell gas temperature rises to 510 °C (950 °F) due convective heating from the molten salt, which causes the reactor cell pressurization. The peak reactor cell pressure is below the opening differential pressure on the burst disks to the vapor condensing tank. Consequently, the vapor condensing region of the containment remains isolated from the reactor cell. The molten salt spill height in the reactor cell is also not sufficient to spill over into the connected drain cell compartment (see Figure 4-4).

The full spill calculation considered cesium vaporization from the GRTR model. However, the cesium vaporization release fraction predicted in the current calculation was negligible (i.e., $<10^{-8}$).

[9] -2 psig (-13.7 kPa) is shown on Figure 4-3 as 12.7 psia, using 14.7 psia as +0 psig. The reactor building is approximately +0 psig. The peak pressure on Figure 4-3 as approximately 21 psia (145 kPa), which is +6.3 psig (+43.4 kPa)

The low cesium vaporization release can be explained by an example from a fluoride high-temperature reactor (FHR) accident scenario [5]. Figure 4-5 was developed from a FHR accident scenario that heated the molten salt to a boiling condition (i.e., ~1340 °C or much higher than the MSRE spill, which was less than 635 °C). The FHR results illustrate negligible cesium vapor releases when the molten salt temperature is less than 975 °C. The molten salt in the cited FHR accident eventually heated to ~1275 °C at 24 hr where larger cesium vaporization releases were predicted. Consequently, the negligible cesium vaporization release fraction in the MSRE spill scenario is expected due to the low temperature of the spilled molten salt relative to the temperature needed for an appreciable release.

As discussed in Section 3.5, the demonstration calculation will use the radionuclide releases from the maximum credible accident in the MSRE safety analysis report [8]. The radionuclide releases from the MSRE safety analysis report allows the subsequent demonstration of the radionuclide behavior, which is described in the Section 4.2.

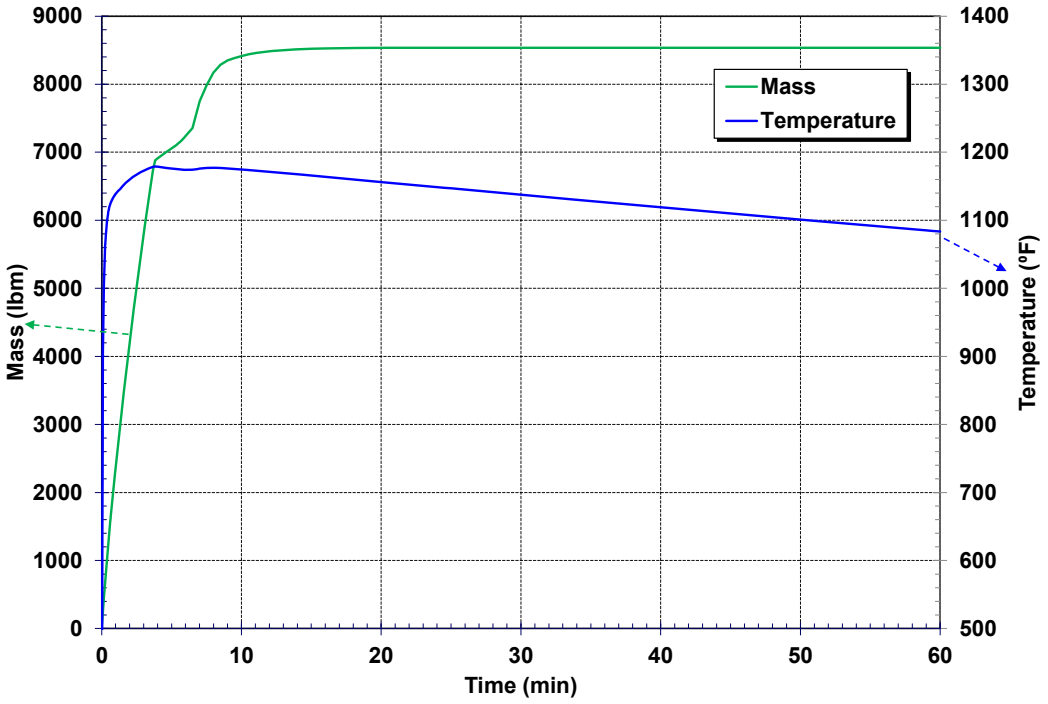

Figure 4-1 Mass and temperature of molten salt spilled into the reactor cell.

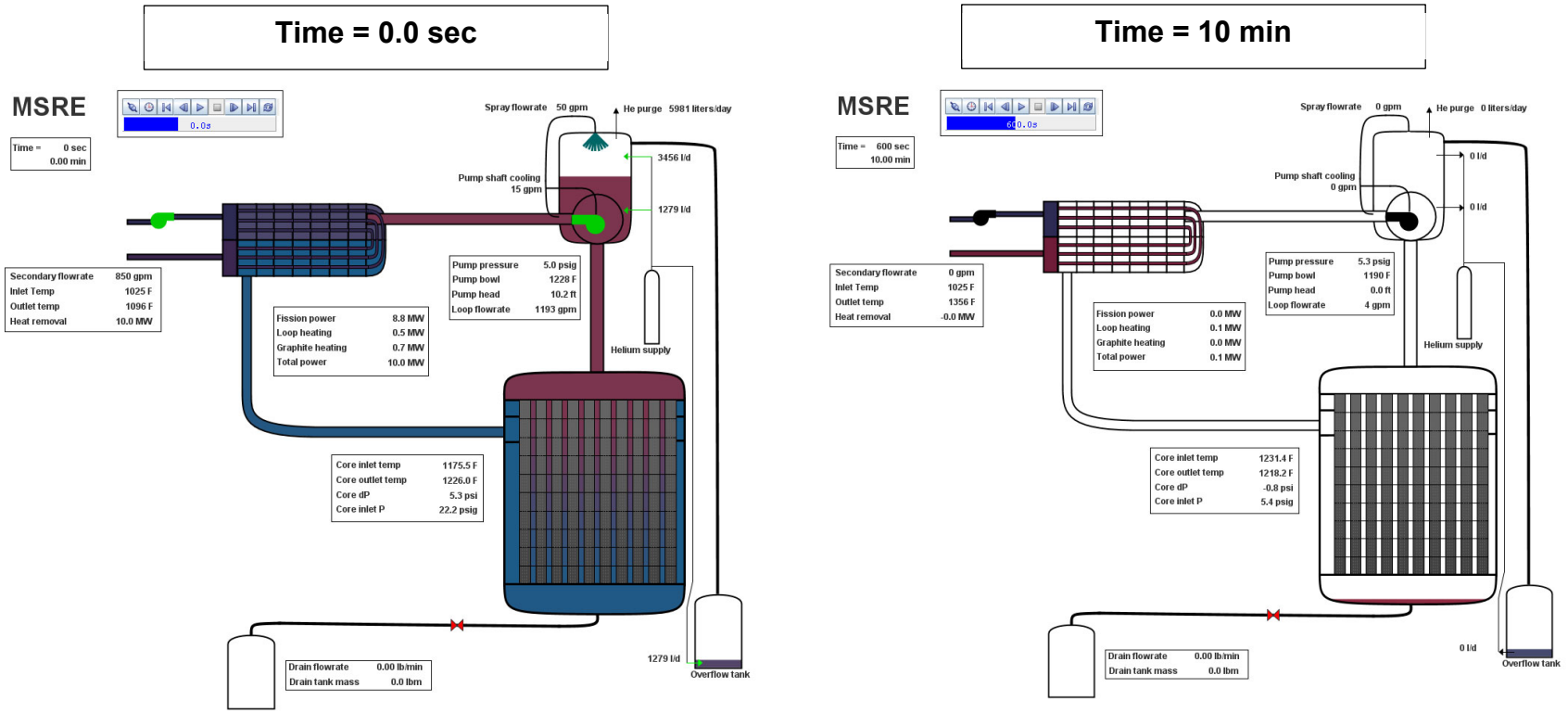

Figure 4-2 MSRE molten fuel salt spill.

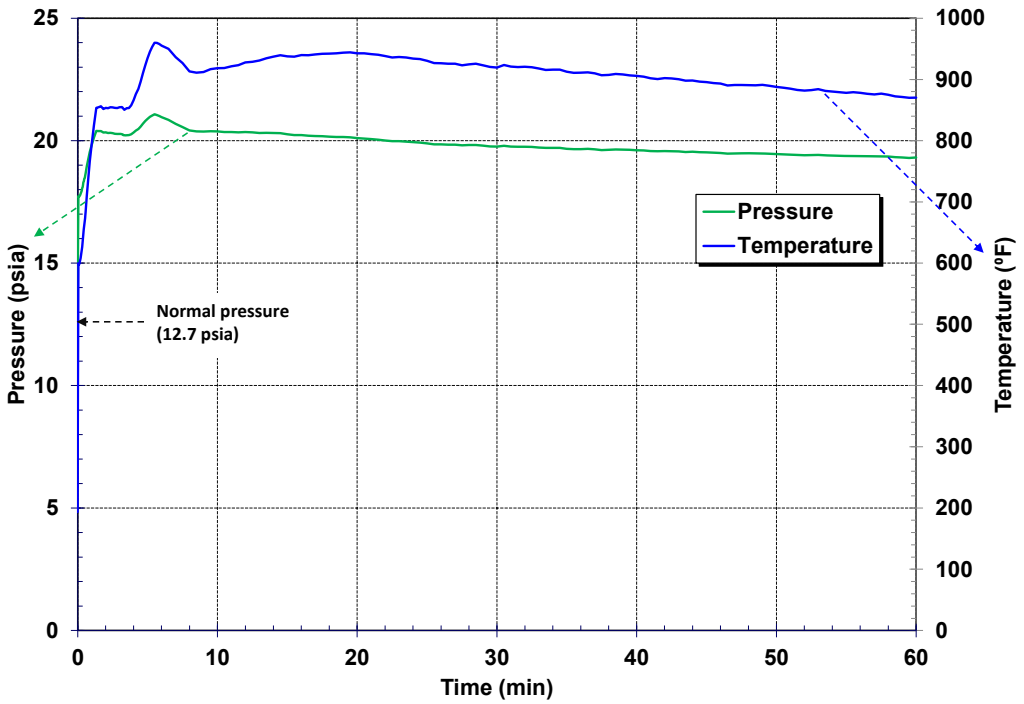

Figure 4-3 Reactor cell pressure and gas temperature.

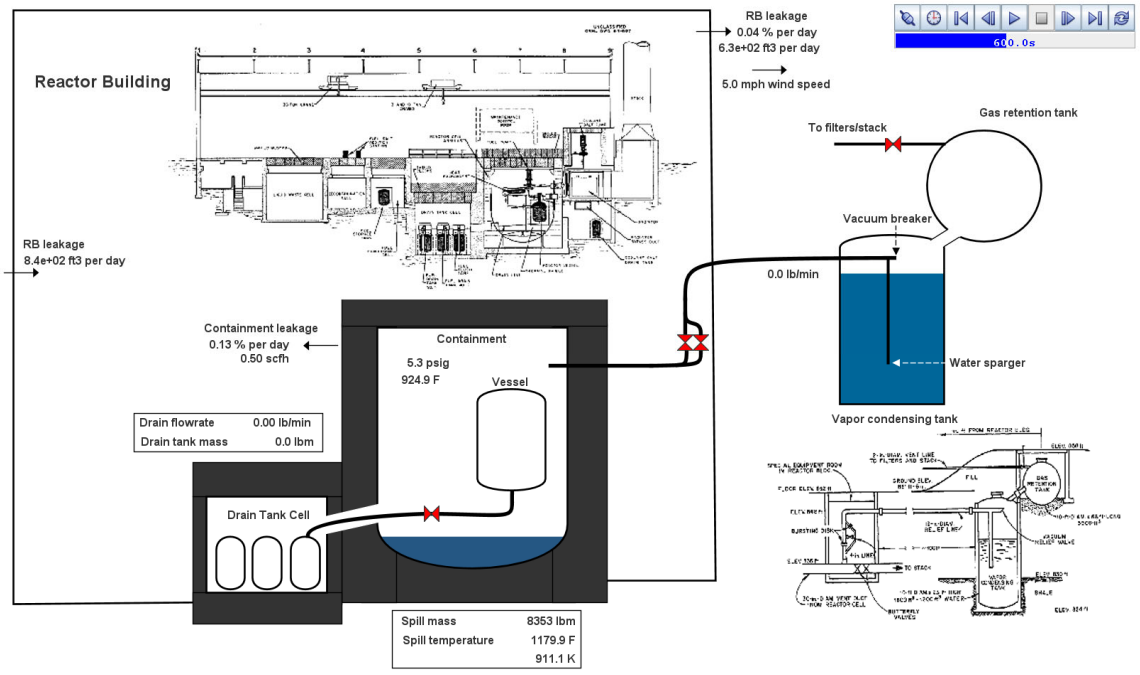

Figure 4-4 Reactor cell status at 10 min.

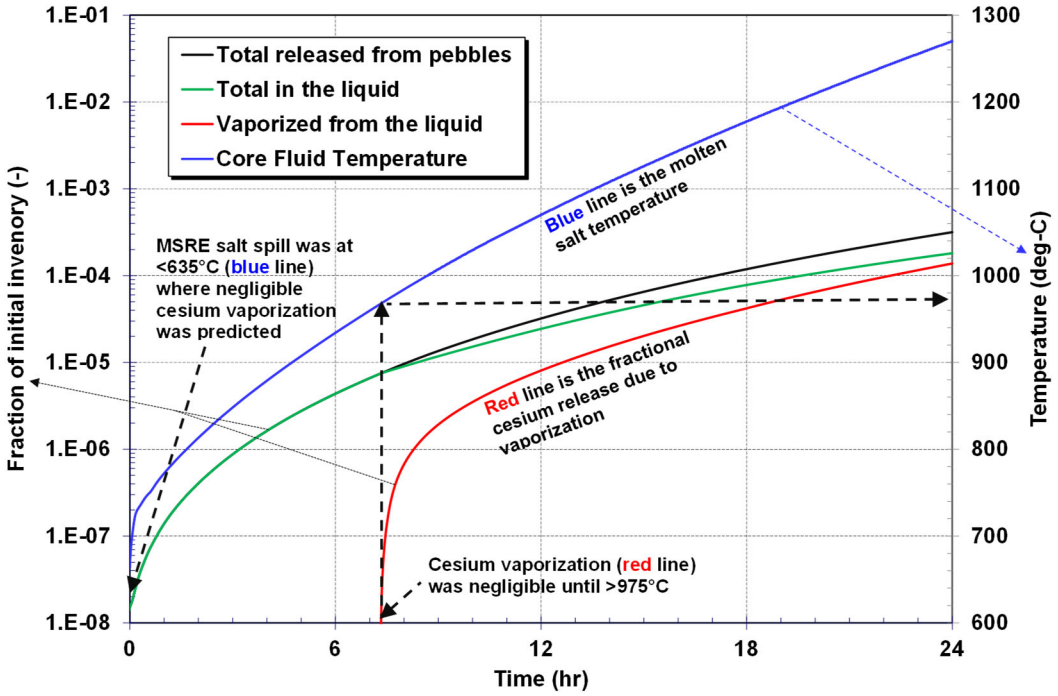

Figure 4-5 Cesium and cesium fluoride vaporization releases (i.e., an example from a fluoride high-temperature reactor (FHR) accident with much higher temperatures [5]).

4.2. Long-term response modeling approach

As described in Section 3.5, the new GRTR fission product chemistry and release model is still under development. Consequently, the radionuclide releases from the spilled molten salt were specified as previously reported in the MSRE safety analysis report [8] to demonstrate MELCOR's capabilities to simulate radionuclide transport, deposition, and release to the environment. Table 4-1 shows the radionuclide release fractions from the MSRE maximum credible accident (MCA). The specified releases were assumed to enter the reactor cell atmosphere over the first 100 sec of the accident. The subsequent 24-hr behavior of the radionuclides was calculated using the MSRE MELCOR model of the reactor cell and reactor building (see Figure 3-12) and the offgas system (see Figure 3-13).

Table 4-1 MSRE safety analysis maximum credible accident release fractions [8].

Parameter	Release fraction *
Noble gases	100%
Iodine	10%
Volatile fission products	10%
Non-volatile radionuclides	10%

Notes:
* The radionuclide inventory was calculated by SCALE and shown in Table 3-4.

Iodine and cesium are volatile and can form compounds before and after release from the fuel salt. MELCOR allows exploration of different chemical compounds. For the long-term source term calculations, it is assumed that 5% of the released iodine is elemental iodine (i.e., I_2), which is a gas. The remaining iodine is assumed to combine with a portion of the cesium to form cesium iodide (CsI). The remaining cesium is assumed to be cesium fluoride (CsF). The cesium and iodine chemical form(s) in a MSR are being actively researched (e.g., Reference [22]) due to its importance to the source term. Reference [22] identifies that CsF is highly soluble and will be retained in the fuel salt. In contrast, CsI has a low solubility and is more volatile for vaporization. However, splashing and entrainment are mechanical aerosol formation processes. Consequently, low soluble elements or compounds could be released in spite of their solubility. MELCOR allows exploration of alternate chemical forms, which will be needed until the molten salt thermochemical database is more complete (see Section 3.5).

In the long-term response model, the reactor vessel and the salt recirculation system (see Figure 3-11) were not included. Also, the condensable fluid was changed from molten salt to water to simulate the hydrodynamic steam loads from the molten salt-water mixing. The spilled molten salt was simulated as a heated surface on the floor of the reactor cell. The steam production was calculated based on the transfer of the sensible heat in the spilled molten fuel salt to the water.

The long-term model was used to simulate a number of variations of the MSRE maximum credible accident, which are shown in Table 4-2. First, the median aerosol size due to splashing and entrainment has uncertainties. A relatively small value of 1 μm was selected as the default aerosol size for all cases but one. MCA2 used a larger aerosol size to see the sensitivity in the aerosols size on the radionuclide transport. The aerosols are sourced into the reactor cell gas space using a logarithmic distribution. A geometric standard deviation of 1.5 was used to distribute between larger and smaller aerosols from the specified mass median diameter.

Table 4-2 MSRE molten fuel salt spill sensitivity cases.

Case	Aerosol size	Bldg Ventil	Aux. Filters	Water Spill
MCA1	1 μm	Yes	No	No
MCA2	10 μm	Yes	No	No
MCA3	1 μm	No	No	No
MCA4	1 μm	Yes	Yes	No
MCA5	1 μm	No	Yes	No
MCA6	1 μm	Yes	No	Yes
MCA7	1 μm	Yes	Yes	Yes
MCA8	1 μm	No	Yes	Yes
MCA9	1 μm	No	No	Yes

Any leakage from the reactor cell is assumed to go into reactor building (i.e., CV-520 in Figure 3-12). If the reactor building ventilation system is operating, then the radioactive airborne aerosols and gases in the reactor building can be transported to the building filters. There are competing processes for aerosol settling, transport to the offgas system filters, and leakage from the reactor building to the environment when the building ventilation system is operating. If the building ventilation system is off, then the airborne aerosols in the reactor building will not be transported to the filters and plant stack.

The offgas system included provisions to filter any airborne gases and aerosols in the reactor cell using the auxiliary filter train (see Figure 3-8 and Figure 3-13). The auxiliary filter is usually offline but can be manually started by an operator action. The timing for this mitigating action was assumed to occur at 1-hr, which is relatively close to start of the accident and at a time when most of the released radionuclides are still airborne in the reactor cell. Consequently, the sequence variations with and without the auxiliary offgas flow provides insights on the impact of the auxiliary filter on the source term.

The second variation is a coincidental water spill with the molten salt spill. The MSRE used water for the reactor cell air coolers, pump motor shaft cooling, and in the thermal shield around the reactor. The maximum credible accident in the MSRE safety analysis assumed water and molten salt spilled simultaneously onto the reactor cell floor. The interaction between the molten salt and the water creates a large steam source that rapidly pressurizes the reactor cell. The MSRE safety analysts concluded that the reactor cell could reach 860 kPa (110 psig) [8]. This possibility led to the addition of the vapor condensing and gas retention tanks to reduce the pressure in the maximum credible accident. MCA6 through MCA9 investigate the system response with a coincidental water spill (Section 4.4) while MCA1 through MCA5 assume a dry reactor cell (Section 4.3).

4.3. Long-term source term response without a water spill

MCA1 is selected as the base case for the scenarios without a water spill. After discussing the response of MCA1, the impacts of the scenario variations in MCA2 through MCA5 will be discussed. MCA1 had the following attributes,

- The median aerosol size for the radionuclide release from the spill is 1 μm.
- The building ventilation system is operating.
- The auxiliary filter is not operating.
- There is no coincident water spill.

Figure 4-6 shows the radionuclide release into the reactor cell during the reactor spill. The release fractions follow the values specified in the MSRE MCA safety analysis, which are shown in Table 4-1. As described in Section 4.2, the iodine release included cesium iodide and gaseous iodine. The release fractions of each are specified to be 10%, which has a net 10% iodine release. 100% of the noble gases are released and 10% of all other radionuclides are released over 100 seconds.

Due to the high temperature in the reactor cell after the molten salt spill (see Figure 4-3), the phase of some released radionuclides is impacted. The vapor pressures of some key radionuclides are shown in Figure 4-7. Elemental iodine (i.e., I_2) is a gas at 510 °C (950 °F). Due to its highly reactive chemical characteristics, no elemental cesium was modeled. However, elemental Cs would be primarily gaseous at the reactor cell temperature following the spill. CsI and CsF have a lower vapor pressure than elemental Cs. If there is a coincident water spill, then some cesium hydroxide (CsOH) may form. Without water, CsF is the likely form. Once the radionuclides leak or flow to cooler regions, any radionuclide gases formed in the hot reactor cell will condense and form small aerosols (i.e., CsI and CsF). The cerium behavior is also shown as an example of a radionuclide that will have a negligible vapor pressure. Cerium is always an aerosol. The impact of the vapor pressures on the radionuclide transport is discussed next.

First, the gaseous noble gas (Xe)[10] and gaseous iodine radionuclide responses are shown in Figure 4-8 and Figure 4-9, respectively. The responses of xenon and gaseous iodine are approximately identical when scaled to the magnitudes of their respective release fractions. The radionuclides remain airborne in the reactor cell and slowly leak to the reactor building. MCA1 includes the reactor building ventilation operation as shown in Figure 4-10. The reactor building ventilation system transports the leaked xenon and iodine gas to filters, which are ineffective at capturing gases. The gases flow out the plant stack to the environment, which is evident in the steadily increasing environmental release fraction in Figure 4-8 and Figure 4-9. Nevertheless, the leakage rate from the reactor cell is very low because most of the radioactive gases are retained in the reactor cell through 10^5 seconds (~27.8 hr). Approximately 0.2% of the initial inventory of Xe reaches the environment and 0.02% of the initial inventory of gaseous iodine.

Next, the behaviors of CsI, which is mainly a gas, CsF, which is part gas and part aerosol, and Ce, which is only an aerosol after release in the reactor cell are shown in Figure 4-11, Figure 4-12, and Figure 4-13, respectively. The long-term reactor stability of the fraction settled[11] is primarily due to the gaseous component of the radionuclide. The CsI evaporates and forms a gas in the reactor cell temperature (i.e., evident when the airborne fraction is approximately equal to the total fraction in the reactor cell). However, any CsI vapor leaked to the reactor building condenses and forms an aerosol, which allows for settling in the reactor building and capture by the filters.

The CsF and Ce results show varied amounts of aerosol settling in the reactor cell. The amount of Ce settling in the reactor cell is the highest because it is only an aerosol. Similar to the CsI results, any leaked CsF forms an aerosol in the reactor building and can be captured by the filters. Consequently, the aerosol release to the environment for CsI, CsF, and Ce are limited relative to the gaseous radionuclides (i.e., xenon and gaseous iodine) due to settling in the reactor cell and/or capture by the filters.

The reactor cell airborne fractions for CsI and CsF stabilizes near 10^{-1} and 10^{-2} due to their high and moderate vapor pressure at the high gas temperature in the reactor cell, respectively. Any leakage from the reactor cell to the reactor building is susceptible to transport by the building ventilation system to the filters. Due to the much lower temperature in the reactor building, any CsI and CsF vapors condense into aerosols and can be captured by the filters. Due to the high leak tightness of the reactor cells, most of the released radionuclides are retained in the reactor cell. For the vapors that leak and condense in the reactor building, they can settle or be swept towards the absolute filter in the building ventilation system. The absolute filter is filter 99.97% effective at removing aerosols larger than 0.3 μm. It is assumed that aerosols smaller than 0.3 μm pass through the filters and out the stack. The CsI and CsF environmental releases are very small relative to the previous Xe and I_2 gaseous releases. The CsI and CsF release fractions to the environment are approximately $2x10^{-4}$ and $3x10^{-5}$, respectively. The difference in the environmental releases between the two compounds is due to the difference in their vapor pressures (i.e., most of the CsI remains as a vapor in the reactor cell, which leads to a higher leakage rate than for CsF).

---

[10] Xenon is the reference element for the Xe radionuclide class but includes the masses of all the noble gases, which have similar chemical properties (see gaseous grouping in Table 3-4). Similarly, the iodine gas class includes other gaseous elements.

[11] The amount of settling in the reactor cell can be determined from the difference between the total fraction in the reactor cell and the airborne fraction in the reactor cell.

The cerium release from the molten salt is always an aerosol in the reactor cell. Unlike the CsI and CsF behavior in the reactor cell, the amount of airborne cerium continues to decrease to a fraction of $3x10^{-6}$ at 10^5 seconds. The continuously decreasing airborne mass (i.e., increasing settled mass) limited the amount available for leakage to the reactor building. This was the first order effect that limited the Ce release to the reactor building and the environment relative to the other radionuclides.

A second factor limiting the Ce environmental release was the aerosol size. The median released size of the Ce aerosols into the reactor cell was 1 μm. Due to its very low vapor pressure, Ce remained in an aerosol form in the reactor cell. Consequently, the Ce aerosols leaked from the reactor cell into the reactor building and remained near their initial this size distribution from the spill. The absolute filter is very effective (i.e., 99.97%) at capturing 1 μm aerosols. In contrast, almost all of the CsI and CsF that leaked into the reactor building was a vapor. When the leaked CsF and CsI vapors condensed in the reactor building, they formed very small aerosols (<0.2 μm). In contrast to the larger Ce aerosols, some of the smaller aerosols formed by condensation can pass through the absolute filter.[12] In summary, the fraction of cerium leaking from the reactor cell was much smaller due to aerosol settling, and the amount subsequently captured by the filter was much higher due to the larger median aerosol diameter. The overall cerium release to the environment was $<10^{-8}$ at 10^5 seconds.

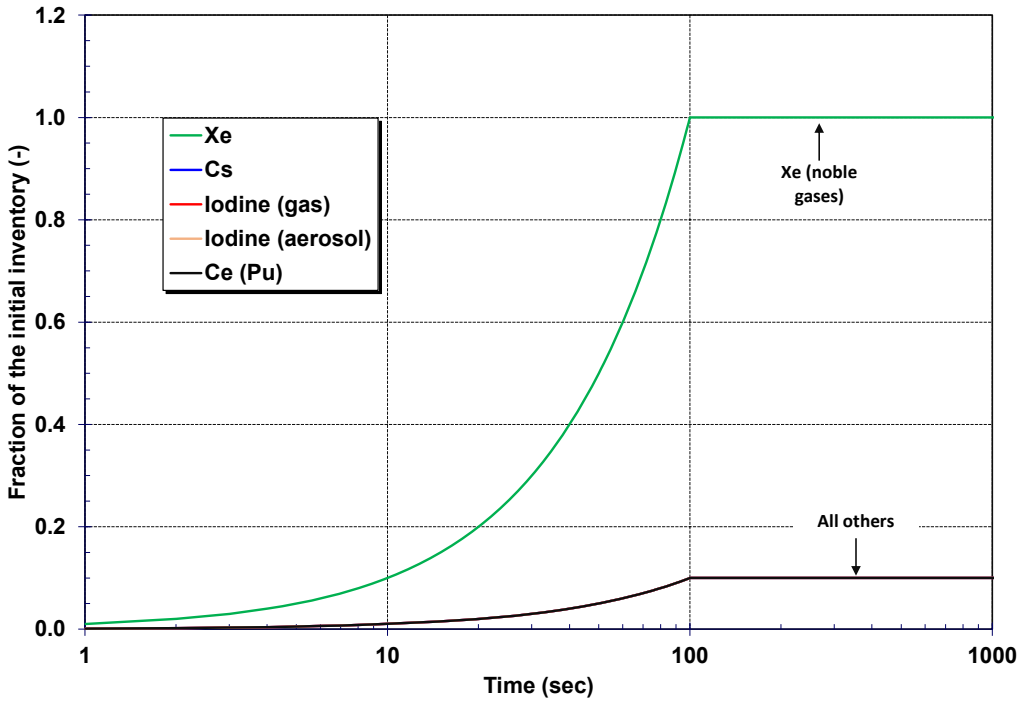

[12] MELCOR includes a variety of models that impact the size distribution of transported aerosols. The aerosols are tracked as a distribution of sizes. Some of the physics that impact the aerosol size distribution includes spontaneous nucleation from the condensation of the radionuclide vapors, condensation onto existing aerosols and structural surfaces, deposition, and agglomeration. The aerosol physics impacts the time-dependent aerosol size distribution and the filter effectiveness.

Figure 4-6 Radionuclide release from the molten salt spill into the reactor cell gas space.

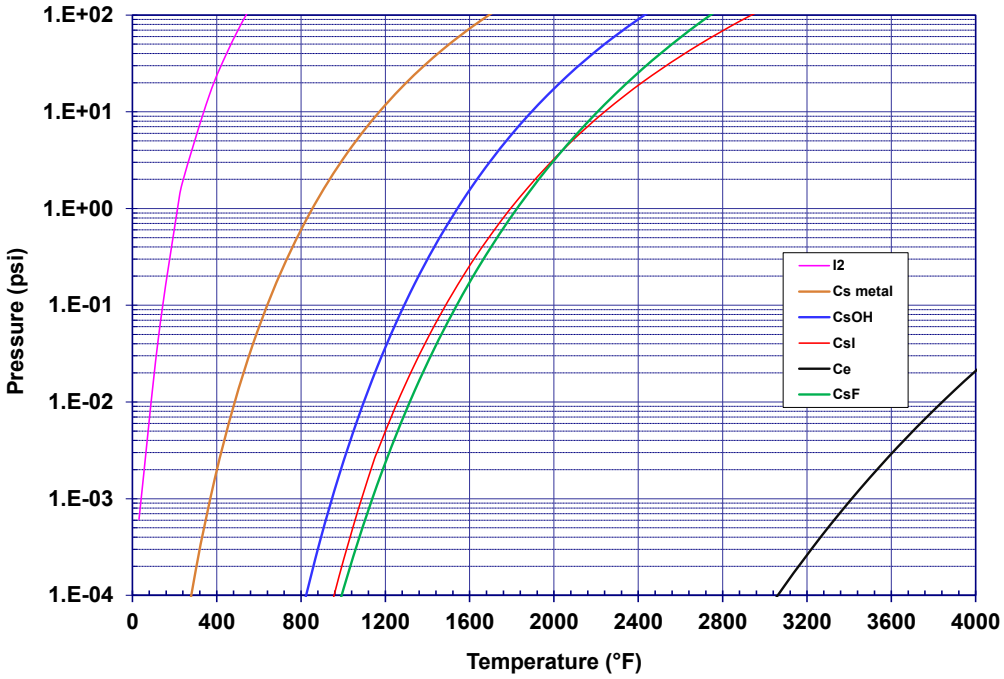

Figure 4-7 Vapor pressures of some released radionuclides.

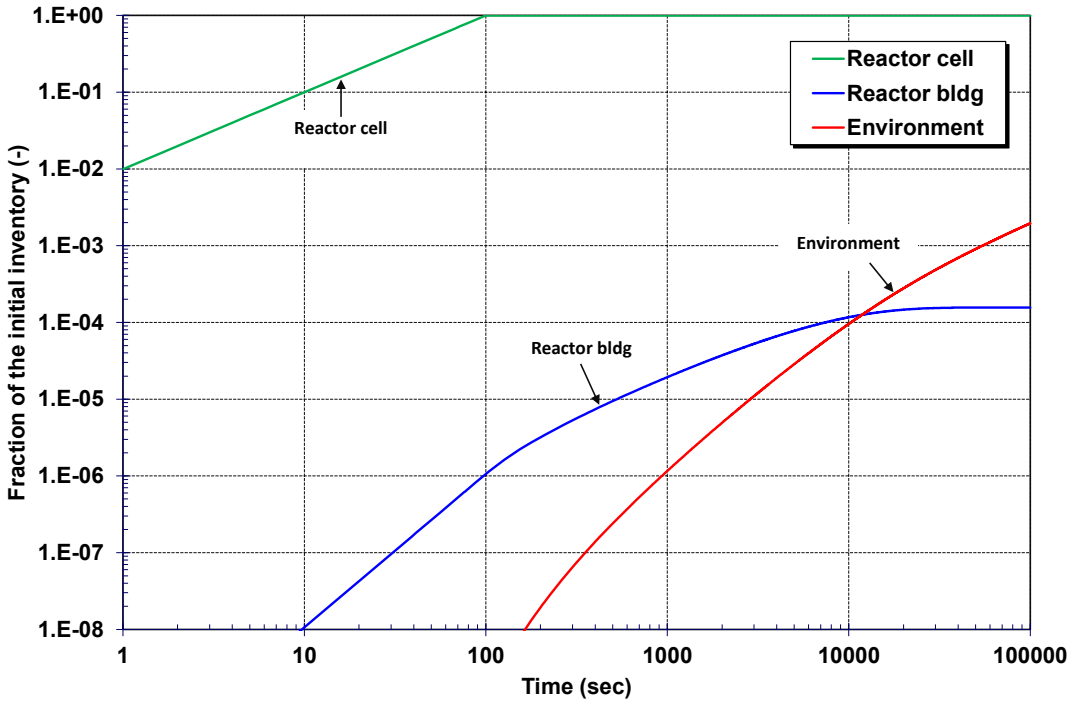

Figure 4-8 MCA1 noble gas (Xe) distribution.

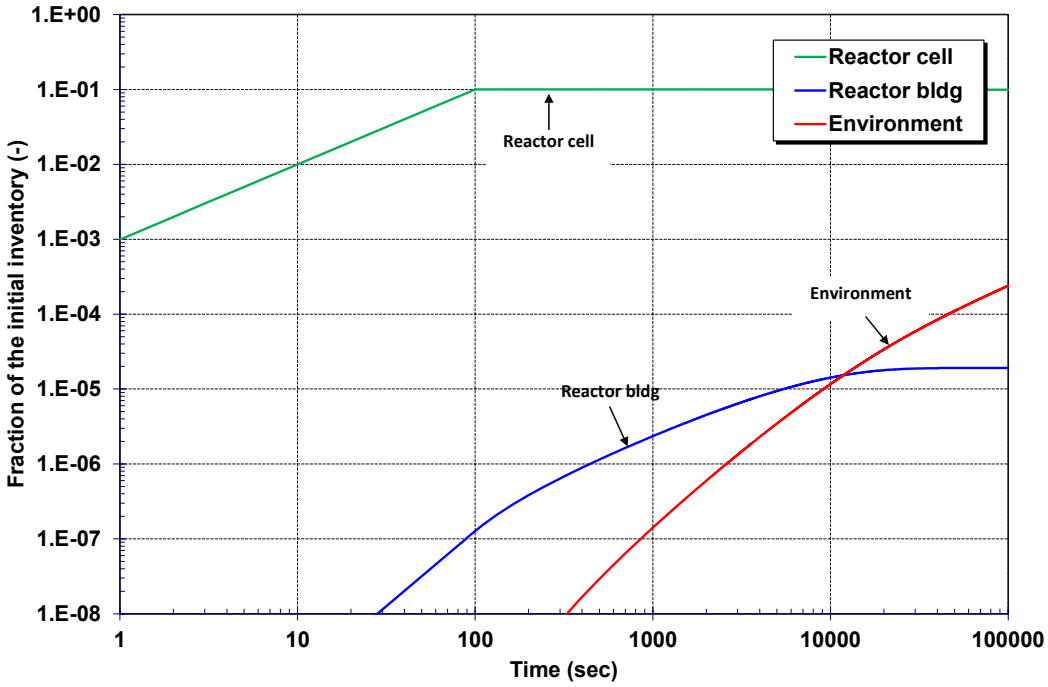

Figure 4-9 MCA1 gaseous iodine (I_2) distribution.

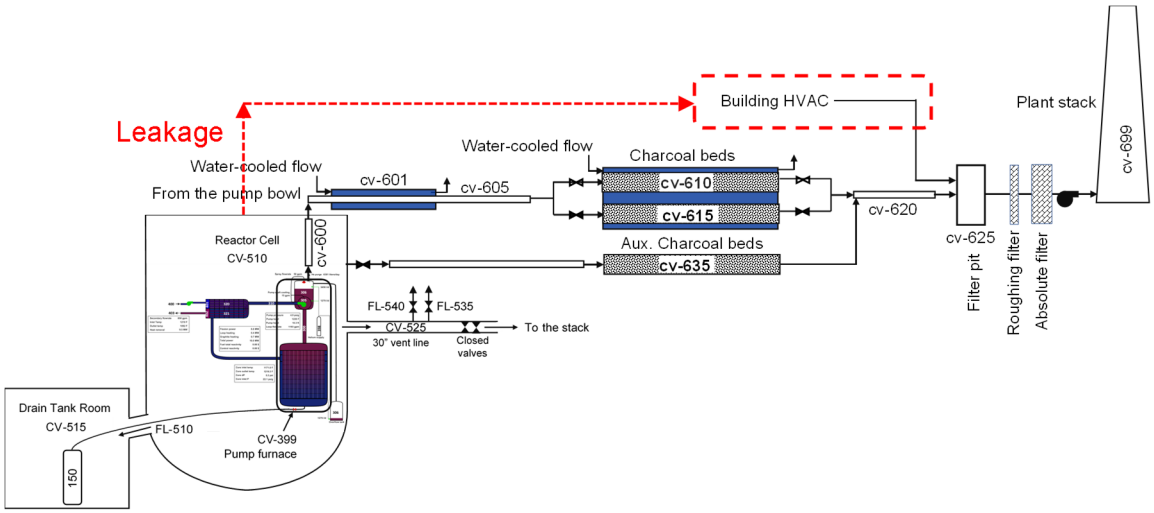

Figure 4-10 MCA1 reactor cell leakage with building ventilation operation.

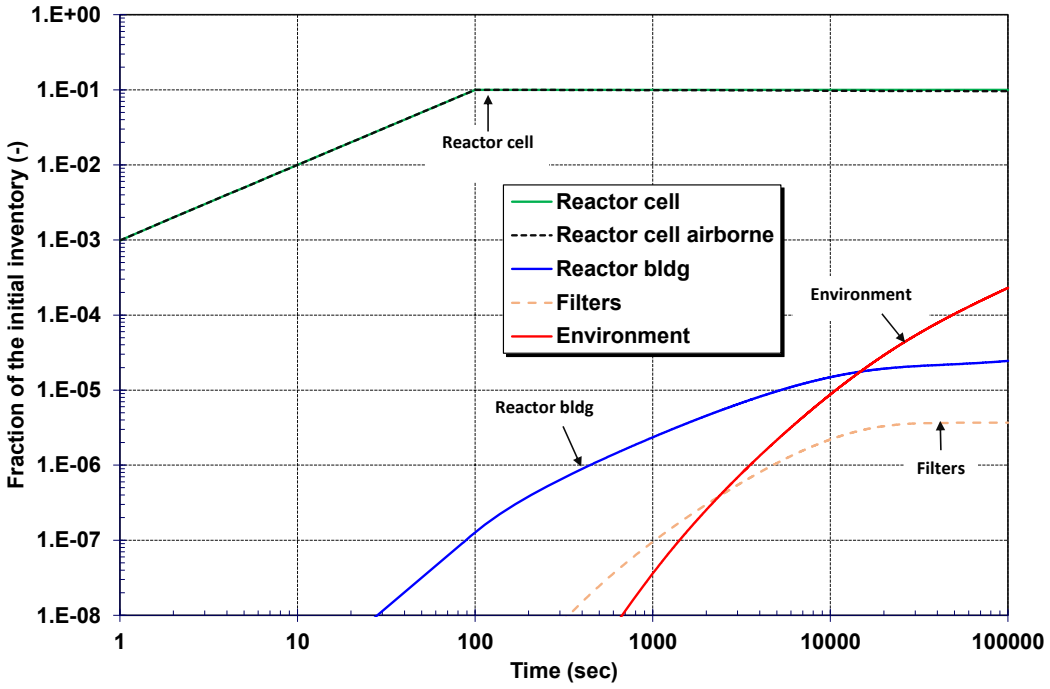

Figure 4-11 MCA1 cesium iodine (CsI) distribution.

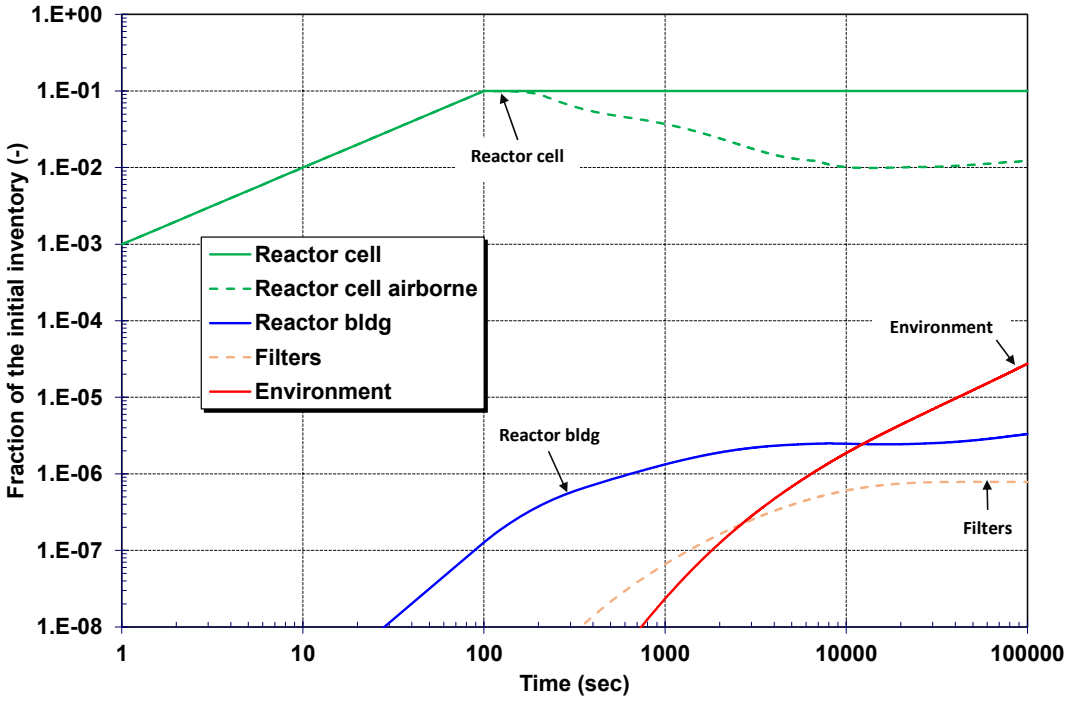

Figure 4-12 MCA1 cesium fluoride (CsF) distribution.

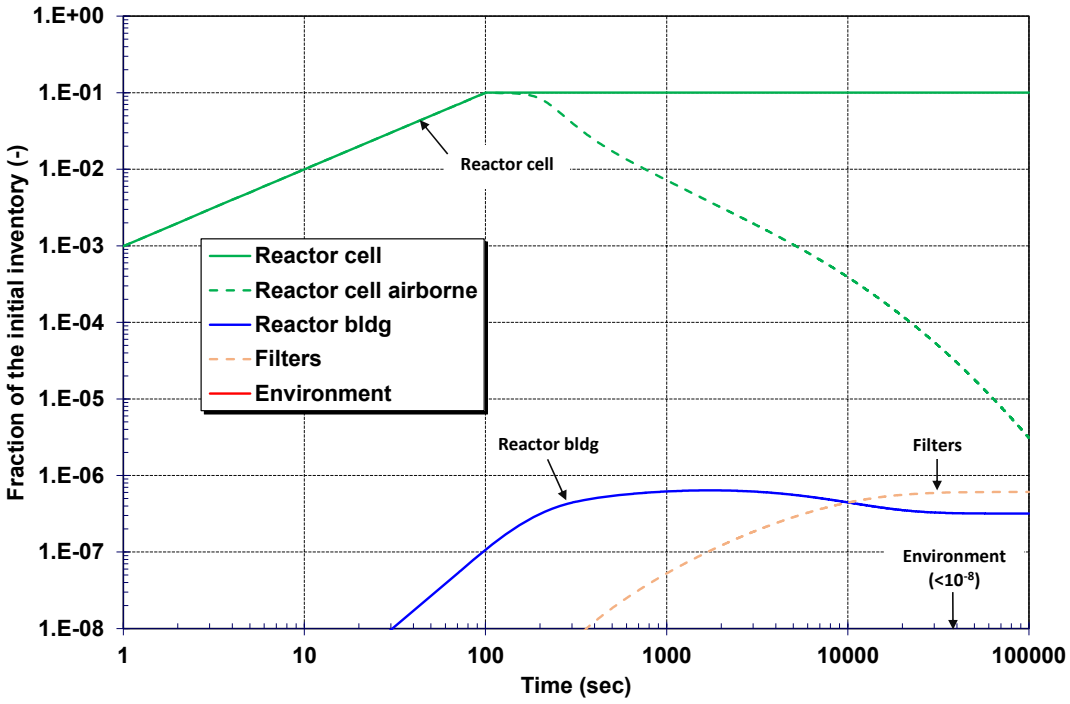

Figure 4-13 MCA1 cerium (Ce) distribution.

There are four variations of the MCA1 base case without a coincident water spill. MCA2 through MCA5 varied some parameters expected to impact the magnitude of the source term (i.e., see below). The parameter variations are intended to provide examples of a phenomenological uncertainty (i.e., aerosol size) and scenario variations (building ventilation, auxiliary filter operation, and a coincident water spill). A more complete uncertainty study would expand the number of parameters and perform random sampling to assess their influence on the source term. The scope of the current study is to demonstrate capabilities and insights from a few parameters varied individually.

Case	Aerosol size	Bldg Ventil	Aux. Filters	Water Spill
MCA1	1 μm	Yes	No	No
MCA2	10 μm	Yes	No	No
MCA3	1 μm	No	No	No
MCA4	1 μm	Yes	Yes	No
MCA5	1 μm	No	Yes	No

The impacts of the variations on noble gas release to the environment are shown in Figure 4-14. MCA4 had the highest release due to auxiliary filter venting of the reactor cell after 1-hr and enhanced transport to the environment due the ventilation flow through the reactor building. There may be some holdup of xenon in the charcoal pores or with new classes of materials (e.g., Reference [23]), which needs further examination and code modeling capabilities. In these calculations, it was conservatively assumed there was no retention of the noble gases by the charcoal.

The manual start-up of the auxiliary filter is evident at 1 hour when the release rate to the environment increases.

MCA3 had the lowest release with no ventilation flow in the reactor building and no auxiliary filter flow. The xenon was not actively transported to the filters via the building ventilation system nor the auxiliary filter flow, which led to higher retention in the reactor building and the reactor cell, respectively.

MCA1 and MCA2 were identical because xenon is not an aerosol. MCA5 did not have enhanced releases due to the building ventilation flow but did include the auxiliary filter flow after 1-hr. The transport to the environment is slower because the small auxiliary filter flow was diluted in the relatively large filter plenum and plant stack. The small auxiliary filter flowrate and the dilution in the filter plenum and stack greatly slowed the transport to the environment.

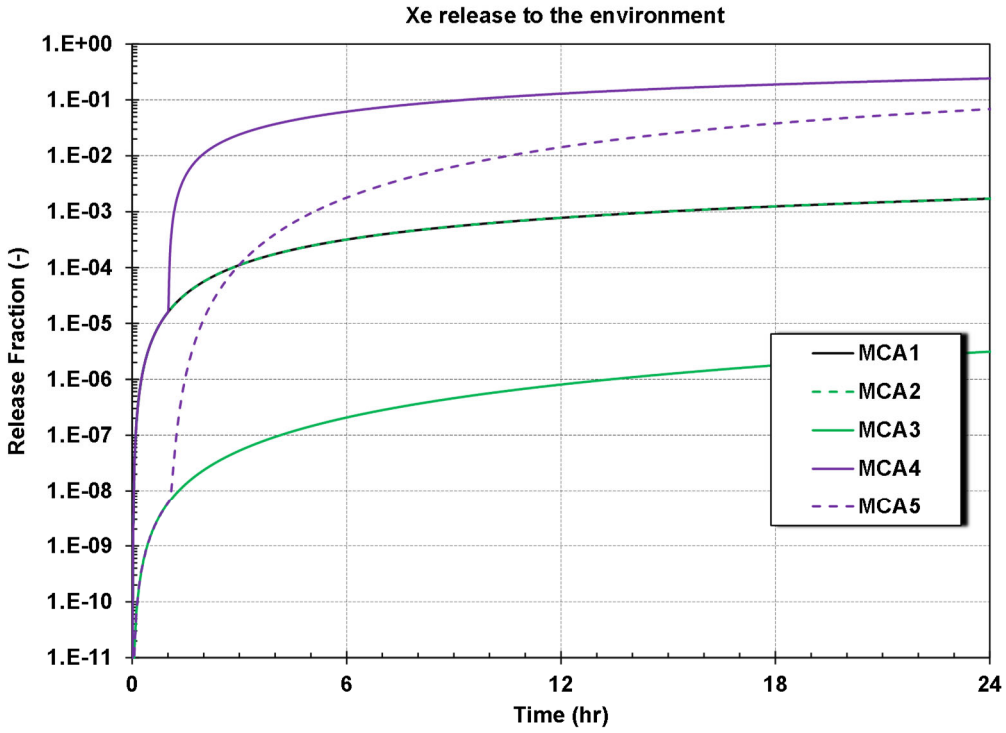

Figure 4-14 Variations in the Xe release to the environment for the cases without a coincident water spill.

Using cerium as an example of the aerosol response, Figure 4-15 shows the variations in the environmental releases. The release of cerium to the environment was very small due to the low-leakage containment, aerosol settling, and effective filtration. MCA4 was initially the highest due to the combination of the building ventilation and auxiliary filter operation. However, the total MCA4 releases at 24 hr were similar to MCA3 and MCA5. Aerosol settling in the reactor cell minimized the transport via the auxiliary charcoal filter after 4 hours. Small aerosols (<0.3 μm) and some bypass

due to incomplete capture leads to a release past the filter.[13] However, the subsequent release to the environment after 4 hours was small due to settling in the reactor cell.

The responses of MCA3 and MCA5 were similar because neither had a building ventilation flow to transport aerosols from the relatively large filter inlet plenum and the plant stack to the environment. Consequently, the aerosols settled in the filter plenum or the stack or were captured in the filters. The releases were dominated by leakage from the reactor building, which was similar in the two cases. In contrast to the response of MCA1, MCA3 and MCA5 had a protracted release of aerosols to the environment. The long-term MCA3 and MCA5 environmental source term eventually reached the magnitude of MCA4. The leakage of the aerosols from the reactor building are not filtered, which eventually generated a similar release to MCA4. In the MCA4 sequence, the aerosols that leaked from the reactor cell were more quickly transported to the environment by the building ventilation system. However, the MCA4 aerosols were effectively filtered and very few passed through the filter to the environment.

MCA2 is a sensitivity of larger median diameter aerosols from the spill and had the lowest environmental release. The larger aerosols settled faster and are more effectively retained by the filter. MCA1 and MCA2 had identical scenario specifications but the median release aerosol size in MCA2 was 10 μm versus 1 μm in MCA1. Figure 4-16 shows the larger aerosol simulation had more rapid settling, which leads to a lower amount leaked from the reactor cell and captured on the filters. Due to the high impact of the faster aerosol settling rate, there was a smaller environmental release in MCA2.

The response of compounds like CsI and CsF with a small vapor pressure had characteristics between the xenon and cerium responses. Figure 4-17 shows the CsF release to the environment. The highest release came from MCA4 due to release pathways via the building ventilation and the auxiliary filter. Since a portion of the CsF is gaseous in the reactor cell, the gases condense upon leaving the reactor cell and form very small aerosols that are more likely to pass through the filters (i.e., whether transported by the building ventilation system after leakage from the reactor cell or vented by the auxiliary filter flow).

Surprisingly, MCA1 and MCA2 have similar responses. The scenario specifications are identical except the median initial aerosol size. However, the evaporation from the aerosols generates similar amounts of gaseous CsF that upon leakage from the reactor cell have the same release characteristics. Consequently, the magnitude of small aerosols formed from gaseous phase of the leaked CsF generated a similar environment source term.

MCA5 does not include the building ventilation system but includes the auxiliary filter flow. The auxiliary filter flow steadily transports the gaseous CsF from the reactor cell to filters where the small and gases aerosols pass through the filter to the environment.[13] As shown in the first hour, MCA4 has a much larger release rate versus MCA5 due to the building ventilation pathway to the environment. In contrast, any CsF aerosols and vapor initially leaked to the reactor building in MCA5 during the first hour were effectively retained. After the auxiliary filter started, the MCA5 releases increased and became the second largest release. The CsF vapor condensed into small aerosols in the auxiliary filter in MCA4, which allowed their bypass through the filter. The MCA5 transport rate through the filter plenum and plant stack was very low relative to MCA4 because the

[13] The absolute filter has a 97.97% effectivity for aerosols larger than 0.3 μm. Consequently, 0.03% of the aerosols pass through the filter. It is assumed all aerosols smaller than 0.3 μm pass through the filter. These are the two sources for bypassing capture by the absolute filter.

building ventilation system was not running. The net effect was an order of magnitude lower environmental release rate in MCA5 versus MCA4.

MCA3 had the highest retention of CsF (see Figure 4-17). There was no active ventilation system to transport the CsF from the reactor cell or from reactor building to the environment. Consequently, the CsF was retained in the reactor cell or the reactor building. The CsF environmental source term was higher than the Ce values due to some CsF gas formation in the hot reactor cell. The CsF gas continued to leak from the reactor cell, which condensed to form small aerosols that more effectively leaked from the reactor building than the larger Ce aerosols. Nevertheless, the MCA3 CsF release was orders of magnitude smaller than the other cases.

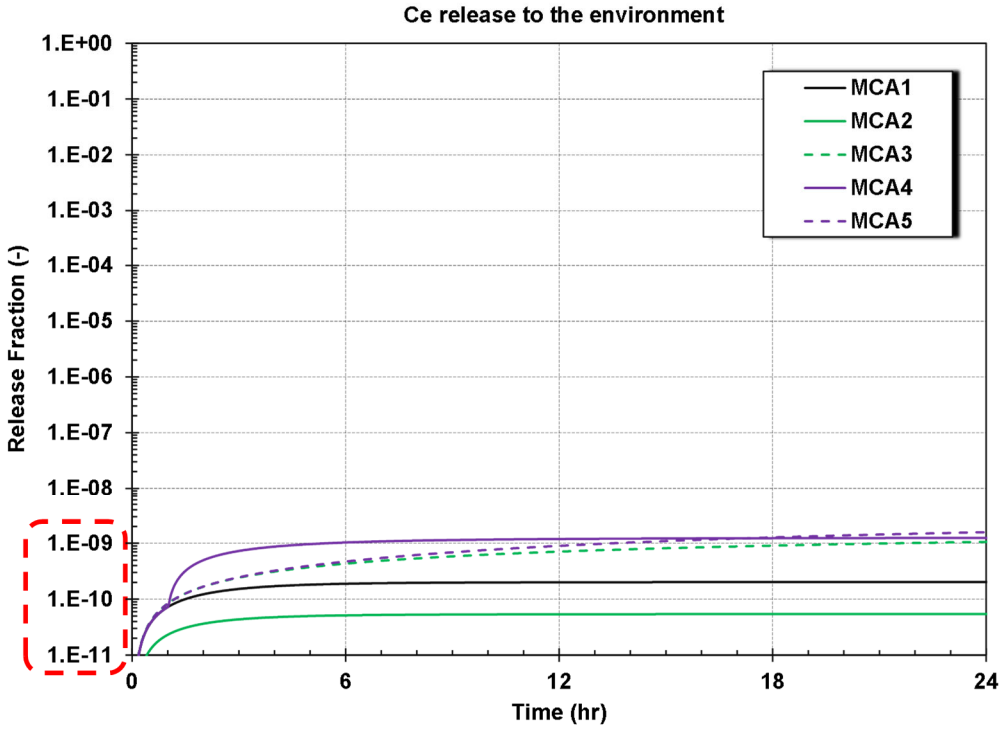

Figure 4-15 Variations in the Ce release to the environment for the cases without a coincident water spill.

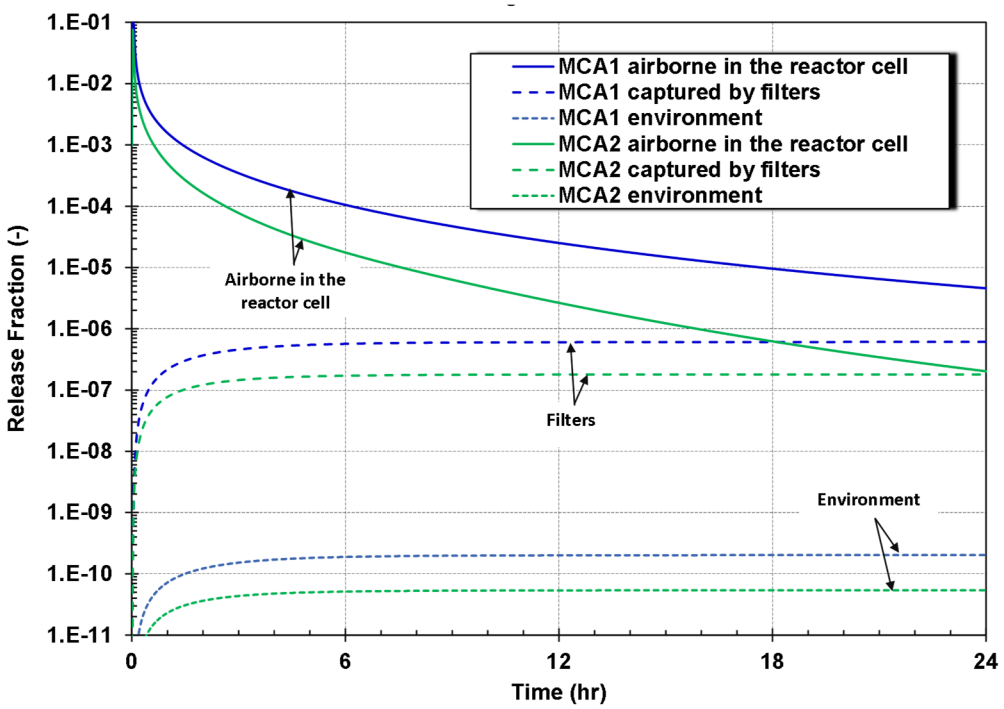

Figure 4-16 Ce aerosol settling and filtration behavior in MCA1 and MCA2.

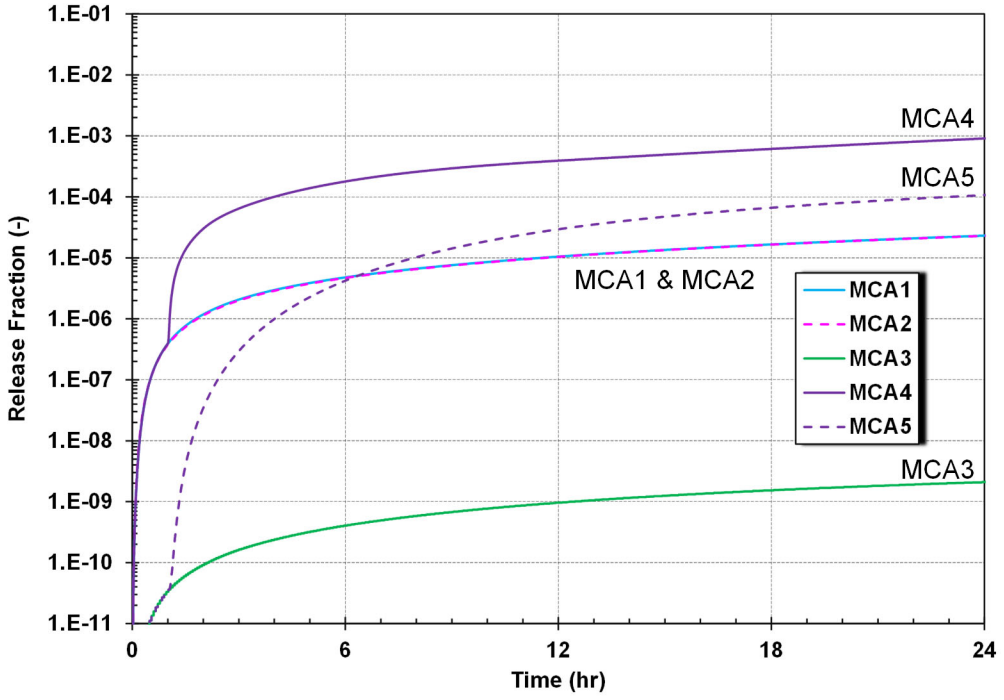

Figure 4-17 Variations in the CsF release to the environment for the cases without a coincident water spill.

4.4. Long-term source term response with a water spill

MCA6 is selected as the base case for the scenarios with a water spill. After discussing the response of MCA6, the impacts of the scenario variations in MCA7 through MCA9 will be discussed. MCA6 had the following attributes,

- The median aerosol size for the radionuclide release from the spill is 1 μm.
- The building ventilation system is operating.
- The auxiliary filter is not operating.
- There is a coincident water spill.

Except for the coincident water spill, the attributes of MCA6 are the same as MCA1.

Case	Aerosol size	Bldg Ventil	Aux. Filters	Water Spill
MCA6	1 μm	Yes	No	Yes
MCA7	1 μm	Yes	Yes	Yes
MCA8	1 μm	No	Yes	Yes
MCA9	1 μm	No	No	Yes

Similar to MCA1 without a coincident water spill, approximately 3860 kg (8500 lbm) of molten fuel salt drains in the reactor cell (Figure 4-1). However, the molten salt is assumed to mix with coincidently spilled water that creates steam. The water and steam limit the reactor cell gas temperature to near steam saturation temperature. The maximum cell gas temperature is 166 °C (330 °F) versus 510 °C (950 °F) in the MCA1 dry floor case.

The reactor cell pressure quickly rose due to the rapid steam generation of the water from the interaction with the spilled molten salt. The 1.03 bar (15 psig) and the 1.38 bar (20 psig) bursting disks opened at 41 seconds and 115 seconds, respectively. The lower pressure bursting disk only opened a 10 cm (4 inch) diameter line, which was inadequate to reduce the pressure. The burst disk opening pressure is calculated based on the differential pressure across the disk. Due to the pressurization of the vapor condensing line after the first burst disk opens, the reactor cell pressure rises to 317 kPa (46 psia) before the second disk opens. The reactor cell pressure begins to decrease following the larger 30 cm (12 inch) diameter line opening at 115 seconds. The reactor cell and vapor condensing tank pressures and temperatures gradually decrease from their peak values after their initial rise.

The steam flow from the reactor cell condenses in the vapor condensing tank water and any non-condensable gases bubble out the water. The vapor condensing tank and the gas retention tank work to reduce the system pressure by condensing steam and adding more volume to the system. The MCA6 pressure response demonstrates the effectiveness of the vapor condensing and gas retention tanks to maintain the peak reactor cell pressure below the design pressure of 377 kPa (54.7 psia). However, the peak gas retention tank pressure is +170 kPa-gauge (24.7 psig), which is slightly above the design pressure of +138 kPa-gauge (20 psig).[14]

[14] Any potential adverse consequence of the gas retention tank rising above the design pressure was not included in the demonstration calculation.

The MCA6 xenon and iodine gas distributions are shown in Figure 4-19 and Figure 4-20, respectively. The responses show some interesting difference relative to MCA1 (i.e., see Figure 4-8 and Figure 4-9) and also to one another. The first effect is the capture in the gas retention tank in MCA6, which was not present in MCA1. The large amount of steam generation in the reactor cell forces most of the released xenon and iodine into the vapor condensing and gas retention tanks. These tanks did not include leakage to the reactor building. Consequently, any radionuclides in these locations are retained there. There is some backwards flow of xenon into the reactor cell through the vapor condensing tank vacuum relief valve as the steam in the reactor cell cools and condenses. The backwards flow shows up as a small redistribution of xenon from the vapor condensing system back into the reactor cell. Consequently, there are competing effects of a higher pressure in MCA6 versus MCA1, which enhances the leakage rate, and less inventory in the reactor cell in MCA6 due to the transfer to the vapor condensing and gas retention tanks. However, the impact of the diversion to the vapor condensing and gas retention tanks is more significant than the higher pressure (i.e., the MCA1 Xe environmental release is $2.3x10^{-3}$ versus $7x10^{-4}$ in MCA6).

The second effect that led to differences in MCA1 and MCA6, is iodine capture in the vapor condensing tank. Although the xenon flows back into the reactor cell when the vacuum relief valve opens, there is no observable iodine flow. The impact on the gaseous iodine distribution is negligible because most of the gaseous iodine is captured in the vapor condensing tank water and immobile (i.e., only airborne gases and aerosols flow back through the vacuum relief valve). Whereas the xenon and iodine behavior are nearly identical in MCA1 (i.e., after scaling by the magnitude of the release, see Figure 4-6), the iodine capture in vapor condensing pool impacts the iodine concentration in the reactor cell and the iodine release to the environment. The iodine release to the environment in MCA1 is 10X smaller than the xenon release (i.e., due to a 10X smaller amount released into the reactor cell). The iodine release to the environment in MCA1 is 22X smaller than the xenon release due to capture in the vapor retention tank. In summary, xenon and iodine behave differently in MCA6 and have lower environmental releases than MCA1.

The cesium fluoride, cesium iodide, and cerium responses are shown in Figure 4-21, Figure 4-22, and Figure 4-23, respectively. These figures are essentially identical because these elements and compounds have a very low vapor pressure at this temperature. The presence of the water and steam in the reactor cell led to a much lower reactor cell temperature that was close to the steam saturation temperature. The water was also important for initially cooling the spilled fuel salt. Depending on the assumption of the amount of water in reactor cell, the reactor cell gas temperature could be higher or lower, which could be explored through uncertainty calculations. Nevertheless, MCA6 illustrates an alternate response from MCA1 where the reactor cell pressure is higher due to the interactions of coincidently spilled water, but the gas temperature is lower.

The cesium fluoride and cesium iodide released from the spill stayed in aerosol form like cerium. In an aerosol form, the release is susceptible to settling and capture on the filters, which is evident in the figures. The results show a rapid decrease in airborne mass in the reactor cell, which limits the amount available to leak into the reactor building. The building ventilation system transports the leaked aerosols that do not settle in the reactor building. Similar to the xenon response, some slight movement of airborne aerosols in the vapor condensing line is evident when the vacuum relief valve opens (i.e., the small increase in airborne mass at 3900 sec). However, most of the CsI, CsF, and Ce aerosols were retained in the vapor condensing tank water, so the aerosol backflow through the vacuum relief valve was very small (i.e., $<10^{-6}$). Most of the gaseous iodine was also retained in the pool and had a negligible backflow into the reactor cell when the vacuum relief valve opened.

In summary, the aerosol radionuclide behavior did not show the same vapor pressure variations as the dry cases. The lower gas temperature in the reactor cell caused the airborne CsF and CsI to have a very low vapor pressure (see Figure 4-7) and behave as an aerosol in the reactor cell. Consequently, the CsF, CsI, and Ce behaved similarly, which was different from the MCA1 results.

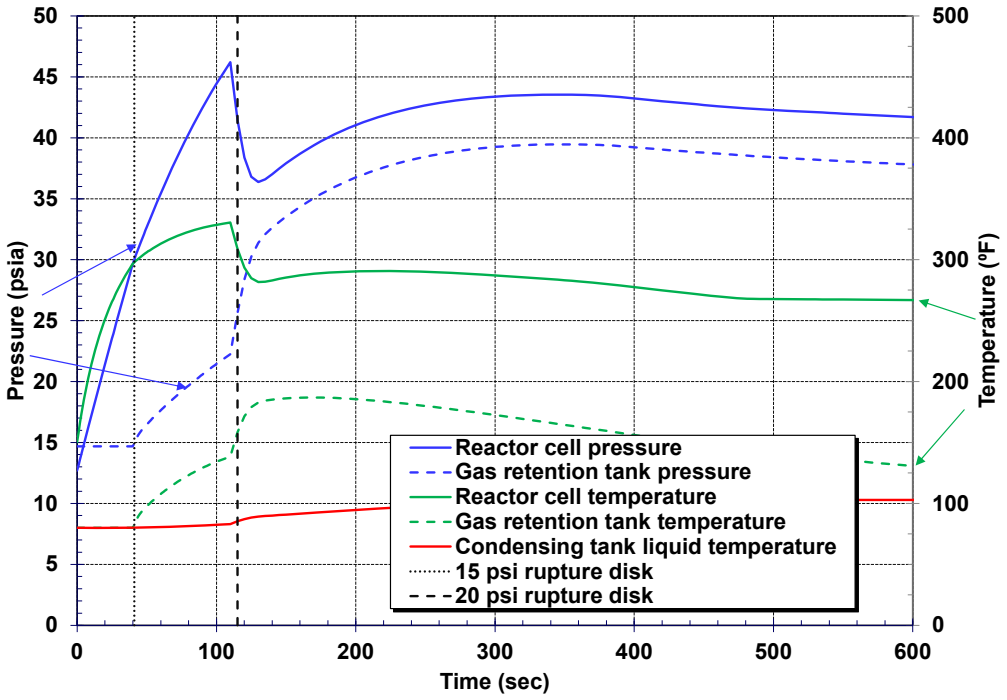

Figure 4-18 MCA6 reactor cell and gas retention tank gas temperature and pressure.

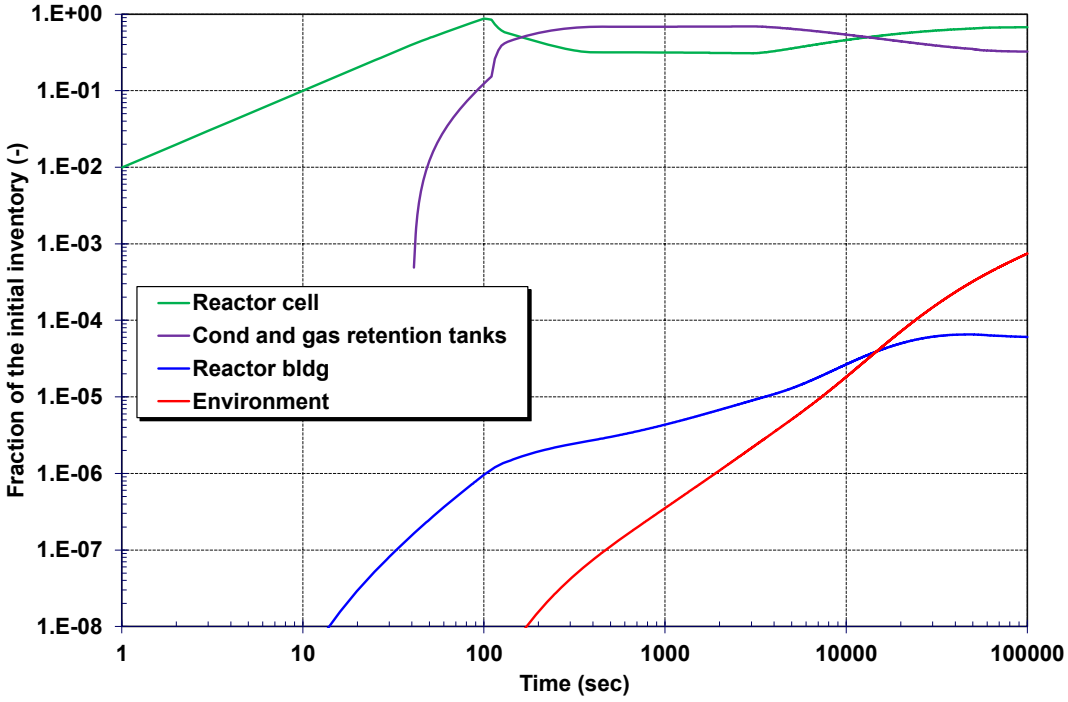

Figure 4-19 MCA6 xenon (Xe) distribution.

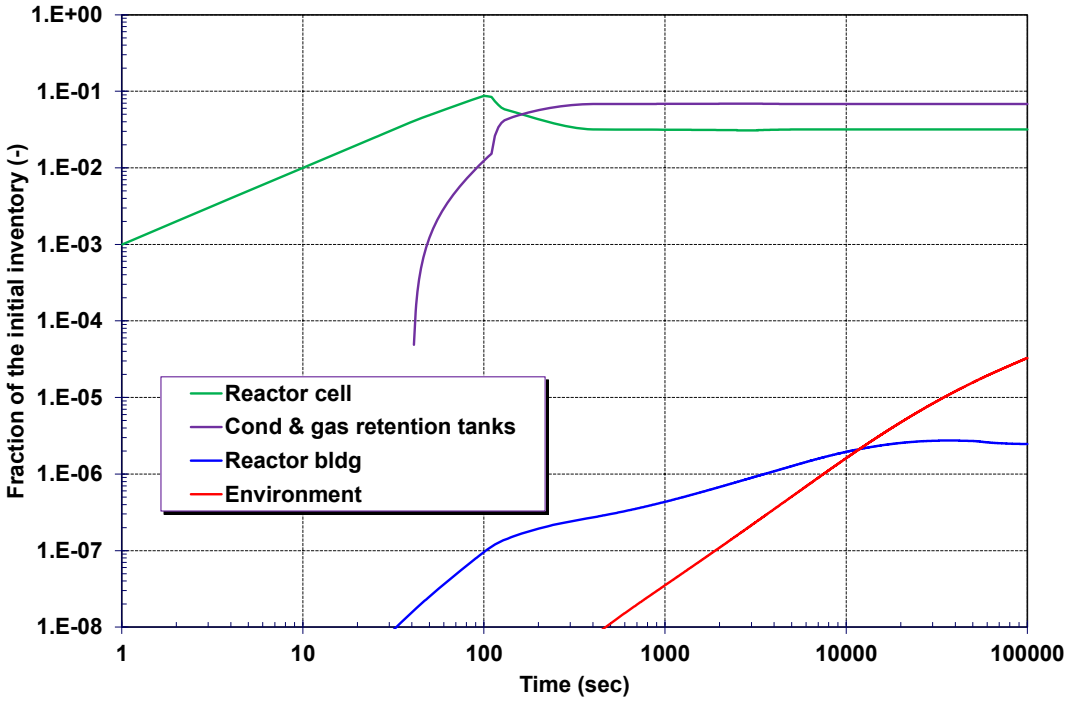

Figure 4-20 MCA6 iodine gas (I_2) distribution.

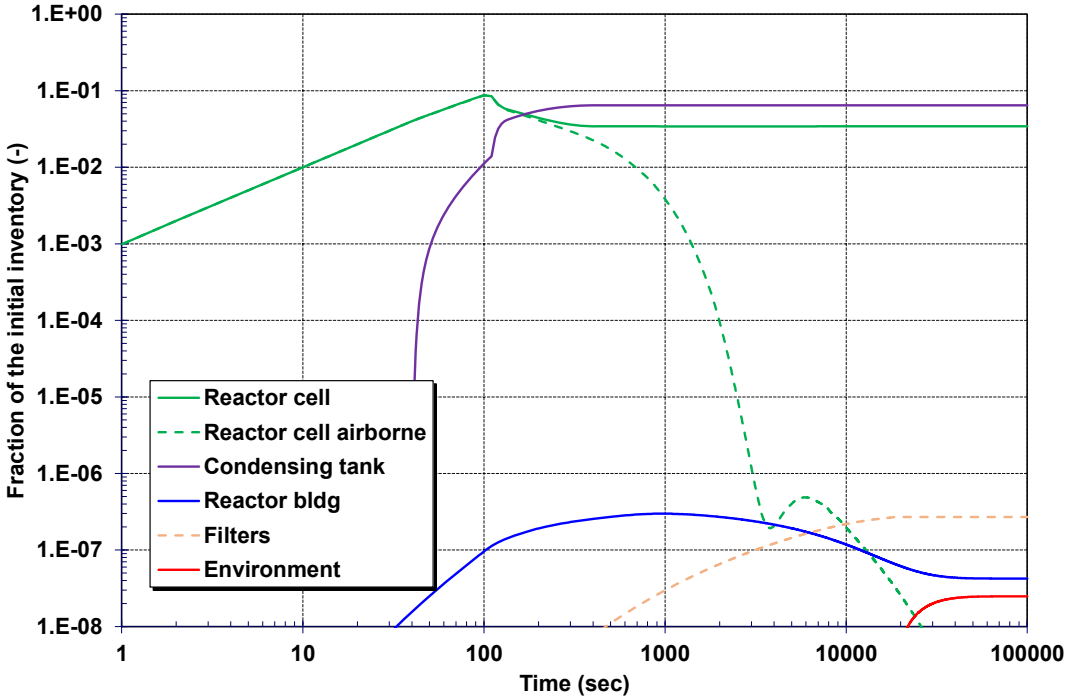

Figure 4-21 MCA6 cesium fluoride distribution.

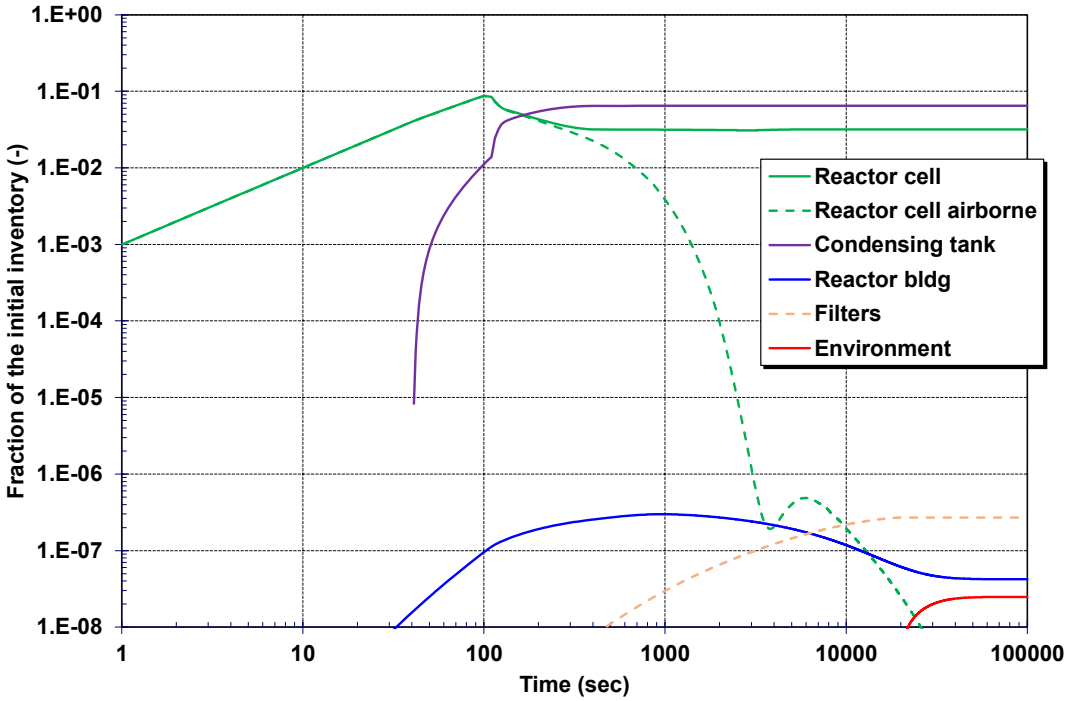

Figure 4-22 MCA6 cesium iodine distribution.

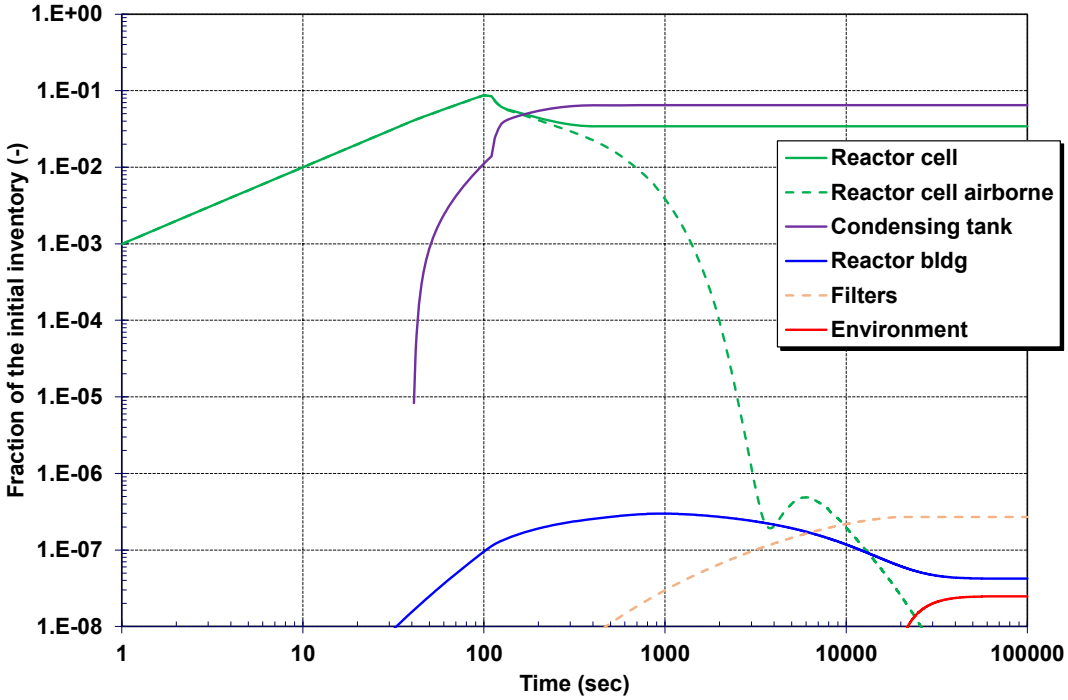

Figure 4-23 MCA6 cerium distribution.

The table below summarizes the boundary conditions for the coincidental water spill sensitivity calculations. Just the cerium results are shown as an example of the aerosol response because cesium fluoride and cesium iodide had similar responses (see previous discussion on their vapor pressure in the reactor cell).

Case	Aerosol size	Bldg Ventil	Aux. Filters	Water Spill
MCA6	1 µm	Yes	No	Yes
MCA7	1 µm	Yes	Yes	Yes
MCA8	1 µm	No	Yes	Yes
MCA9	1 µm	No	No	Yes

The gaseous noble gas (Xe) and gaseous iodine radionuclide responses are shown in Figure 4-24 and Figure 4-25, respectively. The responses of xenon and gaseous iodine show some interesting differences form the dry scenarios. After scaling to the magnitude of their respective release fractions (see Table 4-1), the iodine releases to the environment are lower than the corresponding xenon release fractions. As discussed previously, the impact of the capture in the vapor condensing and gas retention tank in the cases with a coincident water spill reduced the amount available for leakage from the reactor cell. This had a larger impact than the higher pressure due to the steam production. The second overall impact is the iodine capture in the vapor condensing tank water lowered the iodine releases to the environment relative to the xenon. These trends are the same as previously discussed in the MCA6 results discussion.

Similar to the cases without a water spill, the case with both auxiliary filter and reactor building ventilation active (MCA7) had the highest Xe and gaseous iodine releases. The xenon was not filtered so the active ventilation systems enhanced its leakage. Although the iodine was filtered by the auxiliary charcoal filter, the auxiliary filter took suction directly from the relatively high iodine concentration in the reactor cell and 1% passed through without filtering.[15]

The auxiliary charcoal filter capture of gaseous iodine is especially evident in the MCA8 response, which has auxiliary filter operation but no building ventilation. The MCA8 xenon release had the second largest environmental release (i.e., due to no filtering of xenon), whereas the gaseous iodine release was only the third highest because the auxiliary charcoal filters captured most of the gaseous iodine. Nevertheless, the direct connection of the auxiliary filter to the reactor cell transported a relatively high concentration of iodine to the charcoal filters, which retained 99%.

When only the building ventilation is operational (i.e., MCA6), the iodine release was the second largest, primarily because it did not pass through a charcoal filter. The relatively small reactor cell leakage without charcoal filtering had a higher iodine release relative to MCA8 with the charcoal filter. The response of the xenon release between MCA6 and MCA was just the opposite. The MCA6 xenon was third highest because only the small amount that leaked from the reactor cell was vented to the environment whereas MCA8 vented from xenon directly from the reactor cell.

The MCA9 xenon and gaseous iodine releases are the lowest of the various cases. There was no active venting in this case. Consequently, the environmental source term was controlled by leakage from the reactor cell to the reactor building and leakage from the reactor building to the environment. Due to capture in the vapor condensing tank water, there was less iodine available to leak from the reactor cell. A portion of the xenon flowed back into reactor cell from the vapor condensing and gas retention tanks through the vacuum relief valve as the reactor cell leaked and depressurized.

The cerium environmental releases are shown in Figure 4-26. As described in the previous MCA6 discussion, the CsF and CsI responses were essentially identical to the cerium response. Similar to the gas responses, the largest release was from MCA7, which included both building ventilation and auxiliary filter flows. However, the release is very small because the absolute filter captures most of the released aerosols.

The MCA6 Ce environmental release shows a small increase in the environmental release at 6 hr (i.e., not seen in Figure 4-23 due to the scale). Very small aerosols that were not filtered in the vapor condensing tank flowed back through the vacuum relief valve after 1 hr, leaked from the reactor cell, and eventually passed through the absolute filter to the environment. MCA8 and MCA9 did not show this effect because there was no building ventilation flow to carry the small aerosols that leaked into the reactor building through the filter to the environment. The very small effect was also not observable in MCA7. Any impact of the back flow of small aerosols through the vacuum relief valve was negligible relative to the auxiliary filter flow in MCA7.

The results show that MCA8 and MCA9 have essentially the same response, which was unexpected. MCA8 had auxiliary filter flow whereas MCA9 did not. A more detailed comparison of the responses is shown in Figure 4-27. The MCA8 and MCA9 responses are dominated by the aerosol capture in the vapor condensing tank and the rapid reduction in the airborne aerosols available for leakage, which was very similar for both cases and contributed to similar responses. An interesting

[15] The assumed charcoal bed decontamination factor was 100, which corresponds to 99% retention and 1% bypass.

aspect is the comparison of aerosol masses in the offgas system, which includes the auxiliary filter and piping, the absolute filter inlet plenum, the absolute filter, and the plant stack. After the auxiliary filter is started, it draws airborne aerosols from the reactor cell into the offgas piping. However, the auxiliary filter flow is very small relative to the building ventilation flow, so the flow from the auxiliary filter somewhat stagnates in the filter inlet plenum and the plant stack. Therefore, the aerosols transported by the auxiliary filter did not make a meaningful contribution of the release to the environment due to the absence of the building ventilation flow. Instead, the cerium aerosols primarily settled in the absolute filter inlet plenum and to a lesser extent were captured by the absolute filter or settled in the plant stack. These factors led to similar responses in MCA8 and MCA9.

The MCA7 and MCA8 cerium results illustrated in Figure 4-28 confirm the previous conclusions. The two cases differ by the inclusion of the building ventilation flow in MCA7 versus none in MCA8. Both cases have auxiliary filter flow. Similar to Figure 4-27, most of the released mass of airborne cerium aerosols is captured in the vapor condensing tank. The MCA7 results show the impact of the building ventilation flow bringing leaked aerosols to the filter (i.e., offgas region) and the noticeable impact of aerosols from auxiliary filter flow contributing to the increase in the environment release (i.e., via very small aerosols passing through the filter). MCA7 also shows the aerosols entering the offgas region once the auxiliary filter starts. However, the lack of the ventilation flow to transport the aerosols through the inlet plenum towards the absolute filter and the stack contributed to their retention and the lower environmental release.

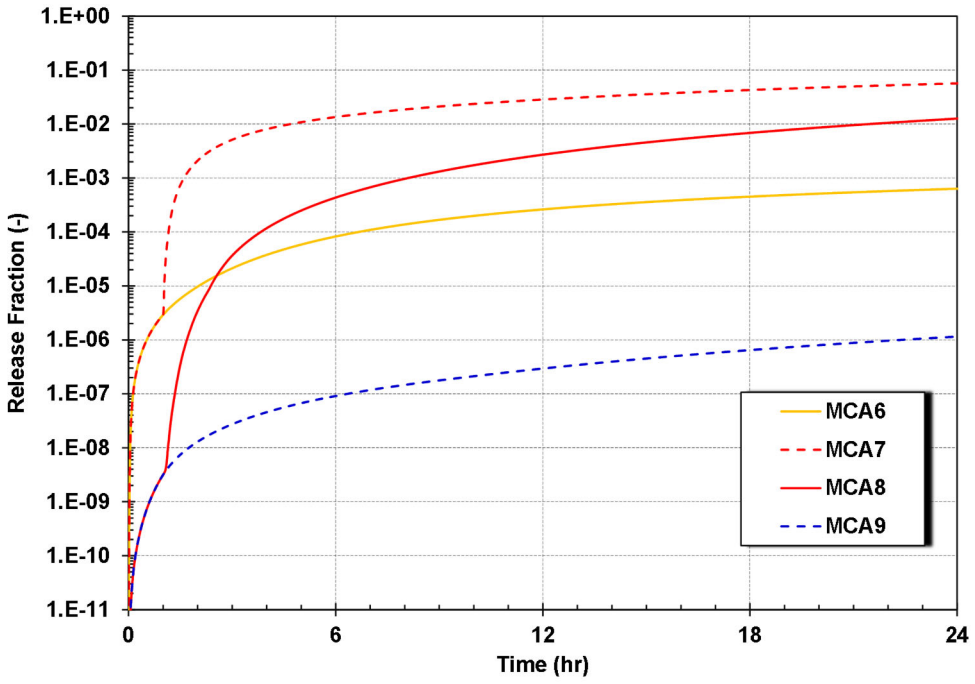

Figure 4-24 Variations in the Xe release to the environment for the cases with a coincident water spill.

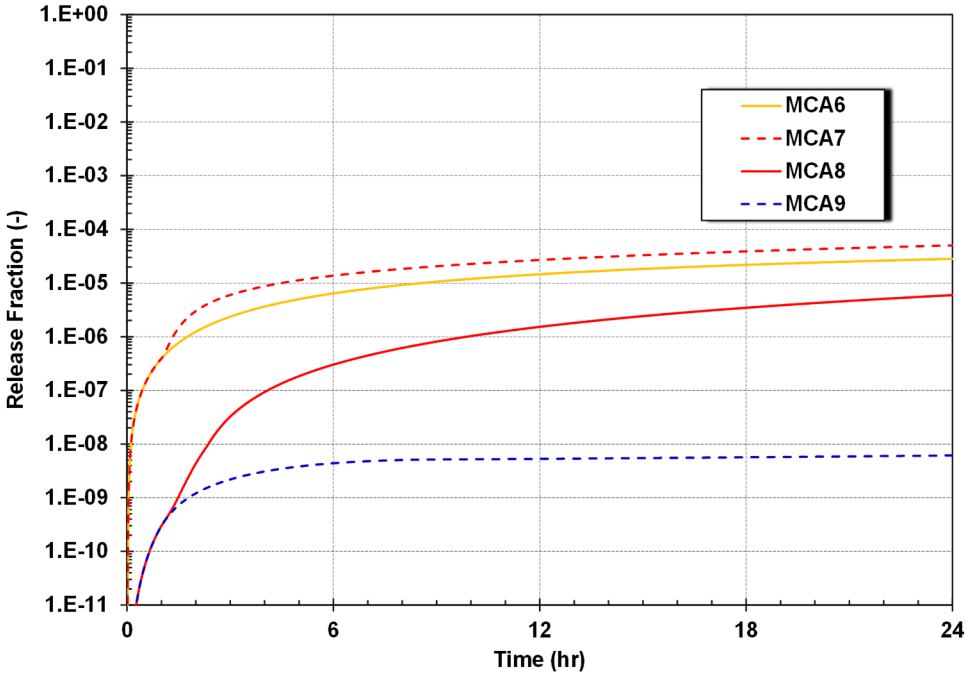

Figure 4-25 Variations in the gaseous iodine release to the environment for the cases with a coincident water spill.

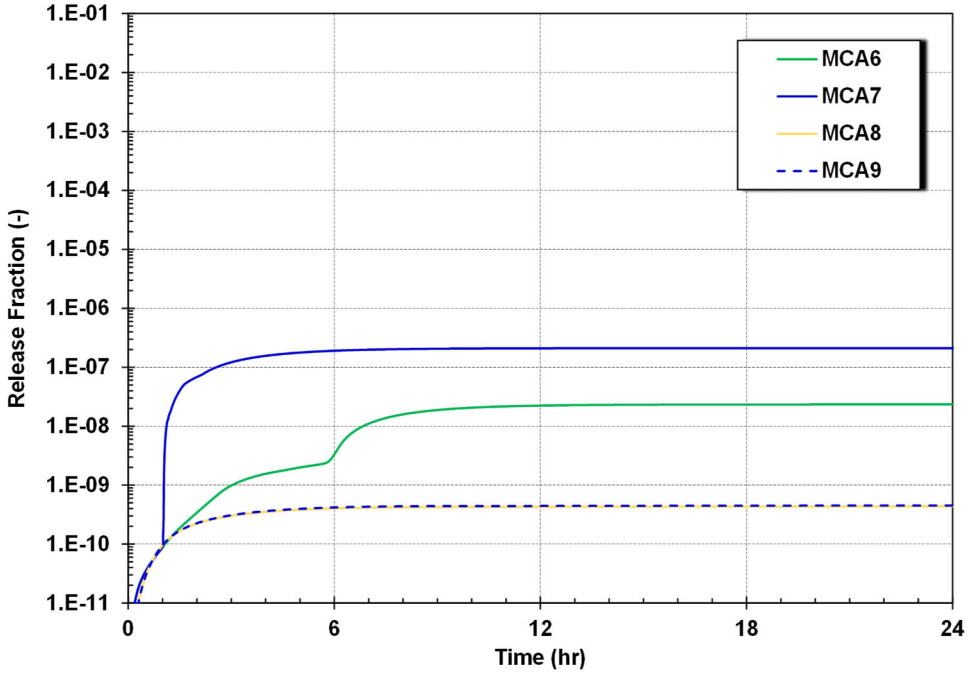

Figure 4-26 Variations in the cerium release to the environment for the cases with a coincident water spill.

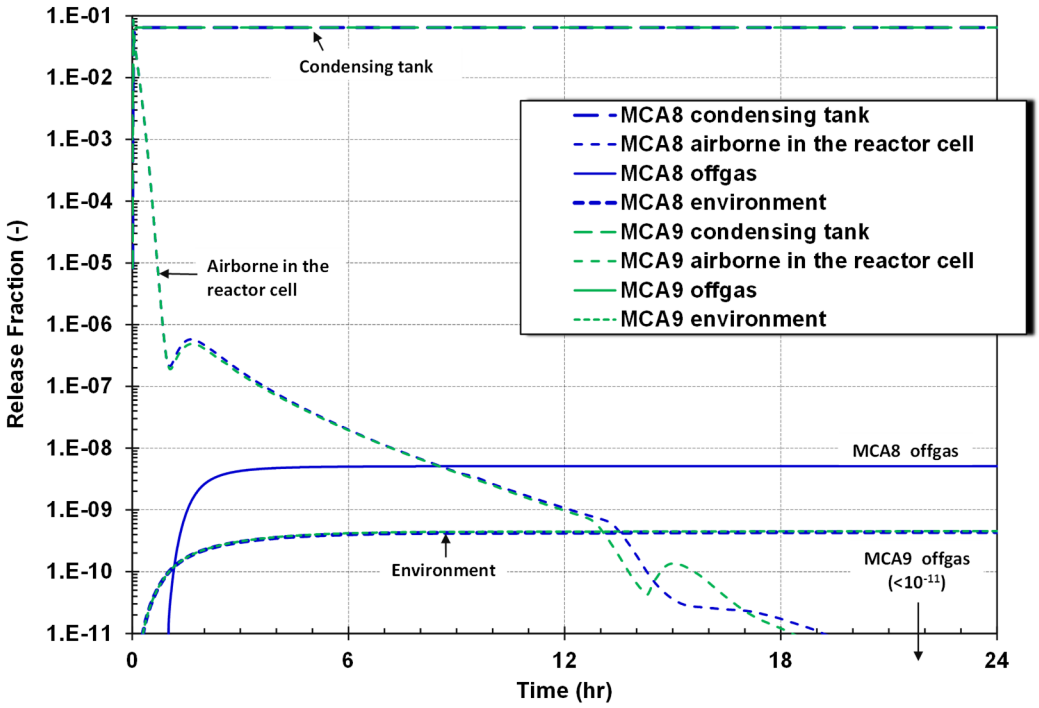

Figure 4-27 Comparison of the MCA8 and MCA9 cerium responses.

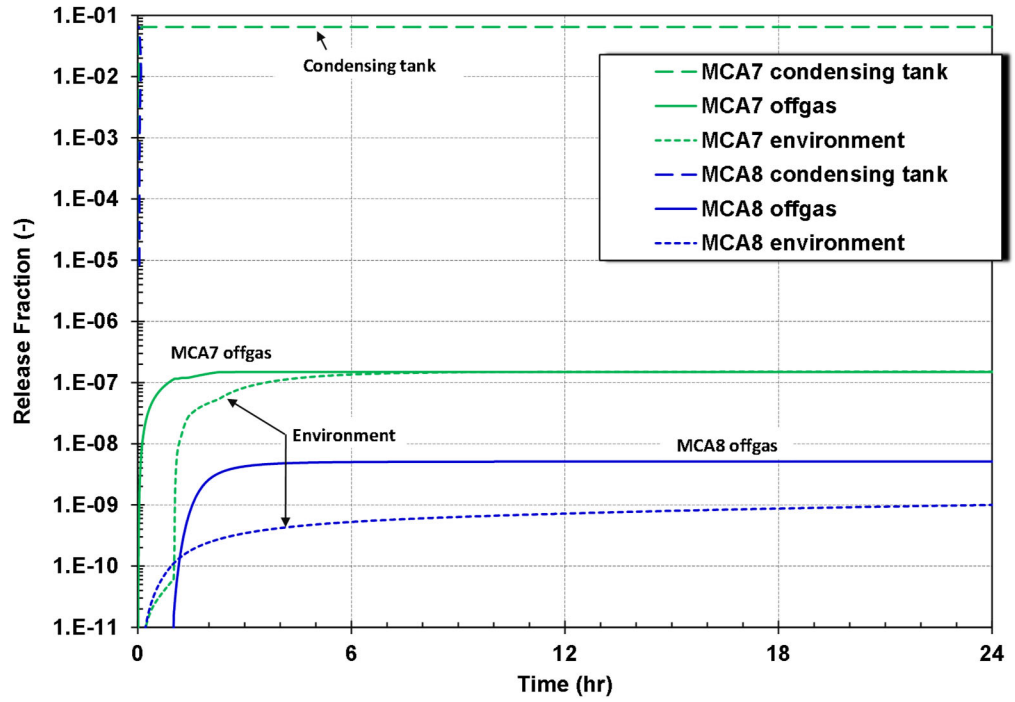

Figure 4-28 Comparison of the MCA7 and MCA8 cerium responses.

4.5. Sensitivity to higher reactor cell and reactor building leakage with an external wind

The last set of calculations examined the potential impact of higher reactor cell and reactor building leakage with an external wind. In the first set of results, the reactor cell leak area is varied with base reactor building leak area and no wind. The second set of sensitivity calculations used the base reactor cell leak area but varied the reactor building leak area and the external wind speed.

As described in Section 3.2.3, the reactor cell leak area was specified to give an inward leak rate of 11.8 liters/min (0.42 SCFH) at the normal operating pressure of 87.6 kPa (-2 psig). The effective leak area is a 1.83 mm diameter hole that was increased by 10X and 100X in the sensitivity studies. The variations illustrate the sensitivity of the reactor cell leak tightness for an alternate design with different leakage specifications.

The reactor building leak area is varied in the second set of calculations. The reactor building leakage rate is based on information used in the safety analysis report. The safety analysis report used a value of 10% per day [8], which was used in these demonstration calculations. The design pressure for the rated leakage was assumed to be 1723 Pa (0.25 psig). However, other MSRE design information in Reference [7] identifies a design pressure of 75 Pa (0.3 in-H_2O). Consequently, using the design pressure value of 1723 Pa (0.25 psig) may be non-conservative because it represents a lower leak area. The building leakage sensitivity study varied the base reactor building leak area by 10X and 100X, which would encompass the leakage characteristics of a lower design pressure. The reactor building leak area variations also included the impact of an external wind as described in Section 3.2.3 that was varied from no wind to 4.5 m/s (10 mph).

The sensitivity cases were based on MCA3 to minimize the effects of the other safety features (i.e., the reactor building ventilation to the absolute filter and auxiliary filter operation). Furthermore, there was no coincident water spill to minimize any benefits from aerosol and gaseous iodine capture in the vapor condensing and gas retention tanks.

Case	Aerosol size	Bldg Ventil	Aux. Filters	Water Spill
MCA3	1 μm	No	No	No

Figure 4-29 and Figure 4-30 show the MCA3 xenon and cerium responses as a function of the reactor cell leak area. The green lines show the fraction in the reactor building. The amount in the reactor building scales approximately linearly with the leak area multiplier for both xenon and cerium. The blue lines show the leakage to the environment. The xenon response follows the trends from the reactor building concentration but shows some non-linear environment release scaling between the leakage cases. The long-term xenon environmental releases increase by 40X for a change from 1X to 10X of the reactor cell leak area multipliers and by 49X for a change from 10X to 100X of the reactor cell leak area multipliers. The enhanced environmental leakage is a result of two key factors that promoted higher reactor building leakage and a larger environmental release. The two factors were more decay heat in the reactor building and the addition of the hot gases from the reactor cell that slightly raised the reactor building gas temperature. The overall impact is a 2000X increase in the xenon source term with a 100X increase in the reactor cell leak area.

The cerium aerosol behavior followed similar trends. Due to aerosol settling in the reactor cell, most of the leakage into the reactor building occurred rapidly following the release of the aerosols during

the molten salt spill. The release rate to the reactor building scaled linearly with the leak area multiplier. The leakage rate from the reactor building to the environment followed a non-linear trend that was slightly different than the xenon results. The long-term environmental releases increase by 33X for a change from 1X to 10X of the reactor cell leak area multipliers and by 55X for a change from 10X to 100X of the reactor cell leak area multipliers. The overall impact is a 1800X increase in the cerium aerosol source term with a 100X increase in reactor cell leak area. The aerosol settling in the reactor cell and the reactor building reduced the cerium values relative to the xenon response. The trends of aerosol leakage to the environment reflect a slower rate due to dilution and settling in the reactor building.

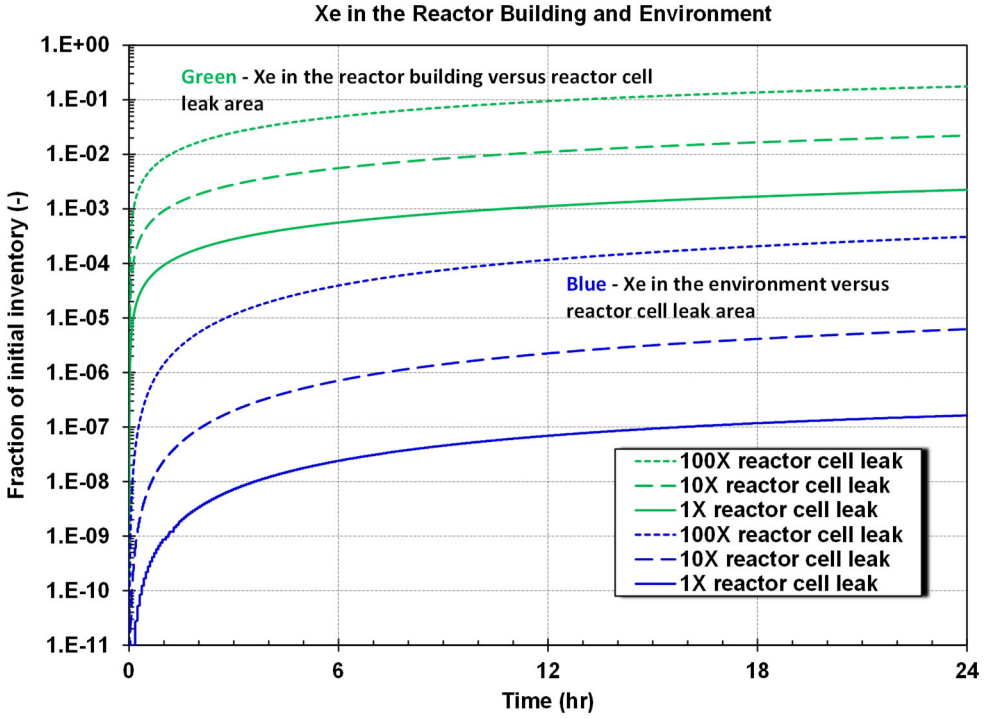

Figure 4-29 MCA3 xenon release to the reactor building and the environment versus reactor cell leak area.

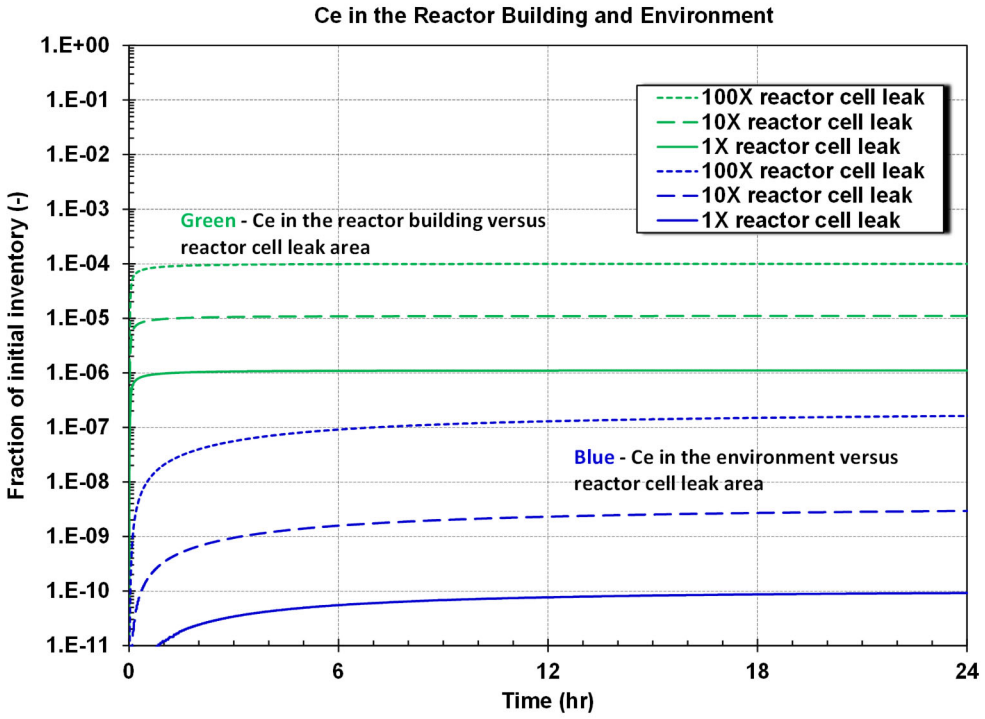

Figure 4-30 MCA3 cerium release to the reactor building and the environment versus reactor cell leak area.

The next calculations show the impact of variations in the reactor building leak area with wind effects. The reactor cell leak area was specified at the nominal value (1X) to eliminate its influence on the other varied parameters. Figure 4-31 and Figure 4-32 show the MCA3 xenon and cerium responses as a function of the reactor building leak area and wind speed, respectively. The results are color coded based on wind speed with varying line types for the leak area multiplier. Unlike the impact of the previous reactor cell leakage variations, the reactor building leakage results do not show linearly scaling results over the time period investigated (i.e., 24 hours). The amount of radionuclides in the reactor building is controlled by the reactor cell leak area, which was not varied. The two figures show the subsequent environmental release, which has a much narrower band of results. The amount of radionuclide leakage to the environment is not significantly impacted by the reactor building leak area or the external wind speed. The impact of the wind speed starts to show a more significant impact with the 100X building leak area multiplier. The variations in the xenon and cerium environmental releases with a 100X building leak area multiplier are 1.6X and 1.4X between no wind and 4.5 m/s (10 mph), respectively. The increased xenon and cerium leakage drops to 1.2X and 1.1X with a 10X building leak area multiplier between no wind and 4.5 m/s (10 mph), respectively. Consequently, a building with a higher leakage rate is more adversely impacted by an external wind. Nevertheless, the impact of the wind and reactor building leakage on the environmental source term is small compared to the reactor cell leakage rate.

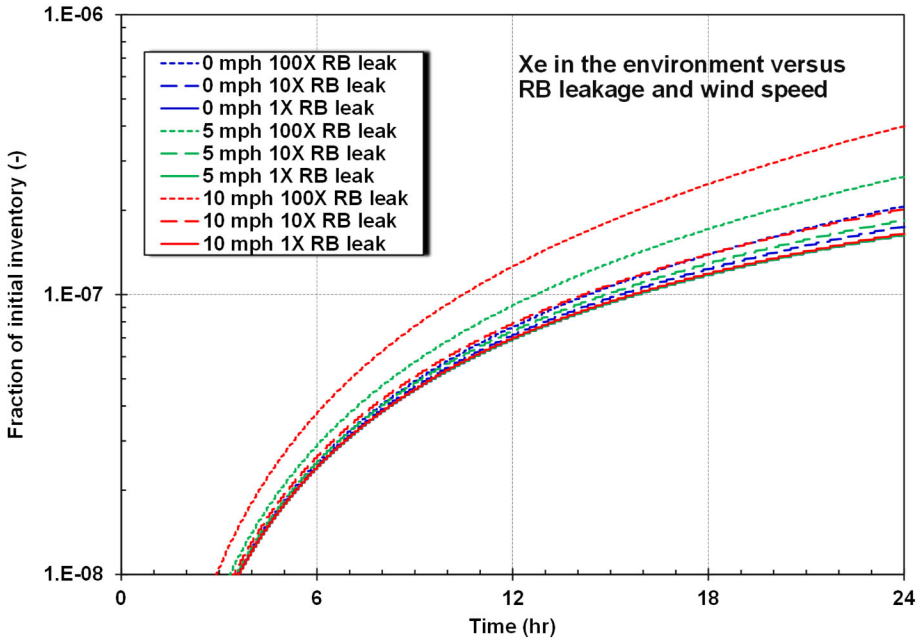

Figure 4-31 MCA3 xenon release to the environment versus reactor building leak area and wind speed.

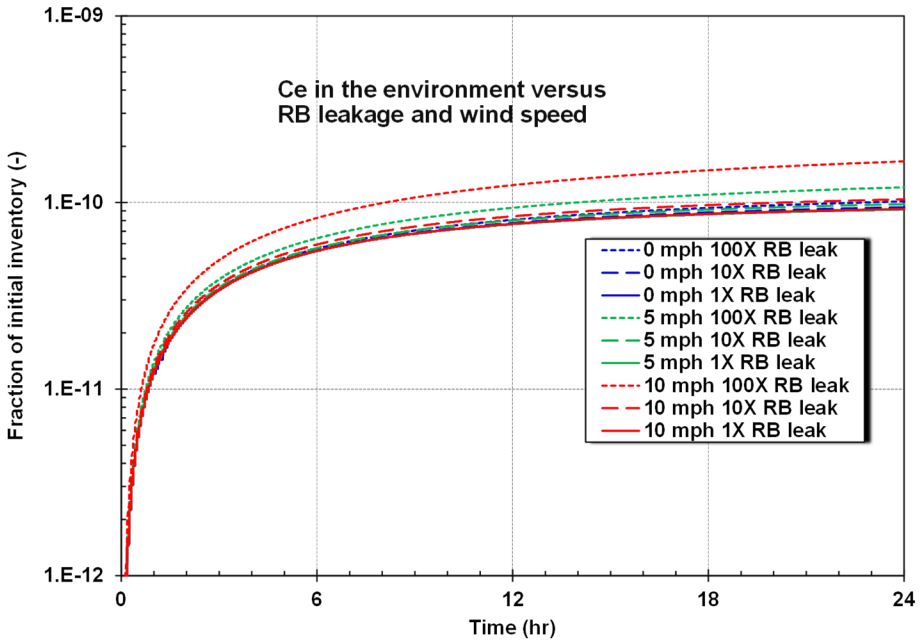

Figure 4-32 MCA3 cerium release to the environment versus reactor building leak area and wind speed.

5. SUMMARY

The MELCOR code has been updated to support NRC safety evaluations of accidents in MSRs. This report presents demonstration calculations for a MSR using the accident radionuclide release from the MSRE safety analysis. A MELCOR model of the MSRE was developed that included the vessel with the molten salt circulation system, the primary heat exchanger, the reactor cell, the vapor condensing and gas retention tanks, the reactor building, the offgas system with the primary and auxiliary charcoal beds, the roughing and absolute filters, the ventilation fans, and the plant stack. Using SCALE results from ORNL, the radionuclide decay heat was specified using a new radionuclide class structure based on the radionuclide solubility in molten salt. SCALE also provided the axial and radial power profile and the fuel and graphite reactor feedbacks. The new MELCOR flowing fuel point kinetics model is used but not significantly demonstrated.

The MSRE input model was used to demonstrate a spill of the molten fuel salt from a broken drain line beneath the vessel. Scenario sensitivity calculations were performed to illustrate the impact of a coincidental water spill, the building ventilation operation, and the auxiliary filter operation. The impact of variations in the aerosol size after the spill, the reactor cell and reactor building leak areas, and an external wind was also shown. The MSRE included important safety features that were modeled in the demonstration calculations. The analyses demonstrate the flexible capabilities of MELCOR to evaluate the accident progression in a MSR. The code can also incorporate evolving data from ongoing research programs and includes flexible inputs for sensitivity and Monte Carlo sampling on uncertain parameters.

REFERENCES

[1] "Non-LWR Vision and Strategy Near-Term Implementation Action Plans," Nuclear Regulatory Commission, ADAMS Accession No. ML16334A495, 2019.

[2] "Nuclear Energy Innovation and Modernization Act," Public Law No: 115-439, January 2019.

[3] Wagner, K., et al., "MELCOR Accident Progression and Source Term Demonstration Calculations for a Heat Pipe Reactor," Sandia National Laboratories, SAND2022-2751, March 2022, https://www.osti.gov/servlets/purl/1854082.

[4] Wagner, K., et al., "MELCOR Accident Progression and Source Term Demonstration Calculations for a HTGR," Sandia National Laboratories, SAND2022-2751, March 2022, https://www.osti.gov/servlets/purl/1854083.

[5] Wagner, K., et al., "MELCOR Accident Progression and Source Term Demonstration Calculations for a FHR," Sandia National Laboratories, SAND2022-2751, March 2022, https://www.osti.gov/servlets/purl/1854081.

[6] B. Rearden and M. Jessee, "SCALE Code System, ORNL/TM-2005/39, Version 6.2.3," UT-Battelle, LLC, Oak Ridge National Laboratory, 2018.

[7] Robertson, R. C., "MSRE Design and Operations Report – Part 1 Description of the Reactor Design", Reactor Division, Oak Ridge National Laboratory, ORNL-TM-0728, January 1965.

[8] Robertson, R. C., "MSRE Design and Operations Report – Part V Reactor Safety Analysis Report", Reactor Division, Oak Ridge National Laboratory, ORNL-TM-0732, August 1964.

[9] "SCALE/MELCOR Non-LWR Source Term Demonstration Project – Molten Salt Reactor (MSR)," NRC Adams Ascension Number ML22353A101, https://www.nrc.gov/docs/ML2235/ML22353A101.pdf, September 13, 2022.

[10] Humphries, L. L., et al., MELCOR Computer Code Manuals: Volume 1; Reference Manual - Version 2.2.18019, Sandia National Laboratories, SAND2019-13442, Jan 2021.

[11] Humrickhouse, P. W., and Merrill, B. J., "Revised Equation of State for FLiBe in MELCOR," Idaho National Laboratory, INL/EXT-17-44148, Revision 0, December 2017.

[12] El-Genk, M. S., and Tournier, J. P., "A Point Kinetics Model for Dynamic Simulations of Next Generation Nuclear Reactor," Progress in Nuclear Energy, Volume 92, September 2016, pp. 91-103.

[13] Wagner, K., et al., "MELCOR Accident Progression and Source Term Demonstration Calculations for a FHR," Sandia National Laboratories, SAND2022-2751, March 2022, https://www.osti.gov/biblio/1854081.

[14] M.H.A. Piro, S. Simunovic, and T.M. Besmann, "Thermochimica User Manual v1.0," ORNL/TM-2012/576, Oak Ridge National Laboratory, December 2012.

[15] Ard, J., et al., "Status Report on the Molten Salt Thermodynamic Database (MSTDB) Development (FY20)," ORNL/SPR-2020/1648, Oak Ridge National Laboratory, 2020.

[16] A. Lo, F. Bostelmann, D. Hartanto, B. Betzler, W. A. Wieselquist, "Application of SCALE to Molten Salt Fueled Reactor Physics in Support of Severe Accident Analyses," ORNL/TM-2022/1844, November 2022, Oak Ridge National Laboratory, Oak Ridge, TN.

[17] Louie, D. L., Humphries, L. L., "NSRD-10: Leak Path Factor Guidance Using MELCOR," Sandia National Laboratories, SAND2017-3200, March 2017.

[18] ASHRAE, "Handbook of Fundamentals," American Society of Heating, Refrigerating and Air-Conditioning Engineers, Inc, 1997.

[19] David F. Williams and Phillip Britt, "Future Research Directions," DOE-NE Molten Salt Chemistry Workshop, April 10-12, 2017, ORNL, https://www.ornl.gov/sites/default/files/Molten%20Salt%20Workshop_Final_092917.pdf.

[20] R. J. Kedl , "The Migration of a Class of Fission Products (Noble Metals) in the Molten-Salt Reactor Experiment," ORNL-TM-3884, Oak Ridge National Laboratory, 1972.

[21] "DOE Handbook Airborne Release Fractions/Rates and Respirable Fractions for Nonreactor Nuclear Facilities, Volume I - Analysis of Experimental Data," Department of Energy, DOE-HDBK-3010-94, December 1994.

[22] O. Beneš, et al., "Cesium and iodine release from fluoride-based molten salt reactor fuel," Journal of Physical Chemistry and Chemical Physics, Vol. 23, April 2021.

[23] D. W. Underhill, "The adsorption of argon, krypton and xenon on activated charcoal," Journal of Health Physics, Volume 71, Issue 2, p. 160-166, August 1996.

DISTRIBUTION

Email—Internal

Name	Org.	Sandia Email Address
David Luxat	08852	dlluxat@sandia.gov
Brad Beeny	08852	babeeny@sandia.gov
Technical Library	01977	sanddocs@sandia.gov

Email—External (encrypt for OUO)

Name	Company Email Address	Company Name
Jason Schaperow	jason.schaperow@nrc.gov	NRC
Hossein Esmaili	hossein.esmaili@nrc.gov	NRC
Shawn Campbell	shawn.campbell@nrc.gov	NRC

Hardcopy—Internal

Number of Copies	Name	Org.	Mailstop

This page left blank

This page left blank

Sandia National Laboratories

Sandia National Laboratories is a multimission laboratory managed and operated by National Technology & Engineering Solutions of Sandia LLC, a wholly owned subsidiary of Honeywell International Inc. for the U.S. Department of Energy's National Nuclear Security Administration under contract DE-NA0003525.